UNIVERSITY OF TURIN

PhD program in
Molecular Medicine

XXXII Cycle

Unleashing anti-tumor immune responses in pancreatic cancer by tumor-associated antigens

Tutor: Prof. Francesco Novelli

Candidata: Sara Bulfamante

Coordinator: Prof. Francesco Novelli

Index

1. Aim of the study ……..……..……..3
2. Table of contents ……...3
3. Tumor-associated antigen in pancreatic ductal adenocarcinoma: alpha-enolase (ENO1) as a potential immunotherapeutic target……....5
4. The role of ENO1 in pancreatic ductal adenocarcinoma adhesion, invasion, and metastasis……9
5. Combined treatments with the DNA vaccine to increase its effectiveness in pancreatic ductal adenocarcinoma……..……24
6. Glycolytic enzymes as novel tumor-associated targets for immunotherapy in pancreatic ductal adenocarcinoma……...28
7. Chemotherapy increases tumor-associated antigens specific immune response and potentiates DNA vaccination in pancreatic ductal adenocarcinoma……..……33
8. Chemotherapy, but not immune checkpoint blockade, enhances tumor-associated antigens specific T lymphocyte effector response in patients with pancreatic ductal adenocarcinoma……..……47
9. Discussion……...……64
10. Bibliography……..70

Aim of the study

To date, the clinical treatments received by patients with pancreatic cancer are not sufficient to inhibit the tumor growth or to increase their survival, which remains very low. Thus, the aim of this thesis is to demonstrate that future pancreatic cancer treatments will benefit from an approach based on immunotherapy, especially on anti-tumor vaccination.

The first goal is to investigate the presence of tumor-associated antigens in pancreatic cancer with a view to using them as targets of the anti-tumor vaccine; moreover, defining their ability in inducing a robust anti-tumor immune response is also necessary.

Secondly, pancreatic cancer is characterized by a strong immunosuppressed state and breaking down this condition is particularly relevant in order to enhance the immune response induced by the anti-tumor vaccine. For this reason, the other aim of this thesis is to evaluate the impact of different pharmacological treatments, with a focus on chemotherapy, on the immune response against pancreatic cancer.

Table of contents

The observations and data contained in this thesis support the potential of tumor-associated antigens (TAA) as targets of new immunotherapeutic strategies for pancreatic ductal adenocarcinoma.

The first part of the work introduces ENO1 as a promising TAA and exposes the immunological effects of the DNA vaccine in preclinical models. The following chapter reports the published data regarding the role of ENO1 in adhesion, invasion and metastasis of pancreatic cancer. Besides, the evidence on DNA vaccination combined with other pharmacological treatments are described in a published review and they are deeply discussed in this thesis. Moreover, several glycolytic enzymes, including ENO1, can be feasible targets for immunotherapy; the relative bibliography is collected in a published review and the main observations are argued in a dedicated section. The next chapter contains the data from a published original article regarding the chemotherapy effect on TAA-specific immune response and DNA vaccination; the relative discussion is addressed in the last section. Finally, in this thesis the unpublished data are presented and discussed, which describe the modulation of TAA-specific T lymphocyte effector response by chemotherapy and immune checkpoint blockade; the related materials and methods are shown at the end of the chapter.

Tumor associated antigen in pancreatic ductal adenocarcinoma: alpha-enolase (ENO1) as a potential immunotherapeutic target

Pancreatic Ductal Adenocarcinoma (PDA) represents the most frequent pancreatic neoplasia and its incidence is increasing, making it the fourth cause of cancer death [1]. PDA remains an almost incurable tumor with a 5-year overall survival rate of 9% [1]. This poor prognosis is due to the lack of early symptomatology and at the time of the diagnosis patients present an advanced tumor stage, which restricts the percentage of who can undergo surgery to 20% [2]. PDA is mostly resistant to chemotherapy (CT), despite in the last decade other chemotherapeutic agents, such as FOLFIRINOX and Nab-Paclitaxel, were administered alone or in combination with the standard drug Gemcitabine (GEM), leading to a slightly increase of PDA patients survival [3–5].

The main reason for chemoresistance is the compositions of the typical tumor microenvironment (TME) of PDA: the tumor mass is surrounded by fibroblasts and pancreatic stellate cells that produce the extracellular matrix (ECM) elements [6,7], indeed desmoplasia can reach almost the whole tumor volume becoming a physical barrier to the drugs [6]. Moreover, PDA TME is poorly populated by leukocyte cells and in advanced stage most of them are represented by immunosuppressive cells, such as tumor-associated macrophages (TAM), myeloid-derived suppressor cells (MDSC), and regulatory T cells (Treg) [8]. Only few effector T cells (Teff) infiltrate the tumor, with no evidence of activation [8]. PDA is considered as a “cold” tumor for both its immunosuppressive state and its low rate of DNA mutations, which does not generate enough neoantigens that can be recognized by immune system [9]; thus the research is increasingly directed towards strategies that trigger and enhance the immune response to cancer cells.

The idea behind the immunotherapy was to exploit the immune system to directly fight tumor progression and it was mostly based on the discovery of specific targets, such as overexpressed tumor-associated antigens (TAA) in cancer, compared to normal tissue [10]. Moreover, the immune system can specifically recognize TAA inducing an anti-tumor response without targeting normal cells. Thus, the crucial point of an effective immunotherapy is to identify the best tumor target to activate the adaptive immune response, ensuring a minimal risk of eliciting autoimmunity, or limiting immunosuppressive mechanisms. Many groups have looked for not yet characterized or more immunogenic new TAA, by developing different approaches. A methodology known as

serological analysis of recombinant cDNA expression libraries (SEREX) has been useful to identify several hundreds of TAA [11,12]. A similar technique, exploiting the presence of antibodies in the sera of cancer patients, coupled with a proteomic approach, is SERological Proteome Analysis (SERPA), which allowed to identify TAA in many kinds of tumors [13,14].

In a study published in 2007, the presence of autoantibodies in the sera of PDA patients was demonstrated using a SERPA approach, and those autoantibodies could discriminate PDA from healthy subjects and from chronic pancreatitis or other malignancies [14]. Among the identified autoantibody-related antigens, alpha-Enolase (ENO1), a glycolytic enzyme, was identified as a promising TAA, because both its ability to induce a high frequency of antibody responses in PDA patients and its very low frequency in healthy donors, chronic pancreatic and non-PDA cancer patients, suggesting also its diagnostic value in PDA [14]. ENO1 overexpression at mRNA and protein level was observed in PDA and in other different tumor types [15]. Beside PDA, ENO1 has been shown to induce antibody production in many types of cancers, such as cholangiocarcinoma, breast cancer, head and neck cancer, leukemia, lung cancer and melanoma [15].

Antibodies from PDA patients specifically recognized two highly phosphorylated acid isoforms of ENO1 (identified as ENO1,2), which were upregulated in PDA compared to normal pancreas and displayed phosphorylation of serine 419 [16]. Importantly, anti-ENO1,2 antibodies were found in PDA patients with normal levels of the diagnostic marker CA19.9, increasing its sensitivity [16]. The presence of anti-ENO1,2 antibodies correlated with a longer progression-free survival and a better clinical outcome in PDA patients treated with the standard GEM-based CT [16]. Interestingly, anti-ENO1 antibodies increased following GEM treatment in PDA patients in which was observed also an increased ENO1-specific Teff response [17]. In general, phosphorylation is associated with a higher affinity of its peptides for human leukocyte antigen (HLA) molecules; indeed, the presence of anti-ENO1,2 antibodies correlated with a higher frequency of the allele HLA-DRB1*8 among PDA patients [18]. Furthermore, peripheral blood mononuclear cells (PBMC) from HLA-DRB1*8 healthy subjects stimulated with phosphorylated ENO1 peptide elicited a significant CD4+ T cell proliferative response compared to the unphosphorylated ENO1 peptide [18].

Many TAA stimulate an integrated humoral and cellular response by activating both T and B cells, and this coordinate response is one of the main effector mechanisms exploitable by tumor immunotherapy [15]. PDA patients with anti-ENO1 circulating antibodies displayed *in vitro* ENO1-

activated peripheral T cells secreting IFN-γ [19]. ENO1 elicited *in vitro* specific proliferation and activation of T cells also from healthy donor PBMC, as well as the differentiation of cytotoxic T cells (CTL) which specifically inhibited HLA-matched PDA cells but not HLA-matched normal fibroblast, *in vitro* and *in vivo* [19].

The response of T cells against ENO1 does not always lead to an effector function as ENO1- specific T cells could display a Treg phenotype. *Ex vivo* phenotypic characterization of infiltrating-tumor T cells (TIL) and infiltrating normal pancreas T cell from PDA patients, showed a significant increase of ENO1-specific Treg from TIL, compared to ENO1-specific Treg from healthy pancreatic tissue [20]. By contrast, T helper1 (Th1) and T helper17 (Th17) cells showed an anti-tumor effector function and were found increased in healthy pancreatic mucosa compared to PDA tissue, suggesting that recruitment of anti-tumor Th17 cells to the tumor site is impaired by Treg immunosuppressive function [20]. Moreover, in PDA patients, circulating ENO1-specific T cells shared the same repertoire of the T cell receptor Vβ chains (TCRB) with ENO1-specific TIL, suggesting the possibility of recirculation between the periphery and the tumor [21]. Despite the existence of ENO1-specific TIL, the intensity of the anti-tumor immune response remained limited, indeed T cells showed mostly a regulatory phenotype [20,21]. By contrast, *in vitro* re-stimulation with recombinant ENO1 could trigger the ENO1-specific T cells from PBMC, with a more pronounced Th1 than Treg phenotype [21]. In PDA patients CT could induce in ENO1 *in vitro*-stimulated PBMC a shift from Treg- to Teff-like phenotype [17]. Finally, PDA patients with a higher number of peripheral ENO-specific T cells showed significantly longer survival, underlying the importance of ENO1-specific response to improve PDA patient anti-tumor immunity [21].

Tumor vaccination is one of the most studied immunotherapeutic approach which directly target the TAA; several clinical trials exploited the vaccination to elicit the immune response, using peptides of overexpressed or mutated proteins, such as MUC1 [22], Telomerase [23], survivin [24], and KRAS [25]; or with whole tumor cells, such as the GVAX which is composed by granulocyte-macrophage colony-stimulating factor (GM-CSF)–secreting tumor cells [26,27]. A recent phase I study investigated the activity of chimeric antigen receptor (CAR)-modified autologous T cells redirected against mesothelin in solid tumors, including PDA [28].

DNA-based vaccines may also represent a suitable and efficient option for immunotherapy, displaying several advantages: they do not contain viral proteins that could down-regulate the immune system or elicit neutralizing antibodies, they are stable and safe, as mutations arising from

a putative integration event are extremely rare [29]. A necked plasmid, pVax vector, approved by the FDA for clinical use, was used to express full length human ENO1 and to vaccinate PDA mouse models, that had been genetically engineered to spontaneously develops PDA due to the pancreas-specific expression of a Cre recombinase that cuts off a STOP cassette before the mutated KRAS and/or TP53 genes [30]. Based on the expression of mutated KRAS alone, or in combination with mutated TP53, mice are called KC or KPC [30]. ENO1 vaccination induced an integrated humoral and cellular response that efficiently prolonged KC and KPC mouse models survival [31]. Furthermore, ENO1 vaccination of KC mice efficiently decreased the tumor size also if the vaccine was received at 8 months, when adenocarcinomas were well established resembling the advanced stage in human PDA at the diagnosis [31].

Several tumor protective immunological mechanisms induced by the ENO1 vaccine were observed, namely high levels of anti-ENO1 IgG able to mediated the complement-dependent cytotoxicity (CDC) of PDA cells, activation of specific Th1 and Th17 cells, a large recruitment of CD3 cells into the tumor, an important decrease of both circulating MDSC and a lower presence of Treg TIL [31,32] (Figure 1).

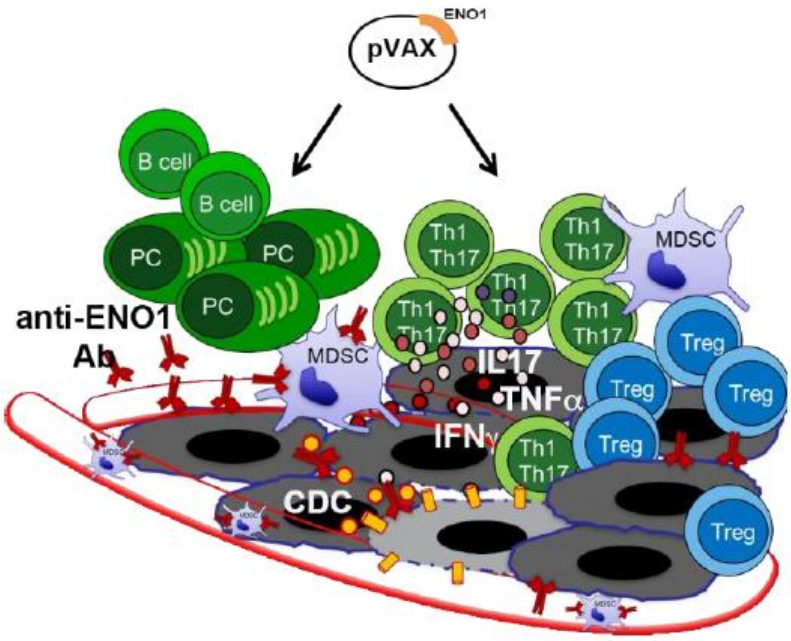

Figure 1. ENO1 DNA vaccination effects in PDA mouse model. Activation of B cells produced anti-ENO1 antibodies (Ab) that affect tumor cells and MDSC invasion and endothelial adhesion (vessels are shown as transparent red tubes). The vaccine induces CDC of tumor cells (grey cells) and T cells, specially Th1/Th17 cells that release IL17, TNFα and IFN-γ cytokines. Yellow circles and cylinders indicate the complement system and the membrane attack complex, respectively, involved in the CDC. Circles represent cytokines.

The crucial role of anti-ENO1 antibodies was confirmed by the observation that ENO1-vaccinated mice showed B cells organized in dense aggregates, the so-called tertiary lymphoid tissue (TLT), correlating with an increased recruitment of T lymphocytes [33]. TLT correlated also with a better prognosis and with a greater infiltration of CD8+ T cells in PDA patients [33]. These observations suggest the induction of TLT as a strategy to favor mobilization of immune cells in PDA.

Anti-ENO1 antibodies also targeted the immunosuppressive function of MDSC, which in PDA patients expressed high levels of ENO1 [34]. Both *in vitro* and *in vivo* MDSC migration was inhibited by anti-ENO1 monoclonal antibody (mAb); moreover, activated T cells in the presence of anti-ENO1 mAb-treated MDSC increased IFN-γ and IL-17 secretion and decreased IL-10 and TGFβ secretion compared to control MDSC [34].

In KC mice models, treatment with GEM prior to ENO1 DNA vaccination unleashed CD4 anti-tumor activity and strongly impaired tumor progression compared with mice that were vaccinated or GEM-treated alone [17]. The ENO1-specific antibodies and IFN-γ secreting T cell induced by ENO1 vaccine, were further increased in combination with GEM-based CT treatment; of note, ENO1 vaccination showed an antigen spreading effect since were detected also antibodies and Teff specific for another glycolytic enzyme, glyceraldehyde 3-phosphate dehydrogenase (G3P) [17].

Overall, ENO1-DNA vaccine elicits an integrated humoral and cellular response to counteract tumor growth, which not only affects the tumor cells themselves but also stromal and reactive cells.

ENO1 is a glycolytic enzyme that catalyzes the conversion of 2-phosphoglycerate to phosphoenolpyruvate and together to the others glycolytic enzymes, such as G3P, resulted overexpressed in PDA cancer cell compared to normal pancreatic tissues [35]. Due to the hypoxic TME, PDA cells display an altered glucose metabolism resulting in its increased uptake; the higher glycolytic rate leads to lactate accumulation and the consequent acidification of the TME results in immunosuppression [35]. The effectiveness of glycolytic enzyme targeting in combination with CT is under investigation in ongoing clinical trials in cancer patients whose survival outcomes are not yet known [35]. These molecules constitute a potential platform of onco-immunology targets both as TAA and because of their role in the reprogrammed cellular metabolism of cancer. This assumption will be discussed in a later chapter.

The role of ENO1 in pancreatic ductal adenocarcinoma adhesion, invasion, and metastasis

The specific ENO1 overexpression in PDA cells together with the presence of ENO1-antibodies in PDA patients, support ENO1 as an eligible target for PDA immunotherapy.
Beside the involvement of ENO1 in inducing an immune response and in the alteration of cancer cell metabolism, ENO1 overexpression has been correlated with size, disease stage, metastasis and prognosis for many tumors [36]. ENO1 was found also on the cell membrane where it acts as a plasminogen receptor; thus, the pro-invasive function of ENO1 seems mainly linked to its role in facilitating the binding of high plasminogen concentrations, which in turn promotes ECM degradation [36]. At the cell surface, ENO1 is part of a multi-protein complex including the urokinase plasminogen activator receptor (uPAR), integrins and cytoskeletal proteins, responsible for adhesion, migration and proliferation [36], while in the cytoplasm, ENO1 interacts with the cytoskeleton to promote migration of tumor cells by providing ATP [37].

In the study of Principe et al. published in 2017 titled “Alpha-enolase (ENO1) controls alpha v/beta 3 integrin expression and regulates pancreatic cancer adhesion, invasion, and metastasis” [38] was investigated the effect of ENO1 silencing on the modulation of cell morphology, adhesion to matrix substrates and cell invasiveness, demonstrating that ENO1, through its role of plasminogen receptor, actually promoted invasion and metastasis formation. The figures mentioned in this chapter refer to the attached article Principe et al. 2017 [38].
The expression of adhesion and cytoskeletal proteins was found altered in ENO1 silencing (shENO1) PDA cells (Figure 1). A down-regulation of proteins involved in cell-cell and cell-matrix adhesion was observed, including alpha v/beta 3 integrin, in shENO1 PDA cells (Figure 4A). The membrane nanostructure analysis revealed a significant increase in the roughness of the cell membrane in shENO1 PDA cells (Figure 2).
This morphological feature was associated with an impaired ability to migrate and invade, since shENO1 PDA cells displayed a reduced adhesion to fibronectin and collagen I and IV, by contrast an increased adhesion to vitronectin (VN) was observed (Figure 3).
The binding to VN by shENO1 was likely maintained via uPAR, indeed its expression was found upregulated in shENO1 PDA cells (Figure 4B). Analysis of uPAR signaling in shENO1 PDA cells resulted

in ERK1-2 and RAC activation, suggesting that the binding of uPAR to VN triggers integrin-mediated signals (Figure 5).

Accumulation of reactive oxygen species (ROS) and senescence were observed in shENO1 cells and the use of an anti-uPAR antibody caused significant reduction of ROS production and senescence, confirming the role of uPAR in shENO1-dependent oxidative stress and senescence in PDA cells (Figure 6). Finally, the impairment of cell migration and invasion due to ENO1 silencing was confirmed also *in vivo*, since a reduced ability to form lung metastasis was observed in shENO1 PDA cells intravenously injected mouse model (Figure 7).

In conclusion this study has shown that ENO1 silencing inhibits adhesion, invasion, and metastasis in PDA cells, due to changes in actin cytoskeleton organization, integrin profile and uPAR expression, confirming the role of ENO1 as a promising target in PDA treatment.

Principe *et al. Journal of Hematology & Oncology* (2017) 10:16
DOI 10.1186/s13045-016-0385-8

Journal of Hematology & Oncology

RESEARCH Open Access

Alpha-enolase (ENO1) controls alpha v/beta 3 integrin expression and regulates pancreatic cancer adhesion, invasion, and metastasis

Moitza Principe[1,2], Simone Borgoni[1,2], Mariafrancesca Cascione[3,4], Michelle Samuel Chattaragada[1,2], Sammy Ferri-Borgogno[1,2], Michela Capello[1,2], Sara Bulfamante[1,2], Jennifer Chapelle[1,5], Francesca Di Modugno[6], Paola Defilippi[1,5], Paola Nisticò[6], Paola Cappello[1,2,5], Chiara Riganti[7], Stefano Leporatti[8] and Francesco Novelli[1,2,5*]

Abstract

Background: We have previously shown that in pancreatic ductal adenocarcinoma (PDA) cells, the glycolytic enzyme alpha-enolase (ENO1) also acts as a plasminogen receptor and promotes invasion and metastasis formation. Moreover, ENO1 silencing in PDA cells induces oxidative stress, senescence and profoundly modifies PDA cell metabolism. Although anti-ENO1 antibody inhibits PDA cell migration and invasion, little is known about the role of ENO1 in regulating cell-cell and cell-matrix contacts. We therefore investigated the effect of ENO1 silencing on the modulation of cell morphology, adhesion to matrix substrates, cell invasiveness, and metastatic ability.

Methods: The membrane and cytoskeleton modifications that occurred in ENO1-silenced (shENO1) PDA cells were investigated by a combination of confocal microscopy and atomic force microscopy (AFM). The effect of ENO1 silencing was then evaluated by phenotypic and functional experiments to identify the role of ENO1 in adhesion, migration, and invasion, as well as in senescence and apoptosis. The experimental results were then validated in a mouse model.

Results: We observed a significant increase in the roughness of the cell membrane due to ENO1 silencing, a feature associated with an impaired ability to migrate and invade, along with a significant downregulation of proteins involved in cell-cell and cell-matrix adhesion, including alpha v/beta 3 integrin in shENO1 PDA cells. These changes impaired the ability of shENO1 cells to adhere to Collagen I and IV and Fibronectin and caused an increase in RGD-independent adhesion to vitronectin (VN) via urokinase plasminogen activator receptor (uPAR). Binding of uPAR to VN triggers integrin-mediated signals, which result in ERK1-2 and RAC activation, accumulation of ROS, and senescence. In shENO1 cancer cells, the use of an anti-uPAR antibody caused significant reduction of ROS production and senescence. Overall, a decrease of in vitro and in vivo cell migration and invasion of shENO1 PDA cells was observed.

Conclusion: These data demonstrate that ENO1 promotes PDA survival, migration, and metastasis through cooperation with integrins and uPAR.

Keywords: Pancreatic cancer, ENO1, Integrin, Atomic force microscopy, Invasion

* Correspondence: franco.novelli@unito.it
[1]Department of Molecular Biotechnology and Health Sciences, University of Turin, Turin, Italy
[2]Center for Experimental Research and Medical Studies (CeRMS), Azienda Universitaria Ospedaliera Città della Salute e della Scienza di Torino, Via Santena 5, 10126 Turin, Italy
Full list of author information is available at the end of the article

BioMed Central

© The Author(s). 2017 **Open Access** This article is distributed under the terms of the Creative Commons Attribution 4.0 International License (http://creativecommons.org/licenses/by/4.0/), which permits unrestricted use, distribution, and reproduction in any medium, provided you give appropriate credit to the original author(s) and the source, provide a link to the Creative Commons license, and indicate if changes were made. The Creative Commons Public Domain Dedication waiver (http://creativecommons.org/publicdomain/zero/1.0/) applies to the data made available in this article, unless otherwise stated.

Background

Pancreatic ductal adenocarcinoma (PDA) is one of the most lethal forms of cancer with a 5-year survival rate of less than 8% [1]. No early detection tests are currently available and, as a result, most patients (80–85%) are not diagnosed until late-stages of the disease, when the cancer has metastasized to other organs [2–4]. In recent years, many proteins have been proposed as new immunological and molecular targets for PDA [5–7] and among these, one of the most promising is alpha-enolase (ENO1) [8].

In PDA and other tumors, ENO1 has a multifunctional role depending on its localization [8, 9]. In addition to its well-known enzymatic function during glycolysis, ENO1 acts as a plasminogen receptor on the cell surface [8, 10] promoting metastatic cancer invasion [11–15]. We have previously demonstrated that the injection of adenovirus expressing cDNA coding for monoclonal antibody that block the binding of ENO1 with plasminogen-inhibited metastases formation of PDA cells in vivo [12]. Many metabolic enzymes, including ENO1, are known to interact with cytoskeletal proteins (e.g., F-actin, tubulin), and these associations provide ATP to promote the migration of tumor cells [16, 17]. Although the roles of ENO1 as a glycolytic enzyme [18, 19] and as a plasminogen receptor [12, 20] have been well characterized, its role in the regulation of cytoskeleton reorganization, particularly in PDA cells, has not been fully clarified. Integrins regulate adhesion-dependent growth and invasion of tumor cells and the integrin alpha v/beta 3 has been reported as a mediator of anchorage independence [21], and its expression has been associated with an aggressive form of disease in different human tumors including PDA [22–27]. In this study, we employed biochemical and functional approaches to investigate molecules involved in cell adhesion and migration of ENO1-silenced (shENO1) PDA cells. AFM (atomic force microscopy) was employed to investigate the nanostructural properties of shENO1 PDA cells. In addition, as cell adhesion, survival and migration are dependent on integrin binding to the extracellular matrix (ECM), and subsequent signals, the roles of alpha V/beta 3 and alpha 5/beta 1 integrins, as well as uPAR (an ECM receptor) were evaluated in shENO1 PDA cells. Moreover, the impact of ENO1 silencing in the in vitro and in vivo invasion and spreading of PDA cells was evaluated. Results from this study indicated that ENO1, by cooperating with integrins and uPAR, is a key regulator of cell survival, adhesion, and motility in PDA.

Methods

Cell culture

Human pancreatic cancer cell lines used were: CFPAC-1 (from ECACC), PT45, and T3M4. Cell lines were cultured in DMEM (Lonza, Milan, Italy) supplemented with 10% FBS (Lonza), L-Glutamine (GE Healthcare, Milan, Italy) and 50 μg/ml of gentamicin (Gentalyn 40 mg/ml, Essex Italia, Segrate, MI, Italy) at 37 °C in a 5% CO_2 atmosphere. Cells were detached using a 1 mM EDTA solution in phosphate-buffered saline (PBS).

Silencing of ENO1 in PDA cell lines

ENO1 was silenced in PDA cell lines using a short hairpin RNA (shRNA), as previously described [12].

Quantitative PCR

Total RNA was extracted using the RNeasy Mini kit (Qiagen, Milan, Italy) and reverse transcription was performed from 1 μg of total RNA using the iScript cDNA synthesis kit (BioRad, Segrate, MI, Italy), according to the manufacturer's instructions. Quantitative RT-PCR was performed using SYBR Green dye (Life Technologies, Monza, Italy) on a Thermal iCycler (BioRad). PCR reactions were performed in triplicate, and the relative amount of cDNA was calculated by the comparative CT method using β-actin RNA sequences as a control. Data are represented as mean ± SEM (standard error of the mean) of three independent experiments. Oligonucleotide primer sequences for Sybr Green qRT-PCR are in the Supplementary Materials and Methods (Additional file 1: Table S1).

CAT microscopy

Images of PDA cells were acquired by using CAT (confocal-atomic force-total internal reflection fluorescence) microscopy, which is a combination of an advanced scanning probe microscope (Bioscope Catalyst, Bruker Inc. USA), a confocal microscope (LSM 700, Zeiss Germany), and a total internal reflection fluorescence microscope (Laser TIRF 3, Zeiss). These devices were mounted on an inverted microscope (Zeiss ObserverZ1, Zeiss). In this study, CAT was used to evaluate topography on living cell surfaces through AFM and internal organization of fibers into cytoskeleton by confocal LSM.

AFM imaging

For topography acquisition, cells were cultured in plastic Petri dishes (Corning by Sigma-Aldrich), as previously described, and were left to grow until 70–80% confluent. Immediately before performing measurements, cells were washed with PBS solution and the medium was replaced with 5 ml of Lebovitz culture medium (L15, Sigma-Aldrich). Topographic and deflection images were acquired on living cells for up to 2 h in contact mode, as previously described [28]. By using V-shaped silicon nitride cantilevers (MSNL-10 VEECO, USA), probes were chosen on the basis of a low range of elastic constant value (nominal constants from 0.01 to 0.03 $N^{*}nm^{-1}$).

Topographic images were acquired at high resolution (512*512 points*line) on a 50*50 μm^2 area, and were used to calculate the roughness values using the Nanoscope Analysis Software. Prior to calculating the roughness, all images were firstly treated with a second order planefit, then with a second order flattening for deleting every bow and minimizing sample three-dimensionality effects. The roughness was evaluated on 25 areas of 1 μm*1 μm, separately acquired on nuclear regions and cytoplasmatic regions. The mean value and its standard deviation were obtained in this way.

Confocal microscopy

For the confocal microscopy study, shCTRL and shENO1 cells were seeded at 4×10^4 cells/chamber well and were incubated at 37 °C in a humidified 5% CO_2 atmosphere. After 24 h, the medium was removed, and cells were washed three times with PBS. Finally, cells were fixed with 4% paraformaldehyde in PBS for 20 min at room temperature and permeabilized with 0.1%Triton X-100 in PBS for 5 min at room temperature. Cells were incubated with anti-ENO1 mAb at a dilution of 1:1000, followed by an Alexa Fluor 488-conjugated goat anti-mouse IgG (H + L) (Life Technologies) at a dilution of 1:250, each for 1 h at room temperature. For actin staining, Phalloidin–Tetramethylrhodamine B isothiocyanate (TRITC) (Sigma-Aldrich) was used at a dilution of 1:1000 for 30 min at room temperature. Cells were then washed with PBS, and samples were covered with a glass slide using Fluoroshiel with DAPI (Sigma-Aldrich) as a mounting medium. DAPI was used for nucleus staining. Samples were kept at 4 °C in the dark until microscopic examination. Confocal acquisitions were performed by using a 100×, 1.46 numerical aperture oil immersion objective. Laser beams with 405, 488, and 555 nm excitation wavelengths were used to detect the blue fluorescence from DAPI, green fluorescence from AlexaFluo 488, and red fluorescence from TRITC, respectively. Finally, confocal data files were processed using ZEN software (Zeiss).

Adhesion assay

For cell attachment to matrix assays, Vitronectin, Fibronectin, Collagen I, and IV (all from Sigma-Aldrich) were diluted to 10 μg/ml in PBS and adsorbed onto 96-well dishes at 4 °C overnight and then blocked for 2 h at 37 °C with 2% BSA in PBS. Wells were then washed three times with PBS before adding cells. PDA cells, either shCTRL or shENO1, were harvested, centrifuged briefly, then resuspended at a density of 5×10^4 cells/ml in DMEM with 2% FBS. Cells were then seeded onto the coated wells and allowed to adhere for 1 h at 37 °C in the presence or absence of anti-human CD61 (beta3 integrin-Santa Cruz Biotechnology) at a concentration of 10 μg/ml. Non-adherent cells were removed by rinsing with PBS three times. Cells were then fixed with 2% glutaraldehyde (Sigma-Aldrich) in PBS for 20 min and stained with crystal violet (Sigma-Aldrich). Stained cells were washed with PBS, and the dye was solubilized with 10% acetic acid (Sigma-Aldrich) for 5 min on a rocker. Attachment was quantified by measuring the absorbance at 570 nm.

Western blot analyses

PDA cells were harvested, lysed, resolved, and transferred to nitrocellulose membranes, as previously described [29]. Membranes were incubated overnight at 4 °C with the following antibodies (all diluted in TTBS with 5% BSA): mouse anti-human integrin alpha v (1:500, clone L230 made in-house), mouse anti-human FAK (1:1000, made in-house), mouse anti-human integrin alpha 5 and rabbit anti-human Src (both at 1:1000, Santa Cruz Biotechnology by D.B.A. Italia, Segrate, MI, Italy), mouse anti-human integrin beta 1 (1:500, BD Bioscience, Buccinasco, MI, Italy), mouse anti-human RAC1 (1:1000 Millipore by D.B.A Segrate, MI, Italy), rabbit anti-human ERK1-2 (1:500, GeneTex by Prodotti Gianni, Milan, Italy); rabbit anti-human integrin beta 3, rabbit anti-human uPAR, rabbit anti-human phospho ERK1-2, rabbit anti-human Paxillin, rabbit anti-human phospho Paxillin, rabbit anti-human phospho FAK, rabbit anti-human p38MAPK, rabbit anti-human phospho p38MAPK and rabbit anti-human phospho Src (all 1:1000, Cell Signaling Technology by EuroClone, Pero, MI, Italy).The mouse anti-human ENO1 (clone 72/1 [30]) and rabbit anti-human beta-actin antibody (Sigma Aldrich, Milan, Italy), both at a dilution of 1:2000 in TTBS, were incubated for 1 h at room temperature. Membranes were then washed with TTBS and probed for 1 h at room temperature with an HRP-conjugated anti-mouse IgG (Santa Cruz Biotechnology) or an HRP-conjugated goat anti-rabbit IgG secondary antibody (Sigma Aldrich), accordingly, at a dilution of 1:2000. Immunodetection was carried out by enhanced chemiluminescence using ECL PLUS (GE Healthcare).

Flow cytometric analysis

A total of 1×10^5 cells were incubated with primary antibody: mouse IgG1 anti-human CD51/61 (alpha v/beta 3 integrin, BD, Milan, Italy), mouse IgG2a anti-human CD41/61 (alpha IIb/beta 3 integrin, BioLegend by Campoverde, Milan, Italy), mouse IgG1 anti-human beta1 integrin (Santa Cruz Biotechnology) or an isotype-matched negative control IgG1 or IgG2a antibody (Ab) accordingly (Dako, Milan, Italy), all at doses of 10 μg/ml for 30 min at 4 °C. After incubation with primary Abs, cells were then incubated with a secondary APC goat anti-mouse IgG Ab (BioLegend) for 20 min at 4 °C. Following this, cells were resuspended in PBS,

acquired with a BD Accuri C6 Flow Cytometer (BD) and analyzed using FlowJo 7.5 software.

RAC GTPase activation assay

To perform the RAC assay, cells were washed twice on ice with PBS and then lysed in 50 mM Tris, 150 mM NaCl, 1% NP40, 10% glycerol, 10 Mm $MgCl_2$, and 10 μg/ml each of leupeptin, pepstatin, and aprotinin. Equal amounts of cell extracts were incubated at 4 °C for 1 h with glutathione-coupled Sepharose 4B beads (GE Healthcare) bound to recombinant GST-PAK CRIB domain. Bound proteins were eluted in 2× Laemmli-reducing sample buffer and immunoblotted for RAC1.

ROS measurement

PDA cells were cultured for 24 h in presence or absence of 10 μg/ml anti-uPAR antibody (clone 3C6, Sigma-Aldrich). ROS measurement was performed as previously described [19].

Analysis of SA-β-galactosidase activity

For the senescence assay on extracellular matrices, vitronectin, and collagen I (from Sigma-Aldrich) were coated onto 96-well dishes, as described above. 3×10^4 cells/well PDA cells, plus either shCTRL or shENO1, were plated onto coated wells for 72 h in presence or absence of 10 μg/ml anti-uPAR antibody (clone 3C6, Sigma-Aldrich). Images were taken at microscope with ×10 objective. The SA-β-galactosidase activity was analyzed as previously described [19].

Apoptosis assay

PDA cells were cultured for 48 h in presence or absence of 10 μg/ml anti-uPAR antibody (clone 3C6, Sigma-Aldrich), and apoptotic cells were analyzed using Annexin V Apoptosis Detection Kits (eBioscience by Prodotti Gianni, Milan, Italy).

Scratch wound healing assay

PDA cells (1×10^5), plus either shCTRL or shENO1, were seeded into each well of ibidi Culture-Inserts (Ibidi by Giemme, Milan, Italy) and grown to confluence. After 12 h, a cell-free gap of about 500 μm was created after removing the Culture-Insert, and cells were washed twice with serum-free medium to remove any floating cells. Cells which had migrated into the wounded area or protruded from the border of the wound were visualized and photographed under an inverted microscope at each time point over a period of 24 h.

In vitro chemo-invasion assay

The invasive potential of the PDA cell lines was determined using a modified two-chamber invasion assay, as previously described [12].

In vivo experiments

ShCTRL or shENO1 CFPAC-1 cell lines were harvested, washed three times, and resuspended in PBS. NOD-SCID IL2Rgamma^{null} (NSG) mice (provided by the animal facility of the Molecular Biotechnology Center, University of Turin, Italy) were injected into the tail vein (i.v.) with 1×10^5 PDA cells (in 0.1 ml PBS). After 28 days, mice were euthanized, necropsied, and examined for the presence of tumor masses. For the in vivo experiments, five mice were used in each group.

Tissue samples and histopathology

Tumor masses and main organs of mice were fixed in 4% (v/v) neutral-buffered formalin (Sigma-Aldrich) overnight, transferred to 70% ethanol, followed by paraffin-embedding. For histological analysis, 5-μm formalin-fixed paraffin-embedded tissue sections were cut and stained with hematoxylin-eosin. Tumor/normal tissue ratios were evaluated with ImageJ software.

Statistical analysis

The Student's *t* test (GraphPad Prism 5 Software, San Diego, CA) was used to evaluate statistically significant differences in in vitro and in vivo tests. Values were expressed as mean ± SEM.

Results

Altered expression of adhesion and cytoskeletal proteins in shENO1 PDA cells

The CFPAC-1 PDA cell line was silenced with a lentivirus that delivered a short hairpin RNA targeting ENO1 3'UTR (shENO1), or a scrambled shRNA (shCTRL) as a control [12]. Previous LC-MS/MS semi-quantitative proteomic analysis using LTQ-Orbitrap on shENO1 CFPAC-1 cells showed significant alterations in the expression of 17 proteins involved in cell adhesion and cytoskeleton organization [19]. Four of these proteins [actin related protein 2/3 complex subunit 4 isoform a (ARPC4), capping protein actin filament muscle Z-line alpha 2 (CAPZA2), secreted phosphoprotein 1 isoform a (SPP1 also named Osteopontin), and breast cancer anti-estrogen resistance 1 (BCAR1 also named p130cas)] were upregulated, and 13 [AHNAK nucleoprotein isoform 1 (AHNAK), anterior gradient protein 2 (AGR2), catenin, delta 1 isoform 1ABC (CTNND1), hypothetical protein LOC64855 isoform 2 (MINERVA), Galectin 3 (LGALS3), catenin alpha 1 (CTNNA1), integrin alpha v isoform 1 precursor (ITGAV), Galectin 4 (LGALS4), Golgi apparatus protein 1 isoform 1 (GLG1), mucin 5AC (MUC5AC), serine or cysteine proteinase inhibitor clade B ovalbumin member 5 (SERPINb5), PDZ and LIM domain 1 (PDLIM1), and cysteine-rich protein 1 intestinal (CRIP1)] were downregulated [19].

Herein, we studied whether the previously observed protein modulation also occurred at the RNA level. Quantitative real-time PCR analysis in shENO1 CFPAC-1 cells indicated that, of the four upregulated proteins, only BCAR1 (p130cas) showed a significant increase in mRNA expression, while the other three proteins had unchanged mRNA expression (Fig. 1). Among the 13 proteins that were downregulated after ENO1 silencing, the expression of mRNA was significantly reduced in nine of them, namely, AGR2, MINERVA, LGALS3, CTNNA1, ITGAV, LGALS4, SERPINSb5, PDLM1, and CRIP1. The mRNA expression was unchanged in three of the remaining four proteins (AHNAH, CTNND1, and GLG1) or was upregulated (MUC5AC) (Fig. 1).

Morphological and nanostructural modifications in shENO1 PDA cells

Semi-quantitative proteomic and mRNA expression analysis of PDA cells concordantly revealed downregulation of nine cell-ECM adhesion-related proteins after ENO1 silencing (Ref. [19] and Fig. 1), and we therefore investigated the impact of ENO1 silencing on the actin cytoskeleton organization and morphology, by confocal analysis. The majority of ENO1 protein (green fluorescence) in shCTRL cells is localized to the cytoplasm (Fig. 2a left panels), while after ENO1 silencing, green fluorescence was lost, as expected (Fig. 2a right panels). Analyzing actin organization (red fluorescence) showed a loss of fluorescence close to the cell membrane in shENO1 cells, with a concomitant increase of cytoplasmic actin with a perinuclear accumulation. Additional experiments performed with lower cell confluence and with images taken at the level of the apical surface showed that shCTRL cells possess well-defined actin filaments (red fluorescence Fig. 2b upper panel), while shENO1 cells showed a loss of cytoskeleton organization and orientation (red fluorescence Fig. 2b lower panel). These confocal microscopy results were then combined with cell surface analysis in atomic force microscopy (AFM). Three-dimensional AFM highlighted that cell-cell junctions were impaired in shENO1 cells (Fig. 2c lower panels) compared to shCTRL cells (Fig. 2c upper panels). The 2-D AFM analysis of the cell surface showed that shCTRL cells had a smooth and intact cell surface and cell membrane ultrastructural components were uniformly distributed (Fig. 2d upper panels). By contrast, shENO1 cells displayed an altered surface morphology with more evident membrane ultrastructure (Fig. 2d lower panels). Quantification of the nanostructural parameters revealed an increase in the cell surface roughness (Fig. 2e) of shENO1 cells, in line with the modification of the expression of proteins involved in the remodeling of the cytoskeleton and adhesion (Ref. [19] and Fig. 1).

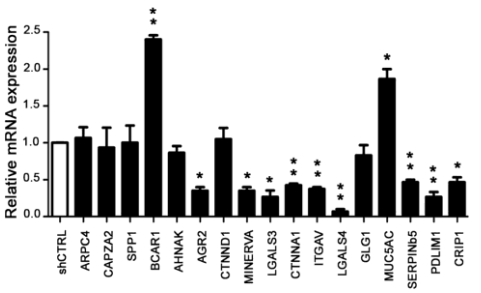

Fig. 1 mRNA expression of modulated proteins in CFPAC-1 shENO1 cells. Using real-time PCR, mRNA expression of different proteins was investigated in CFPAC-1 shENO1 cells. Values are expressed as relative expression compared to control cells. A representative of three independent experiments is shown. Data are mean ± SEM. $^{*}p < 0.05$, $^{**}p < 0.01$, $^{***}p < 0.001$ relative to control cells

shENO1 PDA cells display reduced adhesion to fibronectin and collagens and increased adhesion to vitronectin

As we showed that the proteins involved in ECM cell adhesion were downregulated in shENO1 cells, we evaluated the adhesive ability of shCTRL or shENO1 PDA cells on fibronectin (FN), collagen I (Col-I), collagen IV (Col-IV), and vitronectin (VN). Compared to shCTRL cells, shENO1 PDA cells (CFPAC-1, PT45 and T3M4) showed a significantly lower adhesion to FN, Col-I, and Col-IV, and a greater adhesion to VN (Fig. 3 and Additional file 1: Figure S1a–b). We then evaluated the expression levels of alpha 5/beta 1 and alpha v/beta 3 complexes, the integrins most involved in binding on these extracellular matrices, in shCTRL and shENO1 cells. Alpha 5 integrin was strongly upregulated by shENO1, both at the mRNA (Fig. 4a) and protein levels (Fig. 4b), while the mRNA, protein, and cell surface levels of beta 1 were unchanged (Fig. 4a–c). mRNA and protein levels of alpha v and beta 3 integrins were decreased by shENO1 (Fig. 1, Fig. 4a and b, respectively). Consistently, the surface expression of the complex alpha v/beta 3, evaluated by a specific Ab that recognized the whole complex, was decreased on shENO1 cells compared to control cells (Fig. 4c). To identify the mechanism involved in the increased VN adhesion mediated by ENO1 silencing, we also analyzed the expression of the other VN receptor alpha IIb/beta 3 integrin. However, no surface expression of this complex was detected in either shENO1 or control cells (Fig. 4c). To understand the involvement of beta 3 integrin in the adhesion to VN, a specific anti-beta 3 Ab was employed. In beta 3-expressing shCTRL cells, the anti-beta 3 Ab significantly decreased the adhesion to VN, while in shENO1 cells that did not express beta 3, it had no effect (Fig. 4d). The increase in adhesion to VN in shENO1

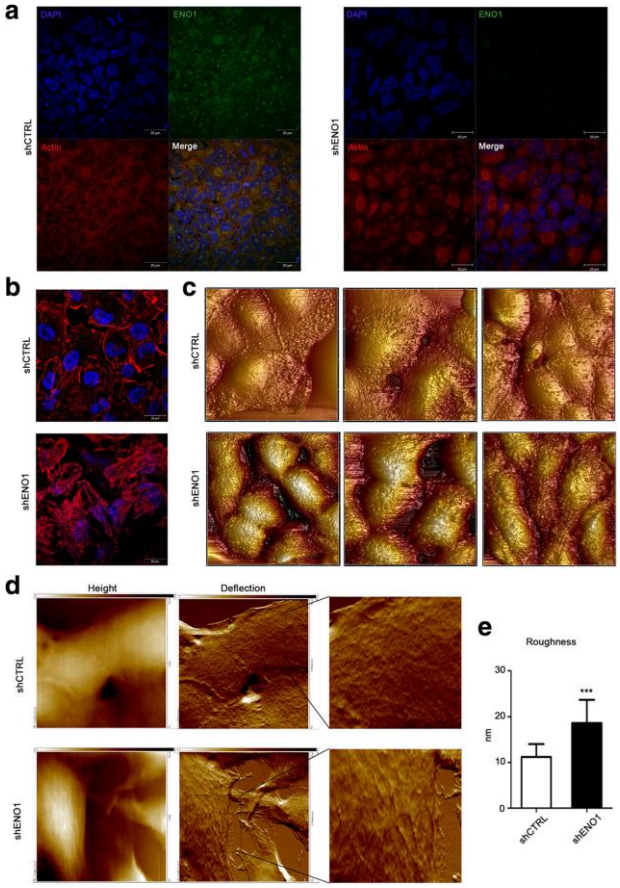

Fig. 2 Morphological analysis and roughness measurements of shENO1 cells. **a** shCTRL and shENO1 CFPAC-1 cells stained for nuclei (DAPI, *blue fluorescence*), actin (Phalloidin-TRITC, *red fluorescence*), and ENO1 (anti-ENO1 mAb followed by anti-mouse FITC, *green fluorescence*). Panels represent images taken at the level of nuclei. **b** Images taken at the level of the cell surface. **c** Three-dimensional topographic images of shCTRL and shENO1 CFPAC-1 performed through the AFM technique (three representative images for each group) (scan size: 50 μm; Z scale 4 μm). **d** Topographic images of shCTRL and shENO1 CFPAC-1 performed through the AFM technique. *Left panels*: height parameter; *central panels*: deflection parameter; *right panels*: magnification of deflection panel. **e** Histograms represent roughness analysis. A representative of three independent experiments is shown. Data are mean ± SEM. ***$p < 0.001$ relative to control cells

cells with a concomitantly reduced expression of the major integrins usually involved in its binding suggested the involvement of other receptors. As uPAR binds VN through the Somatomedin B (SMB) domain [31, 32], its expression in shENO1 cells was evaluated. Quantitative PCR (Fig. 4a) and western blot (Fig. 4b) analysis showed that uPAR expression was markedly increased in shENO1 cells. These data indicated that the lack of ENO1 caused a decrease in the expression of the main integrins affecting cell adhesion. However, shENO1 cells maintained the ability to bind VN by upregulating uPAR.

Analysis of signaling pathways in shENO1 PDA cells

It is known that uPAR, despite lacking a cytosolic domain, activates an intracellular signaling pathway through the interaction with beta 1 and beta 3 integrins, independently of their interaction with VN [33–35]. As beta 1 expression was unchanged at the cell surface of shENO1 cells (Fig. 4 b–c), and it can trigger activation of the ERK1-2/RAC pathway [33, 36], the effect of ENO1 silencing on this pathway was analyzed. Western blot analysis revealed a strong increase in activation of both ERK1-2 (Fig. 5a) and RAC (Fig. 5b)

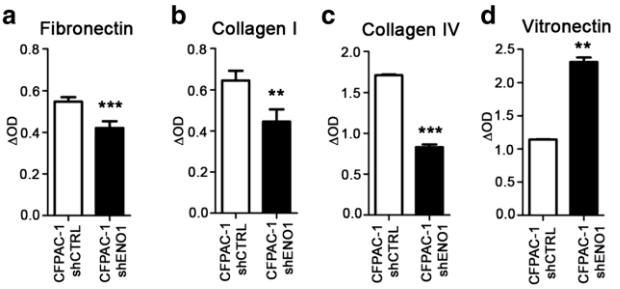

Fig. 3 Adhesion ability of ENO1-silenced PDA cells. Adhesive potential of shENO1 and control CFPAC-1 cells was evaluated by culturing cells for 1 h on fibronectin (**a**), collagen I (**b**), collagen IV (**c**), and vitronectin (**d**). Adherent cells were fixed with 2% glutaraldehyde in PBS and visualized by staining with crystal violet. For quantitative analysis, cells were treated with 10% acetic acid and elutes were read with a microplate reader at a wavelength of 570 nm. Results are expressed as ΔOD (optical density) units = (OD substrate adherent cells)–(OD plastic adherent cells). A representative of three independent experiments is shown. Data are mean ± SEM. $^{**}p < 0.01$, $^{***}p < 0.001$ relative to control cells

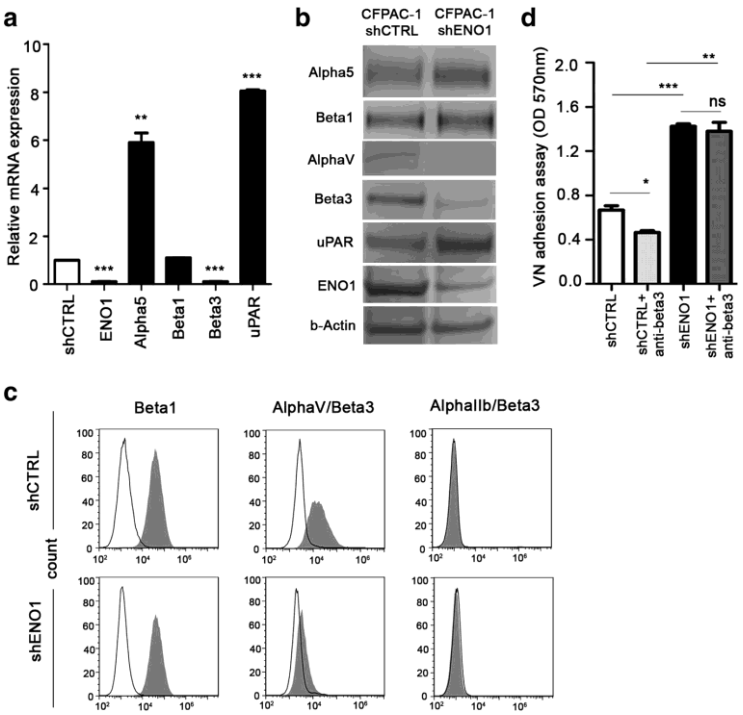

Fig. 4 ENO1-silencing modulates ECM-receptor expression. **a** Using quantitative PCR, mRNA coding for different proteins was investigated in shENO1 CFPAC-1 cells. Values are expressed as relative expression compared to control cells. **b** Western blot analysis was carried out to investigate alpha 5, beta 1, alpha v, beta 3, and uPAR expression on total lysates of shCTRL and shENO1 cells. **c** To determine surface expression of integrins, shENO1, or shCTRL cells were incubated with primary antibodies (*gray peak*) against beta 1, alpha v/beta 3, alpha IIb/beta 3, and or isotype-matched control antibody (*empty peak*) and analyzed by flow cytometry. **d** The adhesion ability of shENO1 and shCTRL cells on vitronectin was evaluated in the presence of anti-beta 3 Ab. Adherent cells were fixed with 2% glutaraldehyde in PBS and visualized by staining with crystal violet. For quantitative analysis, cells were treated with 10% acetic acid and elutes were read with a microplate reader at a wavelength of 570 nm. Results are expressed as OD, optical density units. A representative of three independent experiments is shown. Data are mean ± SEM. $^{*}p < 0.05$, $^{**}p < 0.01$, $^{***}p < 0.001$ relative to control cells

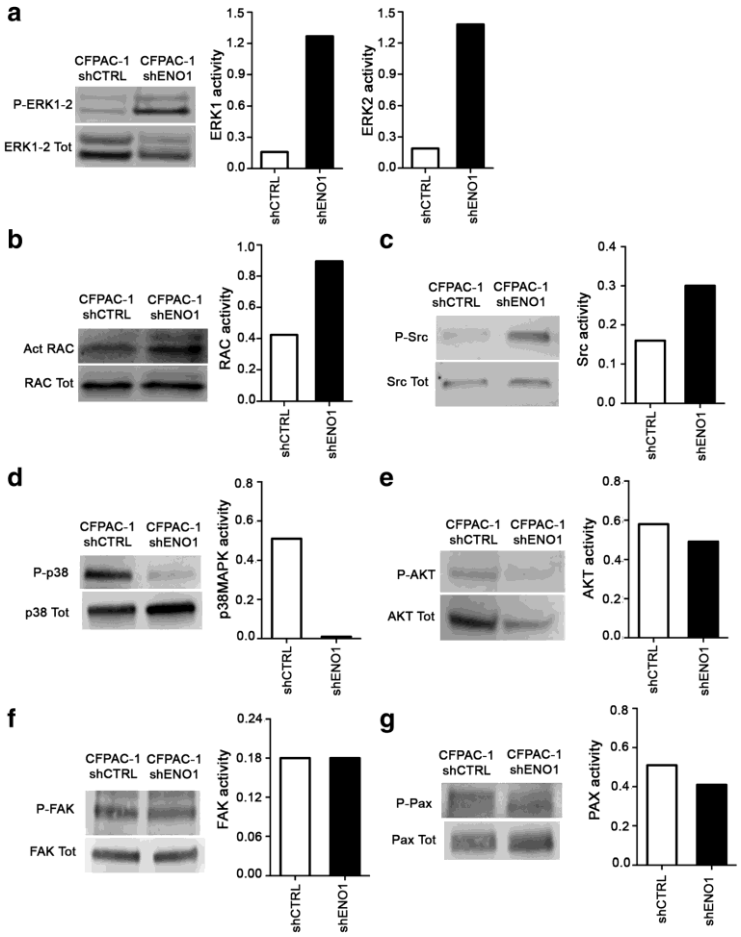

Fig. 5 Analysis of uPAR/integrins pathways. Western blot analysis on total lysates of shENO1 and shCTRL CFPAC-1 cells was carried out to investigate levels of (**a**) phospho- and total ERK1-2, (**b**) activated and total RAC, (**c**) phospho- and total Src, (**d**) phospho- and total p38MAPK, (**e**) phospho- and total AKT, (**f**) phospho- and total FAK and (**g**) phospho- and total Paxillin. Histograms represent the ratios between the phosphorylated and total form of each protein. A representative of three independent experiments is shown

in shENO1 cells compared to control cells. To better clarify the effect of ENO1 silencing on integrin-dependent signaling cascades, other key proteins such as the Src, p38MAPK, AKT, FAK, and Paxillin were evaluated. In ENO1-silenced CFPAC-1 cells, the phosphorylation of Src was increased (Fig. 5c) whereas phosphorylation of p38MAPK were downregulated (Fig. 5d). No significant difference was observed in AKT, FAK, and Paxillin (Pax) phosphorylation (Fig. 5e–g). Thus, ENO1 silencing increases Src activation supporting downstream signals via ERK1-2/RAC signaling.

uPAR blockade in shENO1 cells causes a reduction of ROS and inhibition of cell senescence

Our previous work demonstrated that ENO1 silencing increased reactive oxygen species (ROS) mainly generated through the sorbitol and NADPH oxidase pathways, which affect cancer cell growth and induce senescence [19]. As ERK1-2/RAC activation leads to an increase of ROS and senescence [37], we investigated if uPAR is also involved in these phenomena. ROS were analyzed by measuring intracellular 5-(and-6)-chloromethyl- 2′,7′-dichorodihydro-fluorescein diacetate (DCFDA) fluorescence. Treatment with the anti-uPAR antibody blocked

the binding of uPAR to beta 1 integrin and specifically reduced the production of ROS in shENO1 cells, but not in shCTRL control cells (Fig. 6a).

As uPAR directly binds vitronectin, we observed that the anti-uPAR blocking antibody inhibited senescence of shENO1 cells plated on vitronectin (Fig. 6b upper panel), but not that of shENO1 cells plated on collagen I (Fig. 6b lower panel) suggesting that the senescence can be induced by VN/uPAR downstream effects. The anti-uPAR blocking antibody slightly increased the apoptosis of shENO1 PDA cells (Annexin V positive cells Fig. 6c).

ENO1 silencing impairs in vitro and in vivo PDA cell migration and invasion

Considering the cytoskeleton and integrin pathway alterations in shENO1 cells, we investigated their migration and invasiveness by wound-healing scratch and Matrigel cell invasion assays, respectively. While control cells resulted in more than 60–80% of the wound being closed at 15 h, and 100% after 24 h, there was no wound-healing evident on the shENO1 cell lines (CFPAC-1, PT45, and T3M4), even after 24 h (Fig. 7a and Additional file 1: Figure S1c). Cell invasion through Matrigel also demonstrated a significantly lower ability of shENO1 cell lines to invade compared to control cells (Fig. 7b and Additional file 1: Figure S1d).

To assess the effect of ENO1 silencing in metastasis formation in vivo, shENO1 or shCTRL CFPAC-1 cells were injected intravenously into NSG mice. After 28 days following injection, mice were sacrificed and lungs were excised and checked for the presence of metastasis. Post-mortem observations confirmed that injection with shENO1 cells resulted in a significant reduction of the tumor area in the lungs compared to mice injected with control cells (Fig. 7c). These data confirmed that changes in the adhesion, migration, and invasion ability observed in vitro in shENO1 cells markedly compromised their ability to spread and form

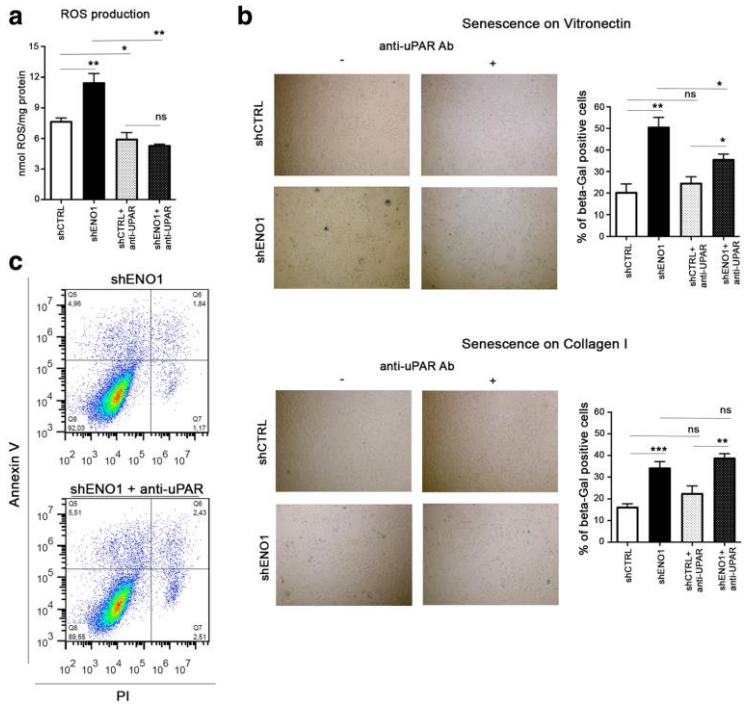

Fig. 6 Analysis of reactive oxygen species (ROS) production, senescence, and apoptosis in shENO1 cells lines after anti-uPAR Ab treatment. **a** Analysis of ROS concentration measured by the DCFDA-AM assay was evaluated in shENO cells and control cells in the presence or absence of anti-uPAR antibody. **b** Senescence-associated β-galactosidase staining. Senescent shENO and shCTRL cells were colored blue upon X-gal staining at pH 6, with or without treatment with anti-uPAR antibody. One representative out of three independent experiments is shown. The graph represents the percentage of X-Gal positive cells with respect to the total number of cells. **c** Dot plot of shENO1 cells apoptotic cells in the presence or absence of anti-uPAR antibody. Apoptotic cells were evaluated as early apoptotic (AnxV pos/ PI negative) + late apoptotic cells (AnxV pos/ PI positive). Data are mean ± SEM. $*p < 0.05$, $**p < 0.01$, $***p < 0.001$ relative to control cells

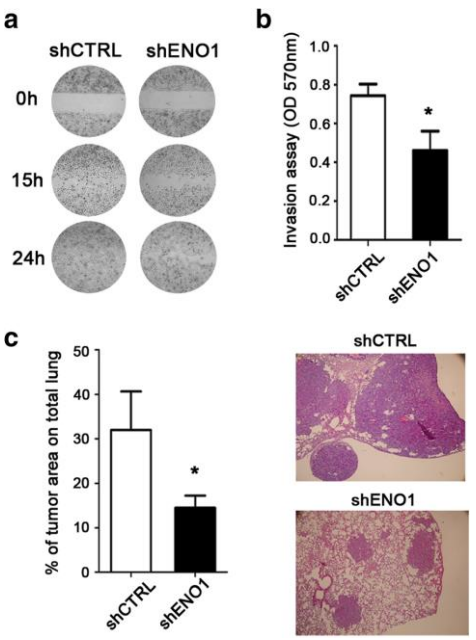

Fig. 7 ENO1 silencing affects in vitro and in vivo cell migration and invasion. **a** Migration ability was evaluated in terms of capacity to close the wound of shENO1 CFPAC-1 cells compared to shCTRL control cells. Representative images are shown for each condition. **b** Invasive potential of shENO1 and shCTRL cells were tested through a Matrigel invasion assay, after 48 h of culture. For quantitative analysis, invasive cells were fixed, stained with crystal violet, treated with acetic acid and elutes were read at a wavelength of 570 nm. Results are expressed as OD. **c** Lung metastatic area was evaluated after 28 days from i.v. injection of shCTRL or shENO1 CFPAC-1 cells in the tail vein of NSG mice. The histogram represents the percentage of metastatic area compared to the total lung (*left panel*). Representative images of the lung are shown for each group of mice (*right panels*). For the in vivo experiments, five mice per group were used. A representative of three independent experiments is shown. Data are mean ± SEM. *$p < 0.05$ relative to control cells

metastasis in vivo, demonstrating that ENO1 may exert a crucial role in invasion and metastasis.

Discussion

In our previous report, we demonstrated that ENO1 cell surface expression is important for plasminogen-dependent invasion, and that targeting of ENO1 with a monoclonal antibody inhibits the invasiveness of pancreatic cancer cells [12]. These data correlate well with previous observations in follicular thyroid carcinoma [38], glioma [13], non-small cell lung cancer [14], and endometrial cancer [15], again supporting the emerging role of ENO1 as a promising target for cancer treatment. However, although blocking surface ENO1 impaired the ability of PDA cells to migrate in vitro and form more metastasis in vivo [12], little is known about the role of ENO1 in regulating cell-cell and cell-matrix contacts. Proteomic analysis of silenced ENO1 in PDA cells revealed a profound modification in their metabolism, which was associated with an increase of oxidative stress and senescence [19]. In addition, although silenced PDA cells also displayed alterations in many molecules involved in adhesion, as well as cytoskeletal proteins, this study aimed to investigate more thoroughly the role of ENO1—a multifunctional protein involved in cell-matrix adhesion, motility and migration, invasion and metastasis in vivo, as well as in survival and senescence.

By employing a combination of confocal and AFM-assisted nanostructural approaches, we investigated the phenotype and morphology of the PDA cells in the presence and absence of ENO1. Profound morphological changes in shENO1 PDA cells were observed, due to the modification of the cytoskeleton organization. Control cells exhibited smooth topography, while the shENO1 cells displayed a rough surface. The increase in surface roughness was consistent with the topographical changes observed with the AFM images. Cell nanostructural parameters, such as elasticity or roughness, may reflect a reorganization of the actin cytoskeleton, which in turn affects cell growth, morphology, cell-cell interactions, cytoskeleton organization, and interactions with the ECM [39]. It is known that ENO1 knockdown induces a dramatic increase of the sensitivity to microtubule-targeted drugs (e.g., taxanes and vincristine) in different tumor cell lines, due to ENO1-tubulin interactions [40], suggesting a role for ENO1 in modulating the cytoskeletal network. Consistently, we demonstrated that ENO1 critically contributed to the organization of the actin cytoskeleton. Indeed, in control cells, actin was organized into filaments that were mostly distributed close to the cell surface, while in shENO1 cells, the organization of the actin filaments was lacking, and actin prevalently relocalized close to the nuclei. This actin modification suggested a profound reorganization of cytoskeleton regulatory proteins, suggesting that ENO1 silencing reduced the ability of PDA cells to adhere to ECM and migrate. This is in agreement with our previous proteomic analysis, which showed that ENO1 silencing downregulated many proteins involved in motility pathways [19].

Consistent with the proteomic data, shENO1 PDA cells showed a decreased adhesion to FN and Cols, and a reduction in migration and invasion. Of the proteins downregulated after ENO1-silencing, we highlight alpha v/beta 3 integrin, a crucial protein involved in spreading and metastasis, the increased expression of which correlates with a poor clinical outcome in PDA [21–23]. FN is recognized by either alpha 5/beta 1 or alpha v/beta 3 complexes, which cooperate in promoting cellular attachment and spreading [41]. Our data show that ENO silencing

downregulates alpha v/beta 3 but increases alpha 5/beta 1 expression. Considering that alpha 5/beta 1 determines adhesion strength through its binding to FN, while alpha v/beta 3 mediates reinforcement of the adhesion through its connection with the actin cytoskeleton [42, 43], we speculate that in shENO1 cells, while the alpha 5/beta 1 complex begins the adhesion process, there is a reduced adherence to FN due to the lack of reinforcement signals controlled by the alpha v/beta 3 complex. Surprisingly, ENO1 silencing is also associated with an increase of adhesion to VN. In cancer, VN interacts with different members of the integrin family (alpha v/beta 1, alpha v/beta 3, alpha v/beta 5, and alpha IIb/beta 3) through the RGD motif [44, 45]. As alpha v and beta 3 subunits were shown to be downregulated in shENO1 cells, none of the abovementioned complexes can be considered to be responsible for the increased adhesion of shENO1 cells to VN. This suggests that a non-integrin receptor is involved in the binding of VN. As uPAR binds VN through a different binding site from that of integrins [34, 46, 47], we hypothesized that uPAR plays a major role in VN binding in shENO1 cells.

uPAR expression is elevated in many human cancers, in which it frequently indicates poor prognosis [48]. uPAR regulates proteolysis by binding to the extracellular protease urokinase-type plasminogen activator (uPA) [49] and also activates many intracellular signaling pathways [50]. Exploiting the above functions, uPAR regulates important functions such as cell migration, proliferation, and survival, and thus makes it an attractive therapeutic target in various different types of cancer [36]. Here, we observed the upregulation of uPAR in shENO1 cells, which have a reduced ability to invade and form metastases, and an increased senescence, suggesting that uPAR may contribute in a different way in this setting. uPAR, lacks a cytosolic domain, and thus signals through its association with integrins, which can also be independent of direct integrin/matrix interactions, in a ligand-independent manner, to promote migration [34]. The major downstream uPAR/integrin signaling (especially beta 1 and beta 3) involves the activation of Src, PI3K/AKT, and MEK/ERK1-2 pathways [50]. In shENO1 PDA cells we observed the activation of Src. The effect of increased Src activity in cells is pleiotropic [51]. In particular, cells with activated Src are characterized by a loss of actin reorganization and reduced cell-ECM adhesion [51], phenomena that perfectly match our observations.

In NSCLC, the downregulation of ENO1 decreased proliferation, migration, and invasion through a FAK-mediated PI3K/AKT pathway [14]. Clustering of integrins activates FAK results in the formation of a complex with Src, and increased phosphorylation of the targets of the FAK-Src complex, such as paxillin [52]. In pancreatic cancer we did not observe an altered phosphorylation of FAK and Paxillin as well as AKT. Instead, in our study, we observed that ENO1 silencing leads to uPAR overexpression that, in turn, triggers Src and ERK1-2 activation, concomitantly with an inactivation of p38MAPK. The activation of ERK1-2 can promote senescence, in accordance with Cagnol et al. [53]. Conversely, activation of p38MAPK can promote apoptosis in cancer cells, including pancreatic cancer [54]. We observed that shENO1 cells, due to the decrease in phosphorylation of p38MAPK concurrently with ERK1-2 activation, slightly inhibit PDA cell apoptosis and favor senescence, in line with our previously reported results [19].

ERK1-2 activation, due to the uPAR-beta 1 integrin interaction is required for RAC activation [36, 55–59]. RAC is a downstream signaling molecule of beta 1 and contributes to the regulation of actin cytoskeleton dynamics, adhesion, and migration and induces cellular reactive oxygen species (ROS) through NAPDH oxidase activation [37]. Expression of the constitutively active RAC1 mutant induces cell cycle arrest, apoptosis, and senescence [37]. We have previously demonstrated that ENO1 silencing induces ROS, mainly through the sorbitol and NADPH oxidase pathway and senescence [19]. Here we demonstrate that, in the absence of ENO1, the upregulation of uPAR leads to an increased activation of the ERK1-2/RAC pathway, which contributes to ROS generation and induces PDA cell senescence, rather than an invasive phenotype. Moreover, the anti-uPAR antibody prevented ROS production and senescence although PDA cell apoptosis was only slightly promoted. These results suggest that a combinatory strategy to simultaneously target ENO1 and uPAR could be effective to inhibit PDA tumor progression and invasion.

Conclusions

Our study has shown, by in vitro and in vivo experiments, that ENO1 silencing can inhibit adhesion, invasion, and metastasis in PDA cells, due to changes in actin cytoskeleton organization, adhesion proteins, and integrin profile expression. ENO1 silencing had a major impact on the alpha v/beta 3 integrin, which accounts for the inability of ENO1-silenced cells to adhere to the ECM matrix and promote PDA invasion. We have reported that, in the absence of ENO1, the upregulation of uPAR does not promote an increase of migration or invasion. These data show that there is an interplay of ENO1 with integrins and uPAR, which critically controls PDA progression.

Additional file

Additional file 1: Table S1. Oligonucleotide primer sequences for SybrGreen qRT-PCR. **Figure S1a–d** Adhesion, migration and invasion ability of PT45 and T3M4 shENO1 PDA cells. Adhesive potential of shENO1 PT45 (a) and shENO1 T3M4 (b) compared to relative shCTRL control cells was evaluated by culturing cells for 1 h on FN, Col-I, Col-IV and VN. Adherent cells were fixed with 2% glutaraldehyde in PBS and visualized by staining with crystal violet. For quantitative analysis, cells

were treated with 10% acetic acid and elutes were read with a microplate reader at a wavelength of 570 nm. Results are expressed as Δ OD (Optical Density) units = (OD substrate adherent cells) − (OD plastic adherent cells). (c) Migration ability was evaluated in terms of ability to close the wound with shENO1 PT45 and shENO1 T3M4 cells compared to shCTRL control cells. Representative images are shown for each condition. (d) Invasive potential of shENO1 PT45 and shENO1 T3M4 were tested by a Matrigel invasion assay, after 48 h of culture. For quantitative analysis, invasive cells were fixed, stained with crystal violet, treated with acetic acid and elutes were read at a wavelength of 570 nm. Data are mean ± SEM of at least three independent experiments. *p < 0.05, **p < 0.01, ***p < 0.001 (DOCX 326 kb)

Abbreviations
Ab: Antibody; AFM: Atomic force microscopy; AGR2: Anterior gradient protein 2; AHNAK: AHNAK nucleoprotein isoform 1; AnxV: Annexin V; APC: Allophycocyanin; ARPC4: Actin related protein 2/3 complex subunit 4 isoform a; ATP: Adenosine triphosphate; BCAR1: Breast cancer anti-estrogen resistance 1; CAPZA2: Capping protein actin filament muscle Z-line alpha 2; CAT: Confocal–atomic force microscopy–total internal reflection fluorescence; Col: Collagen; CRIP1: Cysteine-rich protein 1 intestinal; CTNNA1: Catenin alpha 1; CTNND1: Catenin, delta 1 isoform 1ABC; ECM: Extracellular matrix; ENO1: Alpha-enolase; ERK1-2: Extracellular signal–regulated kinases 1–2; FAK: Focal adhesion kinases; FN: Fibronectin; GLG1: Golgi apparatus protein 1 isoform 1; GST: Glutathione S-transferase; HRP: Horseradish peroxidase; IgG: Immunoglobulin G; ITGAV: Integrin alpha v isoform 1 precursor; LC-MS/MS: Liquid chromatography-mass/mass spectrometry; LGALS3: Galectin 3; LGALS4: Galectin 4; MAPK: Mitogen-activated protein kinase; MINERVA: Hypothetical protein LOC64855 isoform 2; MUC5AC: Mucin 5AC; NSG: NOD/SCID gamma; Pax: Paxillin; PBS: Phosphate-buffered saline; PCR: Polymerase chain reaction; PDA: Pancreatic ductal adenocarcinoma; PDLIM1: PDZ and LIM domain 1; PI: Propidium iodide; RGD: Arg-Gly-Asp; ROS: Reactive oxygen species; SA-beta-Gal: Senescence associated beta-Galactosidase; SEM: Standard error of the mean; SERPINb5: Serine or cysteine proteinase inhibitor clade B ovalbumin member 5; shCTRL: Control cell line; shENO1: ENO1-silenced cell line; shRNA: Short hairpin RNA; SMB: Somatomedin B; SPP1: Secreted phosphoprotein 1 isoform a; TRITC: Tetramethylrhodamine B isothiocyanate; uPAR: Urokinase plasminogen activator receptor; VN: Vitronectin

Acknowledgements
We thank Dr. Radhika Srinivasan for helpful discussion and critical reading of the manuscript, and Roberta Curto for the in vivo experiments.

Funding
This study was supported by the Associazione Italiana Ricerca sul Cancro (AIRC 5 x mille no. 12182 and IG no. 15257); University of Turin-Progetti Ateneo 2014-Compagnia di San Paolo (PC-METAIMMUNOTHER to FN and PANTHER to PC), Italian Ministry of Health, Progetti Ricerca Finalizzata (RF-2013-02354892), Fondazione Ricerca Molinette Onlus and Fondazione Nadia Valsecchi; MP and MSC are recipients of fellowships funded by the Fondazione Ursula e Giorgio Cytron. PD is a recipient of PI AIRC IG 2014N.15399. SL gratefully acknowledges the financial support of the REA research grant no. PITN-GA-2012-316549 (IT LIVER) from the People Programme (Marie Curie Actions) of the European Union's Seventh Framework Programme (FP7/2007-2013). Financial support from MAAT-Molecular NAnotechnology for HeAlth and EnvironmenT Project (number PON02_00563_3316357–CUP B31C12001230005) is also gratefully acknowledged.

Availability of data and materials
All data generated or analyzed during this study are included in this published article [and its Additional file 1].

Authors' contributions
MP designed and performed most of the in vitro and in vivo experiments, analyzed results, generated figures and tables, and wrote the manuscript. SB performed in vitro and in vivo experiments, analyzed data, and wrote the manuscript. MSC, SFB, and SBul performed in vitro experiments and analyzed data. MCap performed proteomics experiments and analyzed data. MCas and SL designed and performed experiments with the CAT microscope and analyzed data. JC performed pull down and immunoblot experiments for activated RAC. PD, FDM, and PN provided reagents, discussed experimental design for the integrin studies and analyzed data. CR performed ROS measurement experiments and analyzed data. PC designed experiments, analyzed data, and revised the manuscript. FN designed experiments, supervised the study, analyzed data, and wrote the manuscript. All authors read and approved the final manuscript.

Competing interests
The authors declare that they have no competing interests.

Consent for publication
Not applicable.

Ethics approval
No human data were collected. Animal data were collected after Ethics approval. Committee's name: Ministero della Salute, Direzione Generale della Sanità animale e dei farmaci veterinari, Italia. Reference no: 378/2015-PR. Date: 15/05/2015.

Author details
[1]Department of Molecular Biotechnology and Health Sciences, University of Turin, Turin, Italy. [2]Center for Experimental Research and Medical Studies (CeRMS), Azienda Universitaria Ospedaliera Città della Salute e della Scienza di Torino, Via Santena 5, 10126 Turin, Italy. [3]Dipartimento di Matematica e Fisica "Ennio De Giorgi", Università del Salento, Lecce, Italy. [4]Euromediterranean Center for Nanomaterial Modelling and Technology (ECMT) of the Consiglio Nazionale delle Ricerche, Istituto Nanoscienze, Lecce, Italy. [5]Molecular Biotechnology Center, University of Turin, Turin, Italy. [6]Regina Elena National Cancer Institute, Rome, Italy. [7]Department of Oncology, University of Turin, Turin, Italy. [8]CNR Nantotec-Istituto di Nanotecnologia, Polo di Nanotecnologia c/o Campus Ecoteckne, Lecce, Italy.

Received: 14 August 2016 Accepted: 30 December 2016
Published online: 13 January 2017

References
1. Siegel RL, Miller KD, Jemal A. Cancer statistics, 2016. CA Cancer J Clin. 2016;66(1):7–30.
2. Yadav D, Lowenfels AB. The epidemiology of pancreatitis and pancreatic cancer. Gastroenterology. 2013;144(6):1252–61.
3. Stathis A, Moore MJ. Advanced pancreatic carcinoma: current treatment and future challenges. Nat Rev Clin Oncol. 2010;7(3):163–72.
4. Wolfgang CL, Herman JM, Laheru DA, Klein AP, Erdek MA, Fishman EK, et al. Recent progress in pancreatic cancer. CA Cancer J Clin. 2013;63(5):318–48.
5. Silvestris N, Gnoni A, Brunetti AE, Vincenti L, Santini D, Tonini G, et al. Target therapies in pancreatic carcinoma. Curr Med Chem. 2014;21(8):948–65.
6. Zagouri F, Sergentanis TN, Chrysikos D, Zografos CG, Papadimitriou CA, Dimopoulos MA, et al. Molecularly targeted therapies in metastatic pancreatic cancer: a systematic review. Pancreas. 2013;42(5):760–73.
7. Uram JN, Le DT. Current advances in immunotherapy for pancreatic cancer. Curr Probl Cancer. 2013;37(5):273–9.
8. Capello M, Ferri-Borgogno S, Cappello P, Novelli F. alpha-Enolase: a promising therapeutic and diagnostic tumor target. FEBS J. 2011;278(7):1064–74.
9. Diaz-Ramos A, Roig-Borrellas A, Garcia-Melero A, Lopez-Alemany R. alpha-Enolase, a multifunctional protein: its role on pathophysiological situations. J Biomed Biotechnol. 2012;2012:156795.
10. Ceruti P, Principe M, Capello M, Cappello P, Novelli F. Three are better than one: plasminogen receptors as cancer theranostic targets. Exp Hematol Oncol. 2013;2(1):12.
11. Hsiao KC, Shih NY, Fang HL, Huang TS, Kuo CC, Chu PY, PLoS One. et al. Surface alpha-enolase promotes extracellular matrix degradation and tumor metastasis and represents a new therapeutic target. PLoS One. 2013;8(7):e69354
12. Principe M, Ceruti P, Shih NY, Chattaragada MS, Rolla S, Conti L, et al. Targeting of surface alpha-enolase inhibits the invasiveness of pancreatic cancer cells. Oncotarget. 2015;6(13):11098–113.
13. Song Y, Luo Q, Long H, Hu Z, Que T, Zhang X, et al. Alpha-enolase as a potential cancer prognostic marker promotes cell growth, migration, and invasion in glioma. Mol Cancer. 2014;13:65.
14. Fu QF, Liu Y, Fan Y, Hua SN, Qu HY, Dong SW, et al. Alpha-enolase promotes cell glycolysis, growth, migration, and invasion in non-small cell lung cancer through FAK-mediated PI3K/AKT pathway. J Hematol Oncol. 2015;8(1):22.

15. Zhao M, Fang W, Wang Y, Guo S, Shu L, Wang L, et al. Enolase-1 is a therapeutic target in endometrial carcinoma. Oncotarget. 2015;6(17):15610–27.
16. Merkulova T, Lucas M, Jabet C, Lamandé N, Rouzeau JD, Gros F, et al. Biochemical characterization of the mouse muscle-specific enolase: developmental changes in electrophoretic variants and selective binding to other proteins. Biochem J. 1997;323(Pt 3):791–800.
17. Walsh JL, Keith TJ, Knull HR. Glycolytic enzyme interactions with tubulin and microtubules. Biochim Biophys Acta. 1989;999(1):64–70.
18. Lohman K, Meyerhof O. Über die enzymatische Umwandlung von Phosphoglyzerinsäure in Brenztraubensäure und Phosphorsäure (Enzymatic transformation of phosphoglyceric acid into pyruvic and phosphoric acid). Biochem Z. 1934;273:60–72.
19. Capello M, Ferri-Borgogno S, Riganti C, Chattaragada MS, Principe M, Roux C, et al. Targeting the Warburg effect in cancer cells through ENO1 knockdown rescues oxidative phosphorylation and induces growth arrest. Oncotarget. 2016;7(5):5598–612.
20. Pancholi V. Multifunctional alpha-enolase: its role in diseases. Cell Mol Life Sci. 2001;58(7):902–20.
21. Desgrosellier JS, Barnes LA, Shields DJ, Huang M, Lau SK, Prévost N, et al. An integrin αvβ3-c-Src oncogenic unit promotes anchorage-independence and tumor progression. Nat Med. 2009;15(10):1163–9.
22. Gruber G, Hess J, Stiefel C, Aebersold DM, Zimmer Y, Greiner RH, et al. Correlation between the tumoral expression of beta3-integrin and outcome in cervical cancer patients who had undergone radiotherapy. Br J Cancer. 2005;92(1):41–6.
23. Hosotani R, Kawaguchi M, Masui T, Koshiba T, Ida J, Fujimoto K, et al. Expression of integrin alphaVbeta3 in pancreatic carcinoma: relation to MMP-2 activation and lymph node metastasis. Pancreas. 2002;25(2):e30–5.
24. McCabe NP, De S, Vasanji A, Brainard J, Byzova TV. Prostate cancer specific integrin alphavbeta3 modulates bone metastatic growth and tissue remodeling. Oncogene. 2007;26(42):6238–43.
25. Takayama S, Ishii S, Ikeda T, Masamura S, Doi M, Kitajima M. The relationship between bone metastasis from human breast cancer and integrin alpha(v)beta3 expression. Anticancer Res. 2005;25(1A):79–83.
26. Sloan EK, Pouliot N, Stanley KL, Chia J, Moseley JM, Hards DK, et al. Tumor-specific expression of alphavbeta3 integrin promotes spontaneous metastasis of breast cancer to bone. Breast Cancer Res. 2006;8(2):R20.
27. Albelda SM, Mette SA, Elder DE, Stewart R, Damjanovich L, Herlyn M, et al. Integrin distribution in malignant melanoma: association of the beta 3 subunit with tumor progression. Cancer Res. 1990;50(20):6757–64.
28. Leporatti S, Vergara D, Zacheo A, Vergaro V, Maruccio G, Cingolani R, et al. Cytomechanical and topological investigation of MCF-7 cells by scanning force microscopy. Nanotechnology. 2009;20(5):055103.
29. Tomaino B, Cappello P, Capello M, Fredolini C, Ponzetto A, Novarino A, et al. Autoantibody signature in human ductal pancreatic adenocarcinoma. J Proteome Res. 2007;6(10):4025–31.
30. Moscato S, Pratesi F, Sabbatini A, Chimenti D, Scavuzzo M, Passatino R, et al. Surface expression of a glycolytic enzyme, alpha-enolase, recognized by autoantibodies in connective tissue disorders. Eur J Immunol. 2000;30(12):3575–84.
31. Wei Y, Waltz DA, Rao N, Drummond RJ, Rosenberg S, Chapman HA. Identification of the urokinase receptor as an adhesion receptor for vitronectin. J Biol Chem. 1994;269(51):32380–8.
32. Zhou A. Functional structure of the somatomedin B domain of vitronectin. Protein Sci. 2007;16(7):1502–8.
33. Madsen CD, Sidenius N. The interaction between urokinase receptor and vitronectin in cell adhesion and signaling. Eur J Cell Biol. 2008;87(8–9):617–29.
34. Ferraris GM, Schulte C, Buttiglione V, De Lorenzi V, Piontini A, Galluzzi M, et al. The interaction between uPAR and vitronectin triggers ligand-independent adhesion signalling by integrins. EMBO J. 2014;33(21):2458–72.
35. Ossowski L, Aguirre-Ghiso JA. Urokinase receptor and integrin partnership: coordination of signaling for cell adhesion, migration and growth. Curr Opin Cell Biol. 2000;12(5):613–20.
36. Smith HW, Marshall CJ. Regulation of cell signalling by uPAR. Nat Rev Mol Cell Biol. 2010;11(1):23–36.
37. Debidda M, Williams DA, Zheng Y. Rac1 GTPase regulates cell genomic stability and senescence. J Biol Chem. 2006;281(50):38519–28.
38. Trojanowicz B, Winkler A, Hammje K, Chen Z, Sekulla C, Glanz D, et al. Retinoic acid-mediated down-regulation of ENO1/MBP-1 gene products caused decreased invasiveness of the follicular thyroid carcinoma cell lines. J Mol Endocrinol. 2009;42(3):249–60.
39. Lian S, Shi R, Huang X, Hu X, Song B, Bai Y, et al. Artesunate attenuates glioma proliferation, migration and invasion by affecting cellular mechanical properties. Oncol Rep. 2016;36(2):984–90.
40. Georges E, Bonneau AM, Prinos P. RNAi-mediated knockdown of alpha-enolase increases the sensitivity of tumor cells to antitubulin chemotherapeutics. Int J Biochem Mol Biol. 2011;2(4):303–8.
41. Charo IF, Nannizzi L, Smith JW, Cheresh DA. The vitronectin receptor alpha v beta 3 binds fibronectin and acts in concert with alpha 5 beta1 in promoting cellular attachment and spreading on fibronectin. J Cell Biol. 1990;111(6 Pt 1):2795–800.
42. Roca-Cusachs P, Gauthier NC, Del Rio A, Sheetz MP. Clustering of alpha(5)beta(1) integrins determines adhesion strength whereas alpha(v)beta(3) and talin enable mechanotransduction. Proc Natl Acad Sci U S A. 2009;106(38):16245–50.
43. Zaidel-Bar R. Job-splitting among integrins. Nat Cell Biol. 2013;15(6):575–7.
44. Hynes R. Integrins: versatility, modulation, and signaling in cell adhesion. Cell. 1992;69(1):11–25.
45. Hynes RO. Integrins: bidirectional, allosteric signaling machines. Cell. 2002;110(6):673–87.
46. Madsen CD, Ferraris GM, Andolfo A, Cunningham O, Sidenius N. uPAR-induced cell adhesion and migration: vitronectin provides the key. J Cell Biol. 2007;177(5):927–39.
47. Pirazzoli V, Ferraris GM, Sidenius N. Direct evidence of the importance of vitronectin and its interaction with the urokinase receptor in tumor growth. Blood. 2013;121(12):2316–23.
48. Noh H, Hong S, Huang S. Role of urokinase receptor in tumor progression and development. Theranostics. 2013;3(7):487–95.
49. Blasi F, Sidenius N. The urokinase receptor: focused cell surface proteolysis, cell adhesion and signaling. FEBS Lett. 2010;584(9):1923–30.
50. Blasi F, Carmeliet P. uPAR: a versatile signalling orchestrator. Nat Rev Mol Cell Biol. 2002;3(12):932–43.
51. Playford MP, Schaller MD. The interplay between Src and integrins in normal and tumor biology. Oncogene. 2004;23(48):7928–46.
52. Mitra SK, Schlaepfer DD. Integrin-regulated FAK-Src signaling in normal and cancer cells. Curr Opin Cell Biol. 2006;18(5):516–23.
53. Cagnol S, Chambard JC. ERK and cell death: mechanisms of ERK-induced cell death-apoptosis, autophagy and senescence. FEBS J. 2010;277(1):2–21.
54. Koizumi K, Tanno S, Nakano Y, Habiro A, Izawa T, Mizukami Y, et al. Activation of p38 mitogen-activated protein kinase is necessary for gemcitabine-induced cytotoxicity in human pancreatic cancer cells. Anticancer Res. 2005;25(5):3347–53.
55. Jo M, Thomas KS, O'Donnell DM, Gonias SL. Epidermal growth factor receptor-dependent and -independent cell-signaling pathways originating from the urokinase receptor. J Biol Chem. 2003;278(3):1642–6.
56. Gargiulo L, Longanesi-Cattani I, Bifulco K, Franco P, Raiola R, Campiglia P, et al. Cross-talk between fMLP and vitronectin receptors triggered by urokinase receptor-derived SRSRY peptide. J Biol Chem. 2005;280(26):25225–32.
57. Chaurasia P, Aguirre-Ghiso JA, Liang OD, Gardsvoll H, Ploug M, Ossowski L. A region in urokinase plasminogen receptor domain III controlling a functional association with alpha5beta1 integrin and tumor growth. J Biol Chem. 2006;281(21):14852–63.
58. Mazzieri R, D'Alessio S, Kenmoe RK, Ossowski L, Blasi F. An uncleavable uPAR mutant allows dissection of signaling pathways in uPA-dependent cell migration. Mol Biol Cell. 2006;17(1):367–78.
59. Smith HW, Marra P, Marshall CJ. uPAR promotes formation of the p130Cas-Crk complex to activate Rac through DOCK180. J Cell Biol. 2008;182(4):777–90.

Submit your next manuscript to BioMed Central and we will help you at every step:

- We accept pre-submission inquiries
- Our selector tool helps you to find the most relevant journal
- We provide round the clock customer support
- Convenient online submission
- Thorough peer review
- Inclusion in PubMed and all major indexing services
- Maximum visibility for your research

Submit your manuscript at
www.biomedcentral.com/submit

BioMed Central

Combined treatments with the DNA vaccine to increase its effectiveness in pancreatic ductal adenocarcinoma

ENO1 DNA vaccine gave promising results in PDA models, although did not completely eradicate the tumor which, after an initial growth inhibition, returns to proliferate again. This led to developing possible strategies for combinatorial treatments aimed to broaden and sustain the anti-tumor immune response elicited by DNA vaccination. In the review by Cappello et al. published in 2018 titled "Next Generation Immunotherapy for Pancreatic Cancer: DNA Vaccination is Seeking New Combo Partners" [32], were discussed the biological bases of a list of possible approaches to use in combination with DNA vaccine, namely chemotherapy, PI3K inhibitors and TAM inhibitors.

Accumulating evidence indicates that multiple anticancer agents, including classic chemotherapeutics, stimulate tumor-specific immune response either by inducing immunogenic cell death or by engaging immune effector mechanisms (Figure 2).

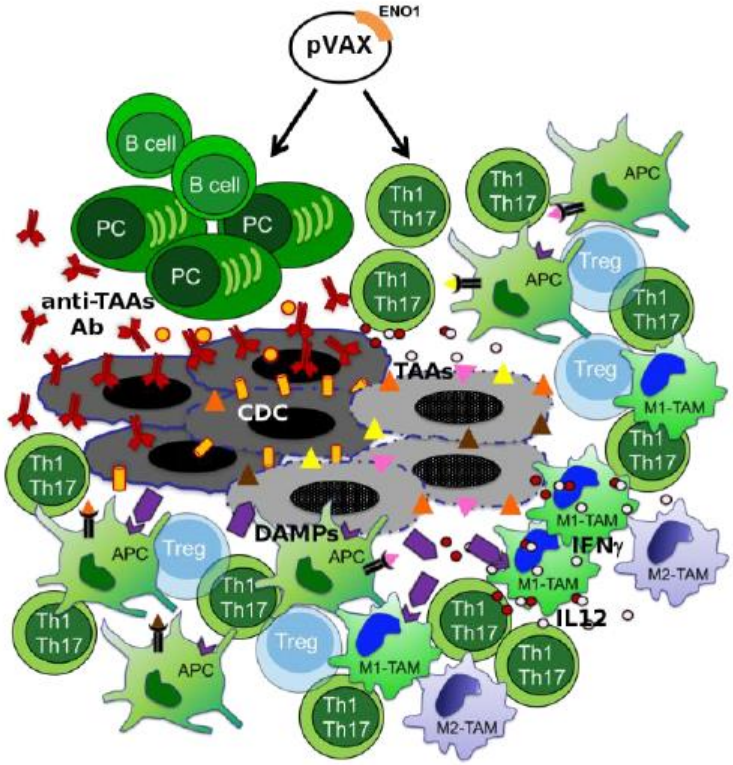

Figure 2. Effects of ENO1 DNA vaccination and chemotherapy combination. Transparent Treg represent inhibited cells; triangles= TAA; violet symbols= DAMP and DAMP receptors.

CT affects cancer cells impairing cell replication, particularly inducing DNA damage and in addition to the typical processes of cell death, namely necrosis and apoptosis, some CT agents induce an immunogenic cell death in which cancer cells express damage-associated molecular patterns (DAMP). These molecules are detected by receptors on a variety of innate immune cells, such as macrophages and neutrophils, but also on antigen presenting cells (APC).

Several studies have demonstrated the positive effect of CT on the anti-tumor immune response in PDA. The number of circulating CD14+ monocytes increase in PDA patients underwent CT and in adjuvant CT-treated PDA patients the TAM density at the stroma-tumor interface was associated with a better prognosis; by contrast in surgical resected patients TAM showed a predominant M2-like immunosuppressive phenotype (M2-TAM) correlating to a worse prognosis. Moreover, GEM synergized *in vitro* also with the cytotoxic effect of M1-TAM and inhibited the pro-tumor effect of M2-TAM.

In the orthotopic PDA mouse model, treatment with 5-Fluorouracile (5-FU) combined with IFN-α increased the number of natural killer cells (NK) in the tumor with a higher cytotoxic capability. In addition, combined GEM treatment with a dendritic cells (DC)-based vaccine led to the elimination of metastasis and recurrence, increasing the overall survival of orthotopic PDA mouse models.

The role of CT in promoting the formation of neoantigens has yet to be explored, while the effect of CT in inducing in PDA novel TAA, or enhancing already established TAA such as ENO1, to enhance the efficiency of DNA vaccination will be deeply discussed in a later chapter.

Phosphoinositide 3-Kinases (PI3K) regulates different pathways involved in cell survival, differentiation, apoptosis, senescence and DNA repair, and in the last years PI3K inhibitors are being used in clinical settings of onco-hematology disease.

PI3K are heterodimers formed by a constitutive catalytic subunit and a regulatory subunit which determines the subclassification into class IA (PI3K-α, -β, -δ) and class IB (PI3K-γ). The catalytic subunit interacts with the regulatory one inhibiting its activity, while in the presence of specific molecules, such as chemokines, growth factors and cytokines, PI3K are recruited to the cell membrane where they are activated. The review focuses on PI3K-γ which is expressed in leukocytes and especially in myeloid cell compartments.

In PDA preclinical model selective genetic deletion and pharmacological inhibition of PI3K-γ significantly impaired tumor growth and metastasis by affecting myeloid cell functions (Figure 3), mainly through the PI3K-γ-dependent activation of Bruton tyrosine kinase (BTK).

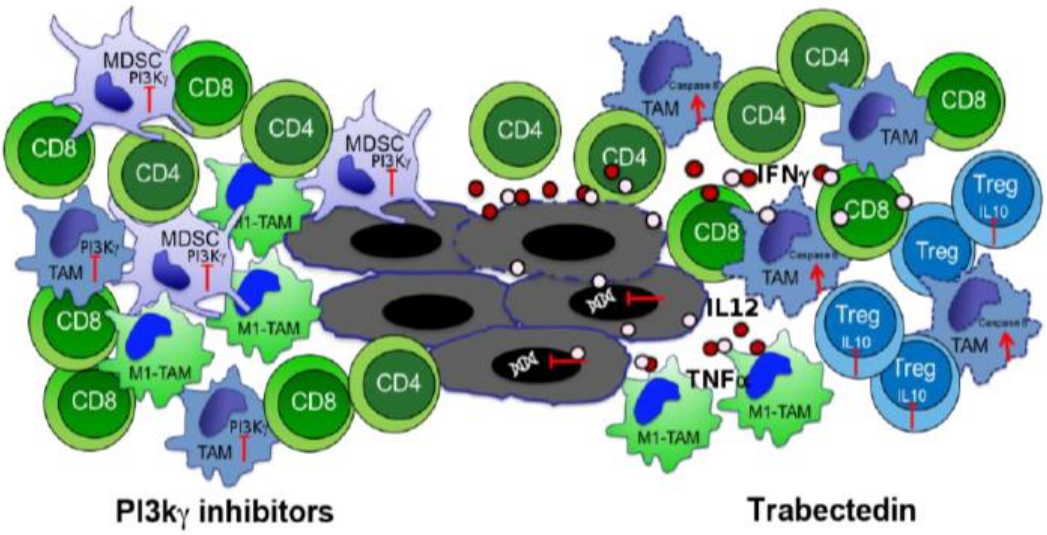

Figure 3. Phosphoinositide 3-Kinase (PI3K) inhibitor (left) and Trabectedin (right) effects on immune cells. CD8 recruitment depends on the M1-TAM switch of TAM and MDSC after PI3K inhibition is represented. Caspase-8 activation and cytokine production induced by Trabectedin in TAM, IFN production by T cells and IL10 inhibition in Treg are shown

Moreover, tumor suppression and increased mouse survival induced by PI3K-γ inhibition has been directly associated with the activation of CD8+ T cells and with the switch from M2-TAM into a more anti-tumoral M1-TAM. The evidence of anti-tumor immune restoring effects strongly suggests PI3K-γ inhibitor as a suitable powerful combinatorial partner to enhance the anti-tumor efficacy of ENO1 vaccination.

In PDA patients the elevated number of both infiltrating CD4+ and CD8+ T cells was demonstrated to correlate with a better outcome and the presence of ENO1-specific T cells was detected both in the tumor and in the blood of PDA patients. However, ENO1-specific TIL were frustrated in their Th1 and Th17 functions. Since also TAM or MDSC could influence the status of T cells in cancer, the effect of depletion of TAM in modifying TIL epigenetic profile was investigated. Trabectedin is a sponge-derived drug that specifically targets mononuclear phagocytes by activating the caspase 8 cascade via TRAIL receptors. When TAM were depleted by Trabectedin treatment in PDA mouse model, CD4+ TIL displayed a higher production of IFN-γ, and much less IL-10, compared

to the same population in untreated tumors (Figure 3); this was confirmed by epigenetic profile of CD4 T cells that showed a significant enrichment of the active mark H3K4me3 at the T-bet promoter and a decrease of the repressive mark H3K4me3 at the Il10 promoter. In presence of Trabectedin i*n vitro* generated macrophages up-regulated IL-2, IL-12, IL-17 and TNF-α production, which are involved in T cell activation. All these effects render Trabectedin a suitable component for combinatorial therapies, moreover it may lead to epitope spreading thanks to its cytotoxic effect on tumor cells and the combined antigen-specific vaccination could enhance T cell reactivity.

Therefore, ENO1 vaccination may benefit from the combined treatments: from CT which induce a progressive increase of antibody and effector response to many TAA, from the effectiveness of the PI3K-γ inhibition to unleash anti-tumor responses, and from the TAM depletion by Trabectedin which epigenetic reprograms TIL into anti-tumor effector cells. As all these approaches utilize drugs or compounds that are used or already approved for clinical purposes, they represent an evaluable springboard for developing a more efficacious protocol for PDA immunotherapy based on DNA vaccination.

Glycolytic enzymes as novel tumor-associated targets for immunotherapy in pancreatic ductal adenocarcinoma

The review by Curcio et al. published in 2021 titled "The glycolytic pathway as a target for novel onco-immunology therapies in pancreatic cancer" [35], analyses the role of emerging glycolytic enzymes (GE) with their related genetic background, in the tumor progression and metastasis, focusing on how they could represent feasible therapeutic targets to counteract PDA. One of the main characteristics that causes aggressiveness in PDA is aberrant glucose metabolism. Indeed, in PDA cells, most of the glucose molecules are quickly transformed into lactate, and glucose becomes the main energy source for the tumor. This mechanism is known as the Warburg effect or aerobic glycolysis, whereby cancer cells favor metabolism via glycolysis to satisfy the increasing needs of nucleotide, lipid and protein synthesis required for cell replication [39]. The enhanced glycolysis and the consequent decrease in oxidative phosphorylation leads to higher lactate production, triggering an acidic and immunosuppressive TME (Figure 4). In this context, the glycolysis rate of T cells is reduced in the tumor niche resulting in inhibition of T cell proliferation and cytokine production, favoring tumor immune evasion.

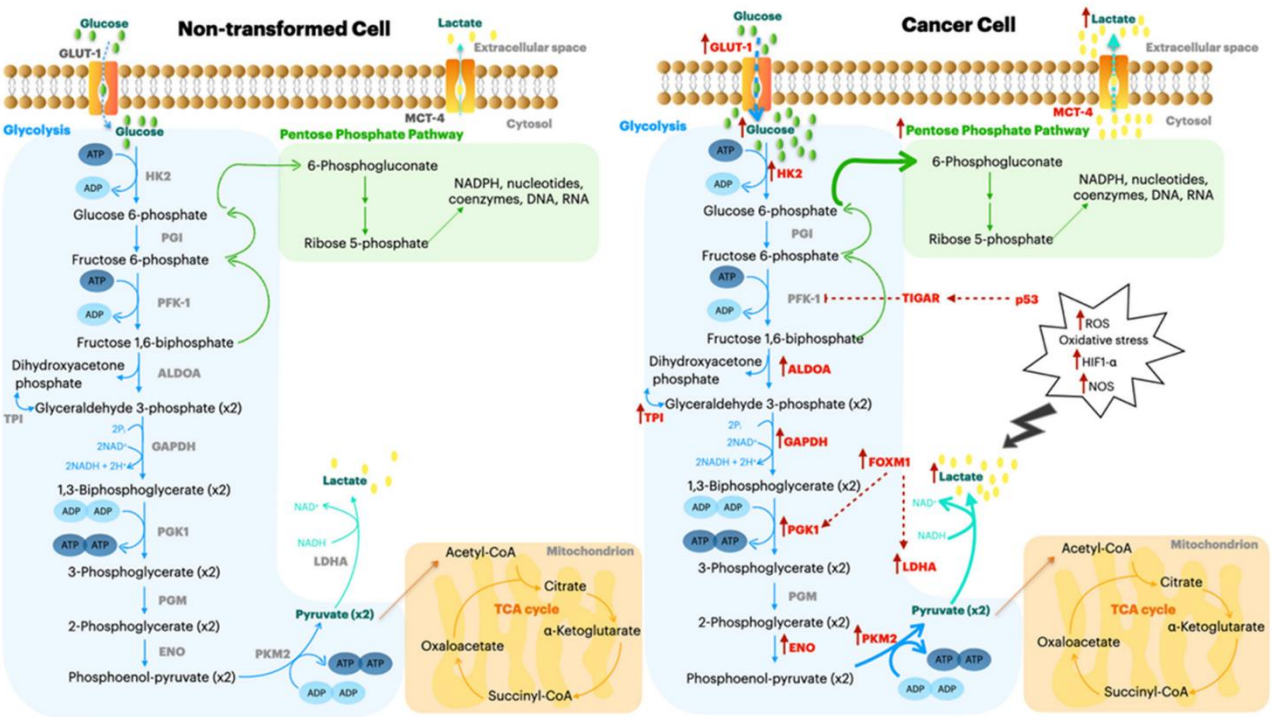

Figure 4. Schematic comparison of metabolic pathways between a not transformed cell and a cancer cell. The enzymes, transcription factors, oncogenes involved in aberrant glycolysis and correlated pathways are highlighted in red and are discussed in detail in the text.

Constitutive KRAS activation drives high proliferation of PDA cells and enhances transcription of several GE, leading to both an increased glycolytic activity and lactate production. KRAS activation in PDA cells was demonstrated to promote inflammatory response, tumor growth and regulation of tumor stroma, through IL-6 and TGF-β secretion. In PDA was studied the effect of mAb to neutralize mutated KRAS. Unfortunately, 30% of PDA cases were able to escape KRAS inhibition, thus targeting KRAS peptides containing different mutations could be a favored strategy. In gastrointestinal malignancies the vaccination targeting KRAS different mutated peptides is under investigation in clinical trials.

Table 1. Schematic summary of potential glycolytic targets in Pancreatic ductal adenocarcinoma (PDA) therapy.

Target	Overexpression		Clinical Outcome			Targeting Approach	Correlation with Immune Response
	Cell Line	Tissue	Survival	PD/M	CT Resistance		
KRAS/TP53		PCR [11] IHC [11,12] RNAseq [13]	↓ [11,14]	↑ M [11]		KRAS interference [11] KRAS/p53 peptide vaccination [11,15–18] RT11-i [19]	Chemokine secretion, macrophage recruitment and lymphocyte and myeloid cell infiltration [11]
GLUT1	qPCR [20] WB [20,21]	RNAseq [15,16] IHC [17,18]	↓ [22]	* ↑ M [21]	[22]	GLUT1 silencing [21] TWIST1 silencing [23] Apigenin [24,25] PON2 [26]	Positive correlation with PD1+ TILs [18] High GLUT1 expression in activated Tregs [27]
HK2	qPCR [28] WB [28,29]	mRNA [30] IHC [30–32] Microarray [33]	↓ [29,31] ↑ [32]	* ↑ M [28]	[28]	HK2 silencing [28] IKA [34]	
ALDOA		IHC [35]	↓ [35]	* ↑ M [35]		ALDOA silencing [35] TDZD-8 [36] TX-2098 [37]	Circulating auto-Ab to ALDOA [10]
TPI	RNAseq [13]	RNAseq [13] IHC [38]	↓ [13,38]		[13,39]		Circulating auto-Ab to TPI [9,10]
GAPDH	mRNA [40] WB [40]	2-DE [41] IHC [41] mRNA [40] WB [40]	↓ [39]	* ↑ M [42]	[39]	2-DG [43] P1DG [44] AXP3009 [45] Genipin [45,46] KA [47]	Humoral and cellular responses to GAPDH [10,48]
FOXM1		Microarray [49] mRNA [50] IHC [51] WB [51]	↓ [50,52]	↑ PD [53] ↑ M [50,53]	[51] * [54]	Genistein [55] FOXM1 siRNA [56,57] FOXM1 RNA interference [58] USP5 inhibition [59] Thiazole antibiotic [60] MG115 and MG132 [61,62] 5,7 Dimethoxyflavone [63]	DC maturation [64,65] T cell proliferation [65]
PGK1	2-DE [66]	mRNA [67] 2-DE [66]	↓ [67,68]	↑ M [69]	[67]		Circulating auto-Ab [10,66,68] High concentration of PGK1 in serum [70]
LDHA	WB [71–74] qPCR [72]	Microarray [71] IHC [71,74,75] mRNA [72] WB [72]	↓ [71]	↑ PD [75]		LDHA RNA interference [72] LDHA siRNA [73,74] EGCG [76] 2-DG [76] Graviola [77] FX11 [78,79]	Negative correlation with CD8+ TIL [71] * Low cytotoxic NK activity [80] * High MDSC activity [80]
ENO1	mRNA [40] WB [40] Microarray [81] Flow cytometry [82]	2-DE [41] mRNA [40] WB [40] Microarray [81] IHC [83]	↓ [39,83,84]	* ↑ M [85]	[39,84]	ENO1 DNA vaccination alone or in combination with GEM [10,86] ENO1 silencing [82,85] Anti-ENO1 mAb [82,87] PhAH [88] ENO1 knockdown [88] Citrullinated ENO1 peptides [89]	Increased level of anti-ENO1 Ab before and after GEM treatment [9,10,90,91] Increased T cell response in vitro and in vivo [81,91] Increased level of ENO1 in plasma patients [83] ENO1-specific Th17 and Treg response [92]
PKM2	WB [71,93,94] qPCR [94]	IHC [31,71,93,94] ↓ IHC [95,96] Microarray [97] Oncomine database [97]	↓ [31,71,97,98]	↑ M [31,99] * ↑ PD [98]	[98]	PKM2 knockdown [94,99–101] PKM2 silencing [97] 2-DG [102,103] Shikonin [103] Betulinic acid and thymoquinone and GEM [104]	Increased level of anti-PKM2 Ab before and after GEM treatment [10] Negative correlation with CD8+ TIL [71]

GAPDH= G3P; CT= chemotherapy; PD= progressive disease; M= metastasis; *= preclinical mouse model; Ab= antibody; IHC= immunohistochemistry; WB= Western blot; qPCR= quantitative PCR; 2-DE= 2-dimensional electrophoresis. Reference numbers correspond to review's bibliography.

All the GE listed in the review were found overexpressed in PDA tissues and cell lines compared to normal ones (Table 1). Interestingly, GE higher expression was correlated with a lower survival of PDA patients, and it was also associated with the presence of metastasis and/or the progression disease condition, suggesting the role of GE also as prognostic biomarkers. Many GE when overexpressed were also associated with the resistance to CT in PDA patients or in PDA cell lines. Interestingly, antibody response against several GE, namely ALDOA, TPI, G3P, PGK1, ENO1 and PKM2, was detected in PDA patients [14] with a greater extent after GEM treatment [17] (Table 1). An increased Teff response was also detected against ENO1 and G3P in PDA patients after CT [17]. These observations support their role as TAA in immunotherapy-based strategy.

Targeting approaches through silencing, knockdown, inhibitor molecules or mAb were deeply *in vitro* and *in vivo* investigated against GE demonstrating a decreased cell proliferation and a reduction in tumor growth due to a lower glycolytic activity. In addition, the block of several GE restored the CT sensitivity of PDA cells. GE blockade not only resulted in glycolysis inhibition, but also in hypoxia-inducible factor 1 alpha (HIF-1α) suppression, protecting cancer cells from apoptosis and suggesting a feed-forward loop in which HIF-1α induced expression of glycolytic enzymes and vice versa. In cancer cells GE overexpression promoted also the vascular endothelial growth factor (VEGF) signaling, one of the pathways involved in invasion, extravasation and colonization at distant organs. HIF-1α inhibitor led to a lower expression of VEGF as well a reduced expression of GE, resulting in a prolonged survival on a PDA xenograft model, supporting the connection between GE, hypoxic stress, and metastasis.

Beside their GE glycolytic upregulation also their cellular localization may affect tumor metabolism. The KRAS-dependent inactivation of TP53 supported glycolysis by impairing the nuclear translocation of G3P, whose levels increased in the cytosol. However, the inhibition of oxidative stress could induce the nuclear translocation of G3P in PDA cell lines, upregulating autophagy-related genes. Indeed, tumor aggressiveness and the higher activity of anabolic pathways seem to be supported by autophagy, since the genetic ablation of autophagy in preclinical models showed impaired cancer progression and invasiveness, demonstrating that autophagy-based strategy could be clinically relevant in PDA treatment.

Several reports have shown that targeting the glycolytic pathway can effectively counteract tumor progression. Moreover, increasing needs of nutrients and glucose in tumors could shift immune cells (Figure 5) and stromal cell metabolism towards glycolytic behavior. Cancer associated fibroblast with a glycolytic phenotype supported oxidative phosphorylation in cancer cells and, consequently, tumor survival and invasive ability. Cytokines secreted by pro-tumoral macrophages induced aerobic glycolysis in PDA cells, promoting tumor survival. In addition, in a glycolytic environment, ENO1 was directed towards the cytoplasm, rather than in the nucleus where it prevented FOXP3 expression and the consequent suppressive phenotype.

Glucose metabolism also plays a pivotal role in suppressive functions and stability of immunosuppression compartment in the TME. In PDA the overexpression of GLUT1 and ENO1 was observed in Treg, and their activation was due to glucose uptake. By contrast, in Teff aerobic glycolysis is required for clonal expansion, cytolytic activity and cytokine secretion. Cytotoxic NK activity was inhibited by PDA cell secreted lactate and in CD8+ T cells, the altered metabolism impaired their effector function, promoting tumor progression. Moreover, in PDA patients, CD8+ TIL were negatively correlated with GE expression.

Overall, high glycolytic cancer cells strongly consume glucose available in the TME and in return they produce massive quantities of lactate. TME acidification and lack of nutrients, together with the higher cancer-dependent ROS production, impair the activation of Teff.

In conclusion, the overexpressed state of GE in PDA and their involvement in tumor progression supports them as a target-group in a novel immunotherapeutic strategy based on the vaccination against one or more GE-related TAA.

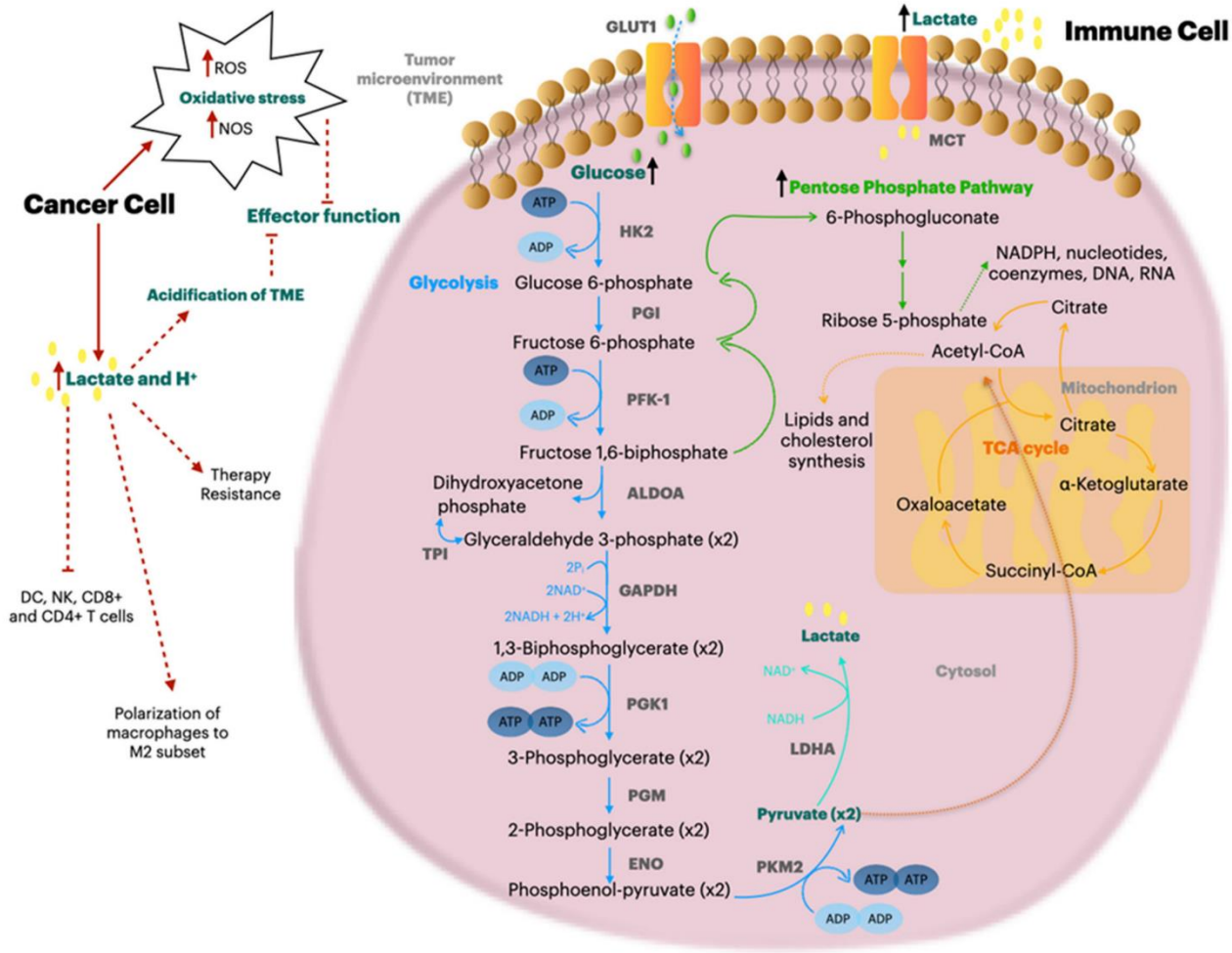

Figure 5. Metabolism of activated T cells and the effect of cancer induced TME acidification on T cell response. Red arrows indicate the effects of altered cancer metabolism on T cell activity and black arrows indicate the involved pathway in T cell activation.

Chemotherapy increases tumor associated antigens specific immune response and potentiates DNA vaccination in pancreatic ductal adenocarcinoma

Has been already demonstrated that CT has immune-modulating properties; particularly CT induces cancer cells DNA damage and cellular stress resulting in cell death. Moreover, these alterations could result in aberrant gene expression and the proteins with abnormal production, in quantity or quality, could be recognized by immune cells as TAA. In the study titled "In pancreatic cancer, chemotherapy increases anti-tumor responses to tumor-associated antigens and potentiates DNA vaccination" published by Mandili et al. in 2020 [17], was investigated the effect of GEM in anti-tumor effector responses to TAA in PDA. The figures mentioned in this chapter refer to the attached article by Mandili et al. 2020 [17].

Sera of 28 PDA patients before and after GEM-based CT were profiled by SERPA to evaluate the presence of autoantibodies specific for proteins from the proteome of CFPAC-1, a human PDA cell line (Figure 1A). In CT-treated patients was observed the enhancement of the IgG-specific response in both the number and intensity of recognized spots, with each spot corresponding to a protein isoform (Figure 1A-B). Interestingly, PDA patient sera after CT showed a higher CDC capability toward PDA cell lines (Figure 1C).

GEM-treated CFPAC-1 modified the expression of several proteins, of which 12 in common with those more recognized by IgG following CT. Moreover, many recognized proteins corresponded to overexpressed genes in The Cancer Genome Atlas (TCGA) PDA, supporting their role as TAA.

Among TAA with high frequency recognition by patients, four TAA were selected to represent metabolic pathways, cytoskeletal and transcription factor; in detail ENO1 and G3P, keratin, type II cytoskeletal 8 (K2C8) and far upstream binding protein 1 (FUBP1) (Figure 2). A positive correlation between anti-G3P and anti-K2C8 antibodies and patient survival was observed (Figure 3A-B). Data from ELISA confirmed both that PDA patients displayed a significantly higher level of antibodies to all four TAA compared to healthy subjects, and the significant increase of antibodies to ENO1, K2C8 and G3P after CT (Figure 3C).

PBMC from 13 of the same PDA patients were *in vitro* stimulated with each of the four selected TAA. Evaluation of cytokine production allowed us to monitor regulatory (IFN-γ/IL-10 ratio <1), effector

(IFN-γ/IL-10 ratio >1), or null cytokine responses (no production of either IFN-γ or IL-10). The TAA-specific proliferation was evaluated indicating the proliferative response with a Stimulation Index (S.I.) ≥ 2; the number of T lymphocyte proliferative responses to selected TAA were significantly increased after CT rounds (Suppl. figure 3A). Analysis of the IFN-γ/IL-10 ratio revealed that CT treatment shifted T cell responses to the four TAA from regulatory to effector, and the concomitant proliferative response increased after CT (Table 2).
A significant increase of the ratio between the percentage of CD8 and Treg after CT rounds was also observed in TAA-stimulated T lymphocytes from PDA patients (Suppl. figure 3B).

To investigate if CT could enhance the anti-tumor efficiency of ENO1 vaccination, mice that spontaneously developed PDA were treated with a suboptimal dose of GEM and inoculated with a ENO1 DNA vaccine. Both ENO1 and GEM+ENO1 treatment induced a significant reduction of PDA and PanIN lesions compared to untreated mice, but GEM+ENO1 treatment further reduced tumor lesions compared to ENO1 alone (Figure 4B).
Combined treatment further increased anti-ENO1 IgG antibodies and ENO1-specific IFN-γ-secreting splenocytes (Figure 4C,E). Of note, GEM+ENO1 treatment caused an increase also of both IgG production and IFN-γ secreting splenocytes specific to G3P, enhancing the preexistence epitope spreading effect of ENO1 (Figure 4D,F).
Finally, only GEM+ENO1 caused a significant increase of tumor-infiltrating CD4+ and CD8+ T cells (Figure 4G-H); however, depletion of CD4+ T cell, but not of CD8+ or B cells, completely reverted the anti-tumor effect of the combined treatment (Figure 4L).

The profiling of the immune response in patients with PDA, together with the preclinical mouse model validation, provide a proof-of-concept that CT combined with TAA vaccination may offer a promising solution for novel PDA treatments.

Journal for ImmunoTherapy of Cancer

In pancreatic cancer, chemotherapy increases antitumor responses to tumor-associated antigens and potentiates DNA vaccination

Giorgia Mandili,[1,2] Claudia Curcio,[1,2] Sara Bulfamante,[1,2] Laura Follia,[1,3] Giulio Ferrero,[3] Emanuela Mazza,[1,2] Moitza Principe,[1,2] Francesca Cordero,[3] Maria Antonietta Satolli,[4,5] Rosella Spadi,[5] Andrea Evangelista,[6] Daniele Giordano,[1,2] Duy Viet,[1,2] Paola Cappello ,[1,2] Francesco Novelli [1,2]

To cite: Mandili G, Curcio C, Bulfamante S, *et al*. In pancreatic cancer, chemotherapy increases antitumor responses to tumor-associated antigens and potentiates DNA vaccination. *Journal for ImmunoTherapy of Cancer* 2020;**8**:e001071. doi:10.1136/jitc-2020-001071

GM and CC are joint first authors.

Accepted 10 September 2020

Check for updates

© Author(s) (or their employer(s)) 2020. Re-use permitted under CC BY-NC. No commercial re-use. See rights and permissions. Published by BMJ.

For numbered affiliations see end of article.

Correspondence to
Dr Francesco Novelli;
franco.novelli@unito.it

ABSTRACT

Background Pancreatic ductal adenocarcinoma (PDA) is an almost incurable tumor that is mostly resistant to chemotherapy (CT). Adaptive immune responses to tumor-associated antigens (TAA) have been reported, but immunotherapy (IT) clinical trials have not yet achieved any significant increase in survival, confirming the suppressive environment of PDA. As CT has immune-modulating properties, we investigated the effect of gemcitabine (GEM) in antitumor effector responses to TAA in patients with PDA.

Methods The IgG antibody repertoire in patients with PDA before and after CT was profiled by serological proteome analysis and ELISA and their ability to activate complement-dependent cytotoxicity (CDC) was measured. Peripheral T cells were stimulated in vitro with recombinant TAA, and specific proliferation, IFN-γ/IL-10 and CD8$^+$/Treg ratios were measured. Mice that spontaneously developed PDA were treated with GEM and inoculated with an ENO1 (α–Enolase) DNA vaccine. In some experimental groups, the effect of depleting CD4, CD8 and B cells by specific antibodies was also evaluated.

Results CT increased the number of TAA recognized by IgG and their ability to activate CDC. Evaluation of the IFN-γ/IL-10 ratio and CD8+/Treg ratios revealed that CT treatment shifted T cell responses to ENO1, G3P (glyceraldheyde-3-phosphate dehydrogenase), K2C8 (keratin, type II cytoskeletal 8) and FUBP1 (far upstream binding protein 1), four of the most recognized TAA, from regulatory to effector. In PDA mice models, treatment with GEM prior to ENO1 DNA vaccination unleashed CD4 antitumor activity and strongly impaired tumor progression compared with mice that were vaccinated or GEM-treated alone.

Conclusions Overall, these data indicate that, in PDA, CT enhances immune responses to TAA and renders them suitable targets for IT.

BACKGROUND

Pancreatic ductal adenocarcinoma (PDA) is very challenging to treat, with only 8% of patients being cured. Gemcitabine (GEM) and FOLFIRINOX are currently considered the chemotherapeutic standard of care for treating advanced PDA.

Targeting the immune system is an active area of research for treating cancer, especially following recent successes obtained with immunotherapy (IT) in many solid tumors.[1–3] Although immune checkpoint inhibitors represent an important breakthrough in the field of IT, they have not yet achieved tumor regression in patients with PDA.[4 5] Significant improvements in IT clinical outcomes cannot be achieved without novel strategies that involve better comprehension of the tumor microenvironment, as well as identifying novel immunological targets.

PDA has a pronounced desmoplasia as a histological hallmark, which is derived from pancreatic stellate cells that are activated to proliferate and produce collagens, laminin, and fibronectin, which differentially shape the stroma.[6] This is also believed to contribute to tumor hypoperfusion and hypoxia[7] and harbor infiltrative macrophages and inflammatory cells with the potential to suppress antitumoral immune mechanisms.[8] In addition to reactive fibroblasts and M2 macrophages, the PDA microenvironment also contains γδ-T cells, which are a source of IFN-γ, and are associated with a poor prognosis.[9]

We have previously shown that DNA vaccination that targets α-Enolase (ENO1), a tumor-associated antigen (TAA) that is upregulated in PDA, effectively prolongs survival in mice that spontaneously develop PDA.[10] This increased survival results from the induction of specific antibodies to ENO1 that activate complement-dependent cytotoxicity (CDC); a decrease in tumor infiltration by regulatory T cells and myeloid-derived suppressor cells

J Immunother Cancer: first published as 10.1136/jitc-2020-001071 on 28 October 2020. Downloaded from http://jitc.bmj.com/ on July 13, 2021 by guest. Protected by copyright.

(MDSC);[11] inhibition of migration and invasion of PDA cells;[12 13] and an increase in tumor-infiltrating T cells[10] that relocalize into tertiary lymphoid tissue.[14]

Considering the immune modulating effects of chemotherapy (CT) in a clinical setting,[15–17] we decided to evaluate whether combining CT with IT can increase therapeutic efficacy in PDA. Here, we observed that, in patients with PDA, CT enhances adaptive immune responses to a number of TAA including ENO1, G3P (glyceraldheyde-3-phosphate dehydrogenase), K2C8 (keratin, type II cytoskeletal 8) and FUBP1 (far upstream binding protein 1). Notably, combining ENO1 DNA vaccination with GEM treatment significantly enhanced antitumor responses and efficacy to counteract tumor progression compared with mice which were vaccinated or GEM-treated only. These data indicate that—in patients with PDA—CT enhances immune responses to TAA and renders them suitable targets for IT.

METHODS

Patients

From 2005 to 2011, 28 patients with newly diagnosed PDA were enrolled in the study approved. Inclusion criteria consisted of an ECOG performance status 0–2, signing of a written informed consent form and no previous CT or radiotherapy. Exclusion criteria consisted of a lack of ability to perform follow-up (1 year) and any previous malignant tumors, with the following exception: adequately treated basal/spino-cell carcinomas, cervical carcinoma in situ, and patients affected by other malignancies, but disease-free for at least 5 years at the date of enrollment.

In this cohort, 14 patients had been subjected to total surgical resection, 4 patients had received palliative resection only, and 10 patients had not been resected. All patients were treated with CT, 26 with GEM-based CT (GEM or GEM plus oxaliplatin) and 2 with capecitabine and bevacizumab (table 1).

Peripheral blood mononuclear cells (PBMC) and sera samples were isolated from venous blood before CT, and after each round of CT, and stored until use.

Cell culture

PDA cell lines CFPAC-1, CAPAN-2, DT6606, and K8484 were cultured at 37°C in a humidified 5% CO_2 atmosphere in DMEM (Invitrogen, San Giuliano Milanese, Italy) supplemented with 20 mM glutamine (Invitrogen), 10% certified fetal bovine serum (FBS) (Invitrogen), and 40 µg/mL gentamycin (Schering-Plow, Milan, Italy).

Proteomics studies

For proteomics studies, CFPAC-1 cells were untreated or treated with 0.25 µg/µL GEM for 24 hours. Procedure details are described in the online supplemental file. For serological proteome analysis (SERPA), CFPAC-1 cells were solubilized and proteins were quantified to perform two-dimensional electrophoresis (DE) and Coomassie staining, as previously described.[18 19] 2-DE gels were transferred to nitrocellulose membranes and incubated with sera from patients before and after CT. Detailed procedures are described in the online supplemental file.

Complement-dependent cytotoxicity

CFPAC-1 or CAPAN-2 cells were seeded in 96-well plates (5×10^4 cells/well). Cells were washed with warm PBS, incubated with sera diluted in PBS (1:1000) for 1 hour at 4°C, then washed again, followed by incubation with fresh reconstituted human complement (Cedarlane, Euroclone, Milan, Italy) diluted at 1:10 in PBS for 1 hour at 37°C. The CytoTox 96 non-radioactive cytotoxicity kit (Promega, Milan, Italy) is based on the ELISA, and detects the release of lactate dehydrogenase (LDH) after 4 hours of incubation from cells that have lost membrane integrity (lysed cells). A LDH positive control was added to empty wells of each plate, and all tests were performed in triplicate.

Antibody detection

The quantity of total IgG in 12 patients was measured using an ELISA kit before and after CT (Bethyl Laboratories, Montgomery, Texas, USA), following the manufacturer's instructions. TAA (ENO1, FUBP1, K2C8, and G3P)-specific IgG responses of sera from 28 healthy subjects and 28 patients with PDA, before and after each round of CT, were analyzed by ELISA (see online supplemental file). Anti-ENO1 and anti-G3P IgG in mouse sera, at different weeks of age, were measured by ELISA using ENO1 or G3P, as previously described.

T cell responses

After thawing, PBMC from 13 patients, before and after each round of CT, were cultured at a density of 5×10^4/well in RPMI (Invitrogen) plus 5% of FBS in 96-well microplates with 5 µg/mL of ENO1, FUBP1, K2C8, or G3P. At day 3, supernatants were collected and IFN-γ and IL-10 levels were measured by ELISA (BioLegend, Campoverde, Milan, Italy), following the manufacturer's instructions. Specific production of IFN-γ and IL-10 in the supernatants was calculated by subtracting the concentration of each cytokine in the medium only from that in PBMC stimulated with TAA. These specific concentration values were pseudocounted (+1) and then expressed as an IFN-γ/IL-10 ratio. At day 5, proliferation was evaluated using a tritiated-thymidine (3H-TdR) incorporation assay (see online supplemental file). Stimulation index (SI) T cell proliferation was calculated by dividing the cpm from PBMC stimulated with each antigen by the cpm of PBMC cultured in medium only. PBMC from five patients were cultured 5×10^5 in 48-well plates in the presence of each TAA, as described above, and at day 3, cells were collected and stained with anti CD4-PercP, CD8-APC, and FoxP3-FITC to perform flow cytometer analysis (see online supplemental file).

J Immunother Cancer. first published as 10.1136/jitc-2020-001071 on 28 October 2020. Downloaded from http://jitc.bmj.com/ on July 13, 2021 by guest. Protected by copyright.

Table 1 Characteristics of patients

Patient	Gender	Age at diagnosis	**Surgical resection**	Stage	CT (I round)	CT (II round)	Survival (months)
142	F	46	Yes	IIB	GEM (3 cycles)	GEM (3 cycles)	38
141	M	66	Yes	IIB	GEM (3 cycles)	GEM (6 cycles)	36
135	M	66	No	IV	Gemox (6 cycles)	Gemox (6 cycles)	11
110	F	57	Yes	IIB	GEM (3 cycles)	GEM (6 cycles)	27
104	M	60	No	IV	Gemox (6 cycles)	Gemox (12 cycles)	13
103	F	62	Yes	IIB	GEM (3 cycles)	GEM (6 cycles)	18
99	M	51	No	III	GEM (3 cycles)	GEM	6
90	M	71	Palliative	IV	GEM (3 cycles)	GEM (6 cycles)	12
87	M	59	Yes	IIA	GEM	Gemox (6 cycles)	46
85	F	64	No	III	Bevacizumab+ Capecitabine (8 cycles)	Bevacizumab+ Capecitabine (8 cycles)	37
84	F	78	Palliative	III	GEM (3 cycles)	GEM (6 cycles)	20
83	M	55	Yes	IIB	GEM (4 cycles)	GEM (6 cycles)	53
82	M	74	No	IV	Gemox (6 cycles)	Gemox (12 cycles)	12
81	F	61	No	III	Bevacizumab+ Capecitabine	Bevacizumab+ Capecitabine	53
77	M	74	No	III	GEM (3 cycles)	GEM (6 cycles)	10
72	M	53	No	IV	Gemox (6 cycles)	Gemox (12 cycles)	14
50	M	46	Yes	IIB	GEM (3 cycles)	GEM (6 cycles)	21
41	F	56	Yes	IIB	GEM (3 cycles)	GEM (6 cycles)	30
36	F	65	No	IV	GEM (3 cycles)	GEM (6 cycles)	14
30	F	72	Yes	IIB	GEM (3 cycles)	GEM (6 cycles)	39
27	M	65	Palliative	IV	Gemox (6 cycles)	Gemox (11 cycles)	16
25	M	72	Palliative	III	GEM (3 cycles)	GEM (6 cycles)	21
19	F	55	Yes	IIB	GEM (3 cycles)	GEM (6 cycles)	25
13	F	71	Yes	IIB	GEM (3 cycles)	GEM (6 cycles)	25
11	M	54	No	IV	GEM+ 5-Fluorouracil (3 cycles)	GEM (6 cycles)	10
10	M	72	Yes	IIB	GEM (3 cycles)	GEM (6 cycles)	28
5	F	58	Yes	IIB	GEM (3 cycles)	GEM (6 cycles)	92
4	M	65	Yes	IIA	GEM (3 cycles)	GEM (3 cycles)	14

In vivo experiments

Pancreatic cancer-prone KC mice were generated by crossing single-mutated KrasG12D with C57BL/6 mice expressing Cre recombinase (see online supplemental file). KC mice were treated twice at week 8 by i.p. injection with GEM (on Monday and Friday) using 1 mg/injection/mouse. The ENO1 vaccine was administered at 9 weeks of age, and every 2 weeks for a total of three rounds of vaccination (see online supplemental file). Mice were sacrificed at 24 weeks of age, and pancreases were fixed in formalin and embedded in paraffin for analyzing tumor lesions and immunohistochemistry (see online supplemental file). Different experimental groups of mice were depleted of CD4, CD8 or CD20 (Bioxcell, West Lebanon, New Hampshire, USA) every 3 days (200 µg/mouse/injected i.p.) until the week after the final vaccination. At 14 weeks, depleted mice were sacrificed, and pancreases were fixed in formalin and embedded in paraffin for evaluating tumor lesions and anti-ENO1 antibody titers. To test the effectiveness of GEM+ENO1 vaccination on established tumors, C57BL/6 mice were injected subcutaneously with pancreatic tumor cells in the right flank (K8484, 1×10^5 cells/mouse) and treated with GEM+ENO1 vaccination when tumors reached 0.2 cm in diameter, as described above.

J Immunother Cancer: first published as 10.1136/jitc-2020-001071 on 28 October 2020. Downloaded from http://jitc.bmj.com/ on Jul 13, 2021 by guest. Protected by copyright.

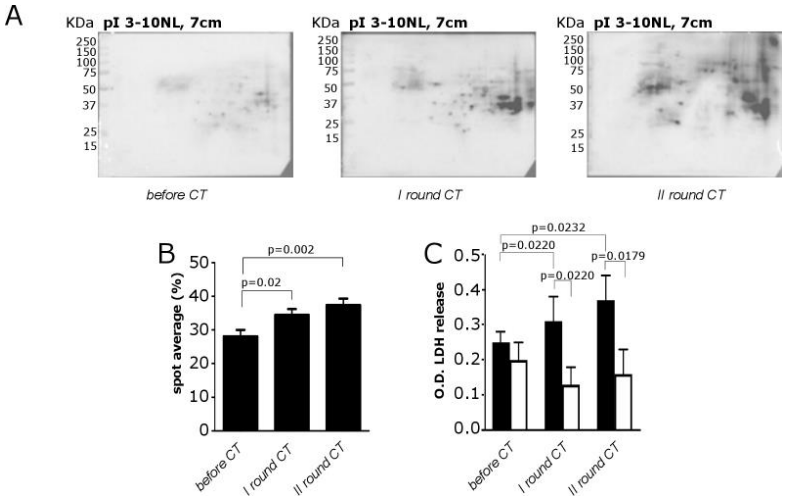

Figure 1 Analysis of the reactivity of sera from patients with PDA to recognize the PDA cell proteome and of their ability to induce CDC before and after CT. (A) Recognition of the proteome 2-DE map of the CFPAC-1 cell line by a representative PDA serum before and after CT. (B) Quantitative evaluation of increased IgG autoantibody recognition before and after CT. Results represent the mean of the percentage of all recognized spots. (C) Bar graph of LDH release measured as OD by damaged CFPAC-1 (black bars) and CAPAN-2 (white bars) cells subjected to CDC by patient sera before and after CT. All graphs indicate mean±SEM from 28 patients with PDA analyzed, and statistical significance is shown. CDC, complement-dependent cytotoxicity; CT, chemotherapy; LDH, lactate dehydrogenase; OD, optical density; PDA, pancreatic ductal adenocarcinoma; 2-DE, two-dimensional electrophoresis.

Enzyme-linked immunosorbent spot assay (ELISpot)

Splenocytes from treated or untreated mice were stimulated in vitro for 4 days in the presence of 10 µg/mL of selected TAA proteins. Recovered T cells were seeded at a density of 1×10^5/well in triplicate and stimulated with DT6606 cells (with a stimulator/effector ratio of 1:100) or 5 µg/mL TAA for 48 hours to evaluate specific IFN-γ production by ELISpot assay (see online supplemental file).

Statistical analysis

Data from SERPA experiments, protein differential expression, overall survival, immunohistochemical and FACS staining, ELISA, and ELISpot were analyzed, as described in the online supplementary file.

RESULTS

Analysis of the autoantibody response to TAA in patients with PDA before and after CT

Circulating IgG from the sera of 28 patients with PDA before and after one or two rounds of CT were profiled by SERPA. In CT-treated patients with PDA, a clear enhancement of the IgG-specific response in both the number and intensity of recognized TAA was observed (figure 1A, B). This increase was not due to a global enhancement of total IgG after two rounds of CT as no difference in sera IgG levels was detected by ELISA (online supplemental figure 1A).

The CDC of sera from patients with PDA before and after CT was evaluated in CFPAC-1 cells (complement sensitive), which do not express complement activity inhibitor CD55, and in CAPAN-2 cells (complement resistant), which do express CD55 (online supplemental figure 1B). A significant difference between sera-induced LDH release in CFPAC-1 and CAPAN-2 cells after the first and second rounds, but not before CT, was observed. A significant increase of sera-induced LDH release against CFPAC-1, but not in CAPAN-2 cells, was found after CT rounds (figure 1C).

Mass spectrometry revealed 91 proteins from 160 isoforms, highlighted by SERPA as distinct spots (online supplemental table 1A and online supplemental figure 1C). Following CT, a widespread and progressive increase of the autoantibody response to TAA was observed (figure 2). There was an increase in 32 TAA recognized in at least three patients after CT (online supplemental figure 1D), among which ENO1 was the most recognized TAA (online supplemental table 1B), in accordance with our previous studies.[20]

Proteomic analysis of GEM-treated CFPAC-1 cells revealed that CT modified the expression of 34 proteins, of which 12 corresponded to TAA whose autoantibody recognition was increased in patients with PDA following CT (online supplemental figure 2A,B and supplemental table 2).

The 32 protein targets of autoantibody responses following CT (online supplemental figure 1D) were

J Immunother Cancer: first published as 10.1136/jitc-2020-001071 on 28 October 2020. Downloaded from http://jitc.bmj.com/ on July 13, 2021 by guest. Protected by copyright.

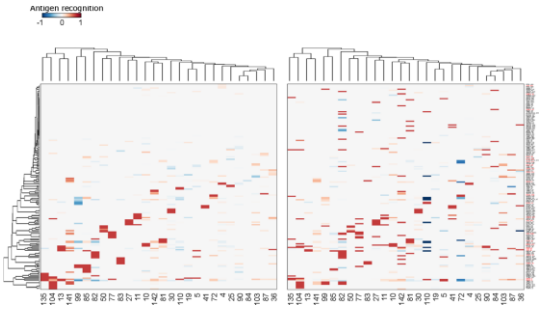

Figure 2 Analysis of the autoantibody response of patients with PDA after CT. Heatmaps representing the variation of antigen recognition level by autoantibodies measured by SERPA in sera from 28 patients with PDA receiving one round (left) or two rounds (right) of CT compared with before CT. Columns represent patients, and rows represent the antigens identified-listed in online supplemental table1A (all the isoforms of ENO1, FUBP1, K2C8 and G3P are indicated in red). Clustering analysis was performed considering data from patients receiving one CT round only (left). Rows and columns of the heat map reported in the right panel are sorted according to this clustering. CT, chemotherapy; PDA, pancreatic ductal adenocarcinoma.

coded by 23 genes transcriptionally overexpressed in The Cancer Genome Atlas (TCGA) patients with PDA (online supplemental figure 3) and gene-set enrichment analysis (online supplemental table 3).

There was considerable TAA recognition by autoantibodies of patients, and 11 TAA were recognized by at least 7 patients before and/or after CT (online supplemental table 1B). Four TAA, namely ENO1, FUBP1, K2C8 and G3P, were selected to represent metabolic-related, cytoskeletal-related and transcription-related molecules. A statistically significant correlation was found between patient survival and the increased autoantibody recognition of G3P and K2C8 after the first round of CT (figure 3A,B). Data from ELISA showed that a group of patients with PDA displayed a significantly higher level of autoantibodies to all four TAA compared with healthy subjects (figure 3C). A significant increase of autoantibodies to ENO1, K2C8 and G3P was measured in patients with PDA after CT (figure 3C), confirming the SERPA results.

T lymphocyte responses to TAA in patients with PDA before and after CT

Peripheral blood T lymphocytes from patients with PDA were stimulated with each of the four selected TAA, and the proliferation, regulatory (IFN-γ/IL-10 ratio <1), effector (IFN-γ/IL-10 ratio >1), or null cytokine responses (no production of either IFN-γ or IL-10) was monitored (table 2).

Overall, the number of patient T cell proliferative responses (evaluated as SI≥2) to selected TAA were significantly increased after CT rounds (online supplemental figure 3A).

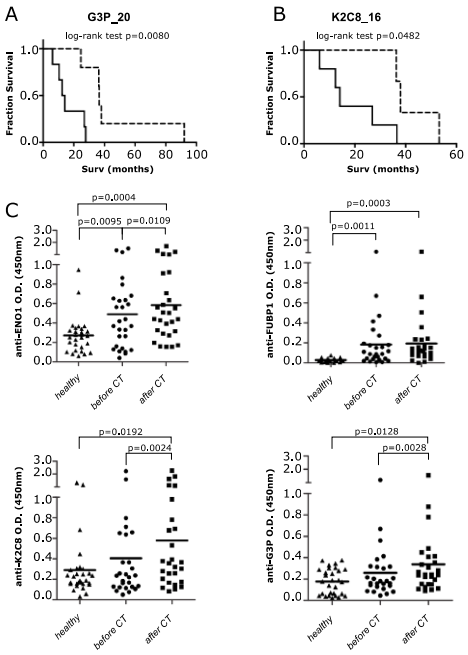

Figure 3 Detection of autoantibodies to TAA before and after CT, and correlation with survival of patients with PDA. (A,B) Survival curves of patients with PDA (n=28) with increased (dotted line) or unchanged/decreased (solid line) of 2-DE western blot reactivity of autoantibodies to G3P_20 (A) and K2C8_16 (B) isoforms after CT. (C) ELISA detection of autoantibodies to ENO1, FUBP1, K2C8 and G3P in healthy subjects and sera of patients with PDA before and after CT. Each graph indicates the OD mean (n=28), and statistical significance is shown. CT, chemotherapy; OD, optical density; PDA, pancreatic ductal adenocarcinoma; TAA, tumor-associated antigens; 2-DE, two-dimensional electrophoresis.

The relationship between proliferative and regulatory/effector responses to each TAA were also analyzed. Before CT, only one patient (pt. 24) displayed an effector response to ENO1. By contrast, seven patients (pt. 3, 9, 10, 24, 30, 32, 87) showed effector responses after CT, with just two of them (pt. 32, 87) being associated with a proliferative response (table 2). Before CT, four patients (pt. 3, 19, 41, 87) displayed effector responses to FUBP1, but only two showed a concomitant proliferative response (pt. 41, 87). After CT, the number of patients that displayed an effector response increased to 11 (pt. 3, 5, 9, 10, 19, 24, 25, 27, 30, 41, 84), with 8 of them (pt. 5, 9, 10, 25, 27, 30, 41, 84) being associated with a proliferative response (table 2). Before CT, six patients (pt. 3, 19, 25, 41, 84, 87) displayed an effector response to K2C8, with four of them (pt. 25, 41, 84, 87) showing concomitant proliferative responses. After CT, there was a regulatory-to-effector shift in three patients (pt. 9, 10, 24); an

J Immunother Cancer: first published as 10.1136/jitc-2020-001071 on 28 October 2020. Downloaded from http://jitc.bmj.com/ on July 13, 2021 by guest. Protected by copyright.

Table 2 TAA-induced cytokine and proliferative response of PBMC from patients with PDA before and after CT treatment

	ENO1						FUBP1						K2C8						G3P					
	Before CT		After CT round				Before CT		After CT round				Before CT		After CT round				Before CT		After CT round			
			I		II				I		II				I		II				I		II	
Patient	IFN-γ/ IL-10	SI	IFN-γ/ IL-10	SI	IFN-γ/ IL-10	SI	IFN-γ/ IL-10	SI	IFN-γ/ IL-10	SI	IFN-γ/ IL-10	SI	IFN-γ/ IL-10	SI	IFN-γ/ IL-10	SI	IFN-γ/ IL-10	SI	IFN-γ/ IL-10	SI	IFN-γ/ IL-10	SI	IFN-γ/ IL-10	SI
3	0.3	0.8	null	1	17.9	1.7	3.1	1.1	17.4	0.7	null	0.6	7.5	0.7	25	0.4	null	0.2	3.2	0.8	38.2	4.1	17.9	0.9
5	null	1.3	null	1.9	null	0.8	0.5	1.2	9.6	2.9	12.9	4.7	0	1.5	0	1.4	null	2.5	0.1	1.6	0	3	0	3.1
9	null	1.1	null	1.3	89.3	1.9	0	0.9	33.9	4.5	5.8	1.4	0	0.9	23.4	3.4	7.9	1.2	0	1.3	466.3	4.4	6.9	2.8
10	null	1.2	null	1.1	16.9	1.2	0.3	1.1	0.4	2.6	25.7	3.5	0.3	1	0.9	3.5	7.4	2.7	null	2	181.3	8	null	2.4
19	null	1.3	null	1	null	0.7	3.4	1.2	17.5	0.9	null	0.8	3.2	1	12.2	0.7	null	1	0	1	75.4	0.8	null	0.6
24	132.7	1.3	0.4	1.2	46.5	0.3	0.3	0.6	2.1	0.4	110.5	0.3	0.2	0.6	0.4	4.6	103.6	6	2.8	0.4	10.8	3.8	163.4	0.3
25	null	1.5	null	1.1	null	2.1	0.4	2.3	0	2.3	1.7	5.2	1.9	2.5	0.5	2.6	0.9	4.4	null	1.9	null	1.6	null	2.7
27	null	1.2	null	1.3	null	1	null	1.4	1.2	2.6	2.2	2.1	null	1	0.7	1.9	0.3	1.4	null	1.2	0	1.5	0	1.5
30	null	1.9	130.3	1.4	null	1.7	0	1.6	4.2	3	5.1	3.9	0.6	1.3	0.7	1.6	0.9	2.6	0	1.2	0	3.2	0	2.6
32	null	1	null	2.1	2.6	13.7	null	1	0.1	0.8	0.7	1.5	null	1	0.1	1.3	0	0.6	null	1	null	0.8	0.1	1.3
41	null	1.6	null	1.3	null	1.3	1.8	5.8	3.7	5.6	0	1.6	3.8	6.8	0.6	4.3	0.3	2.4	0.3	11	0.4	7.4	0.3	5.4
84	0.1	1.2	0.04	2.4	null	1.5	0.2	2.3	0.08	1.9	1.9	2.9	2	2.3	0.25	1.8	0	3	0.3	2.8	0	1.1	0	5.4
87	null	1.9	null	1.6	32	2.8	13.4	2.3	null	1.6	null	3.8	82.9	2.8	40.6	3.2	125.5	4.9	180.3	13.3	null	7.4	76	9

CT, chemotherapy; PBMC, peripheral blood mononuclear cells; PDA, pancreatic ductal adenocarcinoma; SI, stimulation index; TAA, tumor-associated antigens.

J Immunother Cancer: first published as 10.1136/jitc-2020-001071 on 28 October 2020. Downloaded from http://jitc.bmj.com/ on July 13, 2021 by guest. Protected by copyright.

increase in effector responses in three patients (pt. 3, 19, 87); and a decrease in regulatory responses in one patient (pt. 30). Among these seven patients, five (pt. 9, 10, 24, 30, 87) were associated with proliferation (table 2). Before CT, three patients (pt. 3, 24, 87) displayed a G3P-induced effector response, with only one (pt. 87) showing a concomitant proliferative response. After CT, there was a regulatory-to-effector shift in two patients (pt. 9, 19); an increase in effector responses in four patients (pt. 3, 10, 24, 87); and a reduction in regulatory responses in two patients (pt. 30, 41). Among these eight patients, seven (pt. 3, 9, 10, 24, 30, 41, 87) showed T cell proliferation.

A significant increase of the ratio between the percentage of CD8 and Treg after one and two CT rounds was also observed in TAA-stimulated T lymphocytes from patients with PDA (online supplemental figure 3B and supplemental table 4).

Effect of combining CT and ENO1 DNA vaccination on antitumor immunity in the KC pancreatic cancer mouse model

The effect of the combined treatment of CT and DNA vaccination to ENO1, a TAA expressed in the early phases of PDA carcinogenesis (online supplemental figure 5A) was evaluated in KC mice.

KC mice were treated with a suboptimal dose of GEM and then vaccinated with ENO1 (figure 4A). The size of all neoplastic lesions (from PanINs to invasive PDA) was evaluated by H&E staining. Both ENO1 and GEM+ENO1 treatment induced a significant reduction of PDA lesions compared with untreated mice and GEM+ENO1 treatment further reduced tumor lesions compared with the ENO1 vaccine alone (figure 4B). The evaluation of both the number and size of invasive PDA and PanIN lesions showed that ENO1 vaccination and combined treatment reduced the number of both invasive and PanIN lesions, whereas only the size of PanIN lesions were reduced by ENO1 vaccination alone and to a larger extent by combined treatment (online supplemental figure 6).

Smaller tumor lesions were accompanied with an increase of anti-ENO1 IgG antibodies (figure 4C). ELISpot revealed that splenocytes from ENO1-vaccinated mice displayed a significantly higher number of IFN-γ-secreting cells, which was increased in the GEM+ENO1 group (figure 4E). These results were confirmed when syngeneic PDA murine DT6606 cells were used as a stimulus (not shown). GEM+ENO1 treatment caused an increase of both IgG production and IFN-γ secretion specific to G3P, enhancing the epitope spreading effect of ENO1 (figure 4D and F). No increase in anti-K2C8 or anti-FUBP1 IgG and IFN-γ was observed in GEM+ENO1-treated mice (data not shown).

Immunohistochemistry demonstrated that only GEM+ENO1 caused a significant increase of tumor-infiltrating CD4 and CD8 T cells (figure 4G–H and online supplemental figure 5B,C). Compared with untreated mice, an increase of macrophage infiltration was observed in ENO1-vaccinated mice, but not in GEM or GEM+ENO1 treated mice (figure 4I and online supplemental figure 5D). No differences in PD-L1 and FoxP3 expression were observed in tumor lesions among the different groups (data not shown). At 24 weeks, GEM+ENO1 mice showed a significant reduction of circulating CD4 and CD8 T cells, which supported the increased infiltration of these cells in tumor lesions (online supplemental figure 5E,F). In the GEM+ENO1 group, a significant correlation between CD4 and CD8 infiltration was observed (online supplemental figure 5G). Depletion of CD4, but not of CD8 or B cells, completely reverted the antitumor effect of the combined treatment (figure 4L). Anti-ENO1 IgG titers decreased significantly in all subset-depleted mice (online supplemental figure 5H). Finally, a significant delay of the growth of established 0.2 cm tumors was observed in GEM+ENO1 treated mice (figure 4M).

DISCUSSION

It has been established that CT and radiotherapy enhance the antitumor immune response.[21–24] In particular, GEM reduces the amount of MDSC, whereas it favors tumor-associated macrophage polarization to M1, and enhances cytotoxic T lymphocyte function, MHC-I expression by cancer cells, antigen cross-presentation by dendritic cells following GEM-induced apoptosis and increases CCL/CXCL chemokines.[25–29] Here, we demonstrated that, in patients with PDA, CT induced a progressive increase of autoantibodies to many self-TAA, indicating a robust antigenic spreading. To date, antigen spreading has been documented in clinical trials using mesothelin CAR T cells in patients with PDA.[30] Our data showed that antigen spreading is induced by ENO1 vaccination and further increased in combination with GEM, eliciting antibody and T cell responses to G3P.

Many TAA recognized by patients' autoantibodies are highly expressed in PDA (online supplemental figure 3 and supplemental table 3) suggesting their role in PDA development. We showed that after CT, antibodies to ENO1, G3P and K2C8 were increased in just a subset of patients, and additional studies are therefore needed to evaluate whether the increased antibody response to TAA is a useful tool to stratify patients for response to CT.

High ENO1 expression, as well as the specific autoantibody production, has been previously reported in patients with PDA and associated with a more favorable clinical outcome.[20 31] The increase of CDC induced by sera of patients with PDA after CT, which we have documented, could explain the positive correlation between survival and the increased antibody response to G3P and K2C8. In fact, autoantibodies to these TAA predict the patient's outcome in various malignancies.[32–36] However, there is no possibility of comparing the presence of antibodies to K2C8 and G3P in a cohort of untreated patients with PDA to demonstrate the role of CT in these phenomena. This issue requires addressing in a separate study in a PDA mouse model.

The immunosuppressed PDA microenvironment and the consequent T cell exhaustion play a role in

J Immunother Cancer: first published as 10.1136/jitc-2020-001071 on 28 October 2020. Downloaded from http://jitc.bmj.com/ on July 13, 2021 by guest. Protected by copyright.

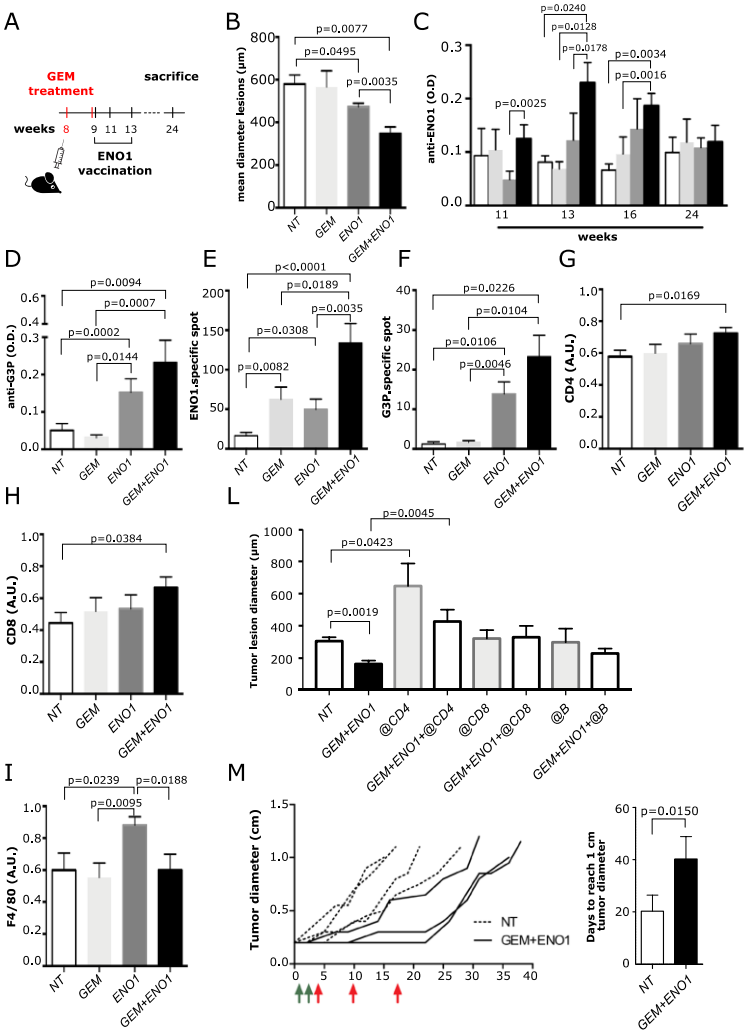

Figure 4 Effect of combination of GEM and ENO1 vaccination in KC mice. (A) Schematic representation of mice treatment schedule. (B) Evaluation of the mean of tumor lesion diameter in treated mice sacrificed at 24 weeks of age. (C) ELISA detection of anti-ENO1 IgG titer (referred to as OD) in sera of mice throughout the treatment period. The experimental groups are indicated as follows: untreated (NT, white bars), GEM (light gray bars), ENO1 (dark gray) and GEM+ENO1 (black bars). (D) ELISA detection of anti-G3P IgG antibody (referred to as OD) in mice at 16 weeks of age. (E,F) ELISpot analysis of IFN-γ-secreting cells (indicated as number of specific spots) in the different treated groups at sacrifice after restimulation with ENO1 (E) or G3P (F) recombinant protein. (G–I) Immunohistochemical staining of CD4 (G), CD8 (H) and macrophages (I) in tumor lesions of mice at sacrifice. (L) Effect of the depletion of CD4, CD8 and B subsets in GEM+ENO1 or untreated mice, evaluated as the mean of tumor lesion diameter. (M) The spaghetti plot indicates the effect of combined treatment (GEM, green arrows; ENO1 vaccination, red arrows) on tumor growth, measured as tumor diameter. Treatment started when the mass of K8484 tumor cells injected subcutaneously reached 0.2 cm in diameter. The bar graph indicated the days required by the tumor mass to reach 1.0 cm of diameter in control and GEM+ENO1 experimental groups. In all experiments, the mice number per group was between 5 and 11; graphs report the mean±SEM values and statistical significance is shown. GEM, gemcitabine; OD, optical density.

immune-resistance.[37–39] We have shown that CT increased TAA-induced effector responses and enhanced the number of TAA recognized by each patient with PDA, which is only partially associated with T cell proliferation.

In this study, we demonstrated that the combination of CT with ENO1 vaccination elicits a strong antitumor activity in KC mice. However, ENO1 vaccination and combined treatment seem to be much more effective

J Immunother Cancer: first published as 10.1136/jitc-2020-001071 on 28 October 2020. Downloaded from http://jitc.bmj.com/ on July 13, 2021 by guest. Protected by copyright.

in reducing PanIN lesions rather than invasive PDA. We are aware that treating KC mice at 8 weeks of age, when only PanIN lesions were present[40] does not recapitulate the human scenario. As advanced, metastatic tumors are diagnosed in most patients with PDA, treating premalignant lesions (PanIN) with IT, in combination with CT, remains a difficult task. However, our data from patients with PDA that show that CT increases the coordinated immune response to TAA may open a therapeutic window for patients with PDA, which deserves to be evaluated for precision IT by targeting one or more TAA that are recognized.

In this study, combination of just one cycle of GEM with ENO1 DNA vaccination reduced PDA lesions compared with ENO1 vaccination alone. The combined treatment also induced antibodies and T cell responses to G3P. While in patients with PDA, antigen spreading involved a progressive increase in the number of TAA recognized by autoantibodies after CT, in mice, increased humoral and cellular recognition to G3P was induced by ENO1 vaccination and was further increased by CT. The epitope spreading effect involved G3P, but not K2C8 and FUBP1, suggesting possible differences in the potential tumor clonality of this model. We cannot rule out that, after combined therapy, the selected tumor cell clones lose K2C8 and FUBP1 expression or increase the expression of other TAA in addition to G3P.

The combined treatment caused a significant increase of infiltration of CD4 and CD8 T cells into tumor lesions, which was associated with a decrease of circulating CD4 and CD8 T cells. In PDA, CT induced the infiltration of CD4 and CD8 T cells to the tumor and correlated with a longer survival in patients, probably because it induced the death of immunogenic tumor cells.[37 41 42] This is in agreement with our data showing that the CD4 and CD8 T cell infiltrate persisted for 3 months after the final vaccination in the GEM+ENO1 group.

Oncolytic virus increased the expression of PD-L1 via induction of IFN-γ, enhancing the effectiveness of combined administration with anti PD-L1 antibody.[43] We did not observe any differences in FoxP3 and PD-L1 in tumor lesions of mice at 24 weeks of age (data not shown). ENO1-restimulated splenocytes from vaccinated mice produced IFN-γ, and to a greater extent in combined treated mice, suggesting that PD-L1 expression was probably not affected. However, we cannot rule out that IFN-γ-induced overexpression of PD-L1 occurred at an earlier time after vaccination. It will be interesting to evaluate the effect of the combination of PD-L1 antibody with CT and ENO1 vaccination.

Macrophages are associated with poor prognosis in PDA[44] and secrete soluble factors that induce GEM resistance.[45 46] Combination therapy did not affect the number of tumor-infiltrating macrophages, suggesting that it prevalently promotes T cell-mediated immunity. We cannot rule out, however, that a different functional polarization in macrophages (eg, M1 versus M2) can be induced by combination therapy. Tumor lesions increase in mice treated with combined therapy and anti-CD4 antibody, unveiling a role for CD4 T cells in GEM+ENO1 treatment in delaying PDA growth. While some reports showed that effective tumor immunity can occur in the absence of CD4 helper T cells, most indicated that CD4 T cells are important for generating tumor-specific CD8 T cells.[47]

Our results are in agreement with data from many vaccination models which show that CD4 T cells play a critical role in inducing antitumor immunity.[48–50] Most of the identified TAA were intracellular and loaded onto MHC class II by antigen-presenting cells after phagocytosis of dying PDA cells exposed to CT.[25–28] Generation of CD4 T cells specific for TAA favors the production of specific IgG by B cells (and favors CDC) and the generation of cytotoxic T lymphocytes by CD8 T cells.[10 46] This supports the notion that the single depletion of these subsets only partially rescues tumor growth. The pivotal role of CD4 in this model is also shown by the observation that depletion of CD4 cells in untreated mice leads to very aggressive growth of tumors. Even if the type of CD4 T cells depleted in GEM+ENO1 treated mice is unknown, it is likely that the subset that was predominantly depleted consisted of T helper 1 and T helper 17 cells, in agreement with present and previous studies.[10] These data are in agreement with those from the analysis of the effector phase of tumor rejection induced by vaccination, indicating a far broader role for $CD4^+$ T cells in orchestrating the host response to tumors.[51] This consists of the simultaneous induction of Th1 and Th2 cytokines, which activate eosinophils as well as macrophages to produce both superoxide and nitric oxide that leads to the induction of systemic antitumor immunity as well as tumor destruction within the growth site.[51]

In conclusion, our profiling of the immune response in patients with PDA, together with the preclinical mouse model validation, provide a proof-of-concept that CT combined with TAA vaccination may offer a promising solution for novel PDA treatments.

Author affiliations
[1]Department of Molecular Biotechnology and Health Sciences, University of Turin, Turin, Italy
[2]Centro Ricerche Medicina Sperimentale, Azienda Ospedaliero Universitaria Città della Salute e della Scienza di Torino, Turin, Italy
[3]Computer Science Department, University of Turin, Turin, Italy
[4]Department of Surgical Sciences, University of Turin, Torino, Italy
[5]Centro Oncologico Ematologico Subalpino, Azienda Ospedaliero Universitaria Città della Salute e della Scienza di Torino, Torino, Italy
[6]Servizio di Epidemiologia Clinica, Azienda Ospedaliero Universitaria Città della Salute e della Scienza di Torino, Torino, Italy

Acknowledgements We thank Roberta Curto for technical support in the in vivo experiments and Dr Radhika Srinivasan for critically reading the manuscript.

Contributors GM and CC designed and performed the majority of experiments, interpreted the results, generated the figures and tables, and wrote the manuscript. CC and PC analyzed immunohistochemical staining. EM performed proteomic analysis. MP, SB and DV performed the in vitro experiments. AE, LF, GF, and FC performed the biostatistics analysis of the patients with PDA and analyzed the results. MAS, RS, and DG recruited patients with PDA. PC supervised and designed the in vivo experiments, interpreted the results, and wrote the

J Immunother Cancer: first published as 10.1136/jitc-2020-001071 on 28 October 2020. Downloaded from http://jitc.bmj.com/ on July 13, 2021 by guest. Protected by copyright.

manuscript. FN supervised the study, interpreted the results, and wrote the manuscript.

Funding This work was supported by grants from the Associazione Italiana Ricerca sul Cancro (5×mille no. 12182 to FN, IG no. 15257 to FN); University of Turin-Progetti Ateneo 2014-Compagnia di San Paolo (PC-METAIMMUN-OTHER to FN and PANTHER to PC); Italian Ministry of Health-Progetti Ricerca Finalizzata (RF-2013–02354892 to FN); Fondazione Ricerca Molinette Onlus (Funds CD38 and Associazione Ursula e Giorgio Cytron); and the Fondazione Nadia Valsecchi.

Competing interests None declared.

Patient consent for publication Not required.

Ethics approval The protocol for human samples was approved by the local research ethics committee (Azienda Ospedaliera Città della Salute e della Scienza di Torino, Turin), and investigations were performed according to the Helsinki Declaration principles. All participants in the protocol signed a declaration of informed consent. Mice were bred and maintained under saprophytic and pathogen-free conditions at the animal facilities of the Molecular Biotechnology Center (Turin) and treated in accordance with EU and institutional guidelines.

Provenance and peer review Not commissioned; externally peer reviewed.

Data availability statement Data are available on reasonable request. All data relevant to the study are included in the article or uploaded as supplementary information. All data generated during this study are included in this published article and its supplementary information files.

Supplemental material This content has been supplied by the author(s). It has not been vetted by BMJ Publishing Group Limited (BMJ) and may not have been peer-reviewed. Any opinions or recommendations discussed are solely those of the author(s) and are not endorsed by BMJ. BMJ disclaims all liability and responsibility arising from any reliance placed on the content. Where the content includes any translated material, BMJ does not warrant the accuracy and reliability of the translations (including but not limited to local regulations, clinical guidelines, terminology, drug names and drug dosages), and is not responsible for any error and/or omissions arising from translation and adaptation or otherwise.

Open access This is an open access article distributed in accordance with the Creative Commons Attribution Non Commercial (CC BY-NC 4.0) license, which permits others to distribute, remix, adapt, build upon this work non-commercially, and license their derivative works on different terms, provided the original work is properly cited, appropriate credit is given, any changes made indicated, and the use is non-commercial. See http://creativecommons.org/licenses/by-nc/4.0/.

ORCID iDs
Paola Cappello http://orcid.org/0000-0002-5321-7794
Francesco Novelli http://orcid.org/0000-0002-6259-5666

REFERENCES

1 Tempero MA. Multidisciplinary management of pancreatic cancer. *J Natl Compr Canc Netw* 2015;13:700–2.
2 Gravitz L. Cancer immunotherapy. *Nature* 2013;504:S1.
3 Nishida S, Ishikawa T, Egawa S, *et al*. Combination gemcitabine and WT1 peptide vaccination improves progression-free survival in advanced pancreatic ductal adenocarcinoma: a phase II randomized study. *Cancer Immunol Res* 2018;6:320–31.
4 Brahmer JR, Tykodi SS, Chow LQM, *et al*. Safety and activity of anti-PD-L1 antibody in patients with advanced cancer. *N Engl J Med* 2012;366:2455–65.
5 Feig C, Jones JO, Kraman M, *et al*. Targeting CXCL12 from FAP-expressing carcinoma-associated fibroblasts synergizes with anti-PD-L1 immunotherapy in pancreatic cancer. *Proc Natl Acad Sci U S A* 2013;110:20212–7.
6 Apte MV, Wilson JS, Lugea A, *et al*. A starring role for stellate cells in the pancreatic cancer microenvironment. *Gastroenterology* 2013;144:1210–9.
7 Olive KP, Jacobetz MA, Davidson CJ, *et al*. Inhibition of Hedgehog signaling enhances delivery of chemotherapy in a mouse model of pancreatic cancer. *Science* 2009;324:1457–61.
8 Clark CE, Hingorani SR, Mick R, *et al*. Dynamics of the immune reaction to pancreatic cancer from inception to invasion. *Cancer Res* 2007;67:9518–27.
9 Xu C, Sui S, Shang Y, *et al*. The landscape of immune cell infiltration and its clinical implications of pancreatic ductal adenocarcinoma. *J Adv Res* 2020;24:139–48.
10 Cappello P, Rolla S, Chiarle R, *et al*. Vaccination with ENO1 DNA prolongs survival of genetically engineered mice with pancreatic cancer. *Gastroenterology* 2013;144:1098–106.
11 Cappello P, Tonoli E, Curto R, *et al*. Anti-α-enolase antibody limits the invasion of myeloid-derived suppressor cells and attenuates their restraining effector T cell response. *Oncoimmunology* 2016;5:e1112940.
12 Principe M, Ceruti P, Shih N-Y, *et al*. Targeting of surface alpha-enolase inhibits the invasiveness of pancreatic cancer cells. *Oncotarget* 2015;6:11098–113.
13 Principe M, Borgoni S, Cascione M, *et al*. Alpha-Enolase (ENO1) controls alpha v/beta 3 integrin expression and regulates pancreatic cancer adhesion, invasion, and metastasis. *J Hematol Oncol* 2017;10:16.
14 Castino GF, Cortese N, Capretti G, *et al*. Spatial distribution of B cells predicts prognosis in human pancreatic adenocarcinoma. *Oncoimmunology* 2016;5:e1085147.
15 Mantovani A, Allavena P. The interaction of anticancer therapies with tumor-associated macrophages. *J Exp Med* 2015;212:435–45.
16 Zitvogel L, Kepp O, Kroemer G. Immune parameters affecting the efficacy of chemotherapeutic regimens. *Nat Rev Clin Oncol* 2011;8:151–60.
17 Di Caro G, Cortese N, Castino GF, *et al*. Dual prognostic significance of tumour-associated macrophages in human pancreatic adenocarcinoma treated or untreated with chemotherapy. *Gut* 2016;65:1710–20.
18 Mandili G, Alchera E, Merlin S, *et al*. Mouse hepatocytes and LSEC proteome reveal novel mechanisms of ischemia/reperfusion damage and protection by A2AR stimulation. *J Hepatol* 2015;62:573–80.
19 Mandili G, Marini C, Carta F, *et al*. Identification of phosphoproteins as possible differentiation markers in all-trans-retinoic acid-treated neuroblastoma cells. *PLoS One* 2011;6:e18254.
20 Tomaino B, Cappello P, Capello M, *et al*. Autoantibody signature in human ductal pancreatic adenocarcinoma. *J Proteome Res* 2007;6:4025–31.
21 Stellas D, Szabolcs M, Koul S, *et al*. Therapeutic effects of an anti-MYC drug on mouse pancreatic cancer. *J Natl Cancer Inst* 2014;106:dju320.
22 Rossi ML, Rehman AA, Gondi CS. Therapeutic options for the management of pancreatic cancer. *World J Gastroenterol* 2014;20:11142–59.
23 Homma Y, Taniguchi K, Nakazawa M, *et al*. Changes in the immune cell population and cell proliferation in peripheral blood after gemcitabine-based chemotherapy for pancreatic cancer. *Clin Transl Oncol* 2014;16:330–5.
24 Zitvogel L, Kroemer G. Subversion of anticancer immunosurveillance by radiotherapy. *Nat Immunol* 2015;16:1005–7.
25 Nishida S, Koido S, Takeda Y, *et al*. Wilms tumor gene (WT1) peptide-based cancer vaccine combined with gemcitabine for patients with advanced pancreatic cancer. *J Immunother* 2014;37:105–14.
26 Suzuki E, Kapoor V, Jassar AS, *et al*. Gemcitabine selectively eliminates splenic Gr-1+/CD11b+ myeloid suppressor cells in tumor-bearing animals and enhances antitumor immune activity. *Clin Cancer Res* 2005;11:6713–21.
27 Galluzzi L, Buqué A, Kepp O, *et al*. Immunological effects of conventional chemotherapy and targeted anticancer agents. *Cancer Cell* 2015;28:690–714.
28 Nowak AK, Lake RA, Marzo AL, *et al*. Induction of tumor cell apoptosis in vivo increases tumor antigen cross-presentation, cross-priming rather than cross-tolerizing host tumor-specific CD8 T cells. *J Immunol* 2003;170:4905–13.
29 Principe DR, Narbutis M, Kumar S, *et al*. Long-Term gemcitabine treatment reshapes the pancreatic tumor microenvironment and sensitizes murine carcinoma to combination immunotherapy. *Cancer Res* 2020;80:3101–15.
30 Beatty GL, O'Hara MH, Lacey SF, *et al*. Activity of Mesothelin-Specific chimeric antigen receptor T cells against pancreatic carcinoma metastases in a phase 1 trial. *Gastroenterology* 2018;155:29–32.
31 Tomaino B, Cappello P, Capello M, *et al*. Circulating autoantibodies to phosphorylated α-enolase are a hallmark of pancreatic cancer. *J Proteome Res* 2011;10:105–12.
32 Suzuki A, Iizuka A, Komiyama M, *et al*. Identification of melanoma antigens using a serological proteome approach (SERPA). *Cancer Genomics Proteomics* 2010;7:17–23.
33 Takashima M, Kuramitsu Y, Yokoyama Y, *et al*. Proteomic analysis of autoantibodies in patients with hepatocellular carcinoma. *Proteomics* 2006;6:3894–900.
34 Wang J, Shivakumar S, Barker K, *et al*. Comparative study of autoantibody responses between lung adenocarcinoma and benign pulmonary nodules. *J Thorac Oncol* 2016;11:334–45.

J Immunother Cancer: first published as 10.1136/jitc-2020-001071 on 28 October 2020. Downloaded from http://jitc.bmj.com/ on July 13, 2021 by guest. Protected by copyright.

35 Heo C-K, Hwang H-M, Ruem A, *et al*. Identification of a mimotope for circulating anti-cytokeratin 8/18 antibody and its usage for the diagnosis of breast cancer. *Int J Oncol* 2013;42:65–74.
36 Capello M, Cappello P, Linty FC, *et al*. Autoantibodies to ezrin are an early sign of pancreatic cancer in humans and in genetically engineered mouse models. *J Hematol Oncol* 2013;6:67.
37 Guo S, Contratto M, Miller G, *et al*. Immunotherapy in pancreatic cancer: Unleash its potential through novel combinations. *World J Clin Oncol* 2017;8:230–40.
38 Bauer C, Kühnemuth B, Duewell P, *et al*. Prevailing over T cell exhaustion: new developments in the immunotherapy of pancreatic cancer. *Cancer Lett* 2016;381:259–68.
39 Tang Y, Xu X, Guo S, *et al*. An increased abundance of tumor-infiltrating regulatory T cells is correlated with the progression and prognosis of pancreatic ductal adenocarcinoma. *PLoS One* 2014;9:e91551.
40 Hingorani SR, Petricoin EF, Maitra A, *et al*. Preinvasive and invasive ductal pancreatic cancer and its early detection in the mouse. *Cancer Cell* 2003;4:437–50.
41 Fukunaga A, Miyamoto M, Cho Y, *et al*. Cd8+ tumor-infiltrating lymphocytes together with CD4+ tumor-infiltrating lymphocytes and dendritic cells improve the prognosis of patients with pancreatic adenocarcinoma. *Pancreas* 2004;28:e26–31.
42 Ino Y, Yamazaki-Itoh R, Shimada K, *et al*. Immune cell infiltration as an indicator of the immune microenvironment of pancreatic cancer. *Br J Cancer* 2013;108:914–23.
43 Ribas A, Dummer R, Puzanov I, *et al*. Oncolytic virotherapy promotes intratumoral T cell infiltration and improves anti-PD-1 immunotherapy. *Cell* 2017;170:1109–19.
44 Sugimoto M, Mitsunaga S, Yoshikawa K, *et al*. Prognostic impact of M2 macrophages at neural invasion in patients with invasive ductal carcinoma of the pancreas. *Eur J Cancer* 2014;50:1900–8.
45 Weizman N, Krelin Y, Shabtay-Orbach A, *et al*. Macrophages mediate gemcitabine resistance of pancreatic adenocarcinoma by upregulating cytidine deaminase. *Oncogene* 2014;33:3812–9.
46 Binenbaum Y, Fridman E, Yaari Z, *et al*. Transfer of miRNA in macrophage-derived exosomes induces drug resistance in pancreatic adenocarcinoma. *Cancer Res* 2018;78:5287–99.
47 Alspach E, Lussier DM, Miceli AP, *et al*. MHC-II neoantigens shape tumour immunity and response to immunotherapy. *Nature* 2019;574:696–701. 2019.
48 Park JM, Terabe M, Sakai Y, *et al*. Early role of CD4+ Th1 cells and antibodies in HER-2 adenovirus vaccine protection against autochthonous mammary carcinomas. *J Immunol* 2005;174:4228–36.
49 Sharma S, Zhu L, Yang SC, *et al*. Cyclooxygenase 2 inhibition promotes IFN-gamma-dependent enhancement of antitumor responses. *J Immunol* 2005;175:813–9.
50 Bos PD, Plitas G, Rudra D, *et al*. Transient regulatory T cell ablation deters oncogene-driven breast cancer and enhances radiotherapy. *J Exp Med* 2013;210:2435–66.
51 Hung K, Hayashi R, Lafond-Walker A, *et al*. The central role of CD4(+) T cells in the antitumor immune response. *J Exp Med* 1998;188:2357–68.

J Immunother Cancer: first published as 10.1136/jitc-2020-001071 on 28 October 2020. Downloaded from http://jitc.bmj.com/ on July 13, 2021 by guest. Protected by copyright.

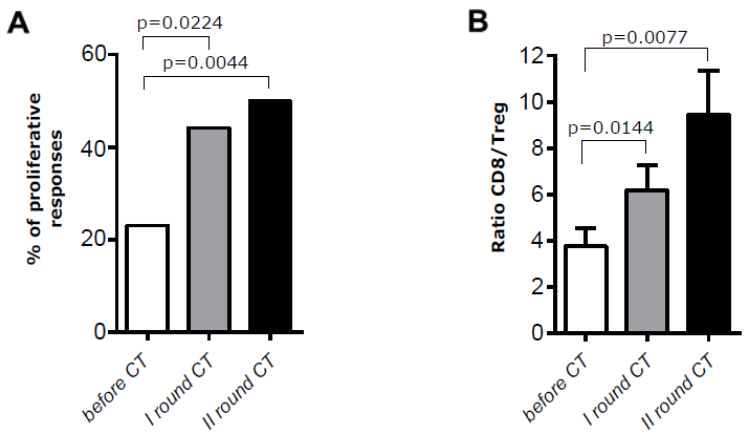

Supplementary Figure 3. A. Bar plot representing the percentage of proliferative responses (SI≥2) from 13 PDA patients' PBMC stimulated with ENO1, G3P, K2C8 and FUBP1 before and after one and two CT cycles. **B**. Ratio between CD8 and Treg (CD4 and FoxP3 double positive) evaluated by flow cytometry on five PDA patients' PBMC stimulated with ENO1, G3P, K2C8 and FUBP1 before (12 responses), after one (9 responses) and two (6 responses) CT rounds.

Chemotherapy, but not immune checkpoint blockade, enhances tumor associated antigens specific T lymphocyte effector response in patients with pancreatic ductal adenocarcinoma

Beside the active immunotherapy, many studies exploited the treatment with immune checkpoint blockade (ICB) in PDA, since important results were obtained in other types of cancer such as melanoma, increasing the survival depending on a strong induction of anti-tumor T cell response [40]. In PDA patients with deficient mismatch repair, resulting in a high number of somatic mutations, anti-PD1 has proven effective; unfortunately, these PDA patients represent only a small percentage [41]. Clinical trials with both anti-PDL1 and anti-CTL4 were not able to substantially increase the survival of PDA patients [42,43]; therefore, the need to find new strategies is increasingly urgent.

CT treatment was already demonstrated to elicit a T cell response to a given TAA [17]. Nevertheless, no data are available regarding the combination of CT with ICB as a feasible approach to unleash and sustain anti-tumor TAA-specific T cells underwent exhaustion. Thus, the purpose of this study is to investigate the Teff response of PBMC stimulated with recombinant proteins of the four preselected TAA (ENO1, FUBP1, K2C8 and G3P) in the presence or not of ICB (anti-PD1 plus anti-CTLA4 mAb) in PDA patients before and after CT treatment.

The ICB effect on the proliferative and cytokine response was evaluated in a cohort of 18 patients through *in vitro* TAA-stimulated PBMC before and after CT and in 13 healthy subjects. Clinical data of patients are reported in Table 2; only one round after CT was analyzed, indeed most of these patients were not unable to continue the CT treatment because of their poor performance status or due to their demise.

Table 2. Clinical data of PDA patients.

Patient	Gender	Age	Surgery	Stage	Metastasis	CT	Response	Survival (months)
6	F	69	Yes	III	No	GEM	PD	5.2
7	F	69	No	IIB	No	GEM	PD	3.9
11	M	54	No	IV	Yes	GEM + 5FU	PD	9.5
16	F	51	No	IV	Yes	GEM	PD	2.2
20	M	59	No	IV	Yes	GEMOX	SD	11.8
24	F	74	No	IV	Yes	GEM	PD	9.8
29	M	59	No	III	No	GEM	PD	13.4
31	F	70	No	IV	Yes	GEM	PD	3.4
32	F	73	Yes	IIB	No	GEM	PR	11.9
35	M	62	No	IV	Yes	GEM	SD	8.2
37	F	67	Yes	IV	Yes	GEM	PD	11.8
50	M	46	Yes	IIB	No	GEM	SD	20.3
51	F	49	No	IV	Yes	GEM	PD	3.1
83	M	55	Yes	IIB	No	GEM	SD	51.7
85	F	64	No	III	No	Bevacizumab+RT+CAP	PR	35.7
143	F	79	No	III	No	GEM	SD	15.0
158	M	55	No	IIB	No	GEM	PD	10.3
184	F	73	Yes	IV	Yes	GEM	PD	9.7
163	M	63	Yes	IIB	No	GEMOX	PD	12.4
186	F	73	Yes	IV	Yes	GEM	PD	34.3
10	F	74	No	IV	Yes	GEMOX	SD	16.4
99	M	96	No	IV	Yes	Folfirinox	SD	9.1
117	F	74	No	III	No	GEM+other	SD	15.2

GEM= Gemcitabine, 5FU= 5-fluorouracil, GEMOX= GEM + Oxaliplatin, RT= radiotherapy, CAP= capecitabine, PD= progression disease, SD= stable disease, PR= partial response. PBMC from underlined patients were analyzed for TRCB sequencing.

Effect of ICB on T lymphocyte proliferation in response to TAA before and after CT

To better investigate the role of ICB, the proliferation rate to TAA was subdivided in two categories. S.I. between 2 and 3 referred to a "low" proliferative response, whereas proliferation was considered "high" with S.I. ≥ 3. The proliferative response < 2 was considered as "null" (Figure 6).

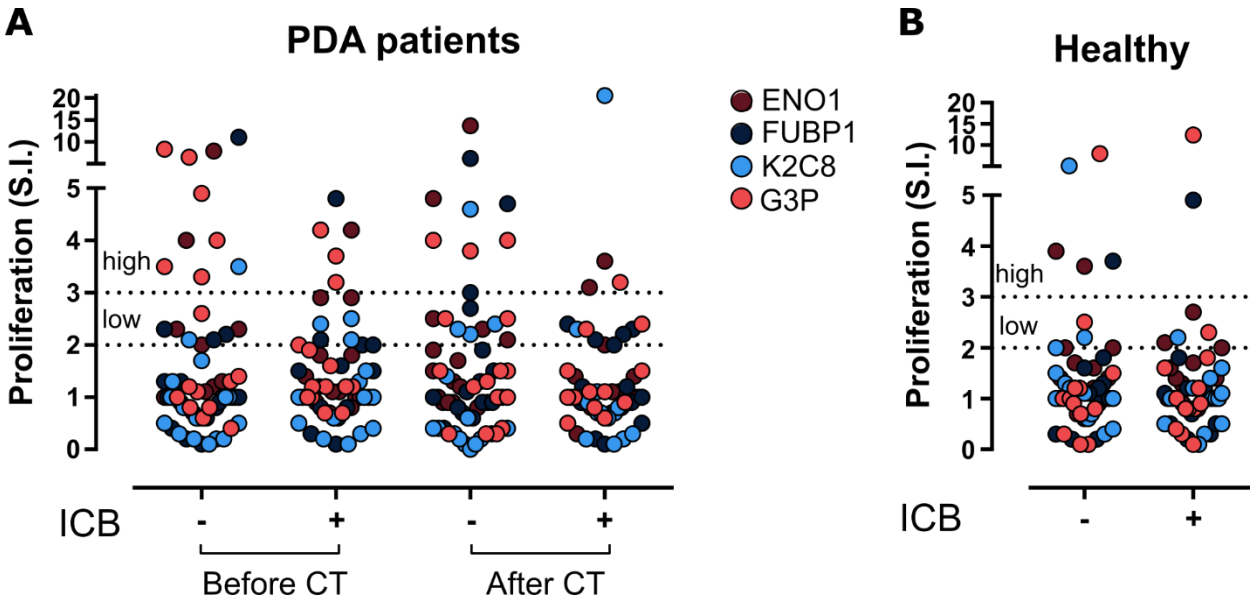

Figure 6. Effect of ICB on proliferation of TAA-activated PBMC. Stimulation Index (S.I.) of PBMC *in vitro* stimulated with TAA (ENO1, FUBP1, K2C8 or G3P) in presence of ICB from **A**. n. 16 PDA patients before and after CT (n. 14 patients in presence of ICB) and **B**. n 13 healthy subjects.

PBMC from 16 patients before CT were stimulated with ENO1, FUBP, K2C8 or G3P and among the 64 expected responses, 13% were low and 16% were highly proliferative. When 14 patients' PBMC before CT were stimulated in presence of ICB the expected responses were 56; while the low proliferative responses were slightly increased, the high responses were 42% reduced compared to the absence of ICB. After CT 16% of responses were low and 13% were high; in the presence of ICB the low proliferative responses remained univariate, but the high responses were 43% reduced.

In 13 healthy subjects the PBMC stimulation with TAA at basal condition showed, out of 52 responses, only 10% of both low and high proliferative responses. In the presence of ICB low proliferative responses remained at 10%, while high responses were halved to 4%.

The proliferation of PDA patients' PBMC to ENO1, FUBP, K2C8 and G3P was heterogeneous. PBMC showed proliferation to different numbers of TAA depending on CT time and/or the presence of ICB (Figure 7A).

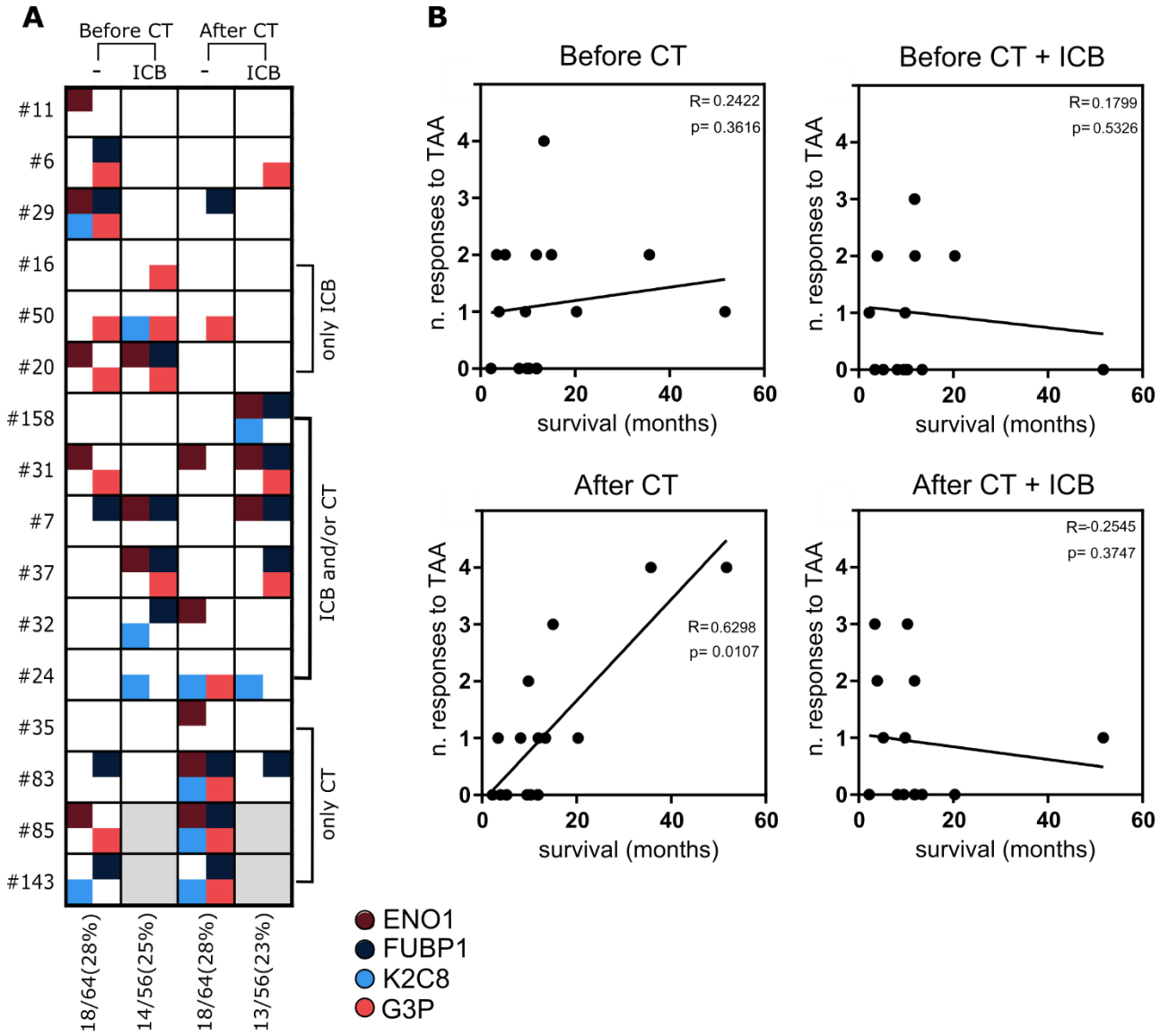

Figure 7. ICB effect on the number of TAA recognized by PBMC from PDA patients before and after CT. A. Representation of the proliferative response (S.I. ≥ 2) to the four TAA (ENO1, FUBP1, K2C8 and G3P) by each patient before and after CT, in presence or not of ICB; frequencies and percentage of proliferative responses are indicated. **B.** Correlation between the number of recognized TAA for each patient and the time survival (months); statistic was calculated with Spearman correlation.

In particular it was possible identify four categories of patients: i) those that did not show any increase in the number of TAA recognition following CT or with ICB addition; ii) those that displayed increased number of TAA recognition only in presence of ICB before CT; iii) those that displayed an increase of recognized TAA number after CT alone or in the presence of ICB, and those which

increased the number of TAA recognition only after CT alone. By contrast, only one among all the healthy subjects increased the number of recognized TAA in the presence of ICB (not shown).

The recognition of TAA number before CT alone or in presence of ICB did not display any correlation with patients' survival and the same was observed after CT in presence of ICB (Figure 7B). By contrast, a positive correlation between the number of TAA recognized by PBMC recovered after CT and the patients' survival was observed (Spearman R= 0.6298, p value= 0.0107).

These data indicate that CT did not significantly alter the proliferative response of TAA-stimulated PBMC, but ICB reduced high proliferative response in PDA patients. Of note, only patients that recognized more TAA after CT had a better survival.

Effect of ICB on IFN-γ production in response to TAA before and after CT

IFN-γ is a cytokine with a well-known anti-tumor effect produced by CTL and Th1 cells [44]. To measure the effect of ICB on anti-tumor effector response against the four TAA, the secretion of IFN-γ was also evaluated. The IFN-γ production by TAA-stimulated PBMC was categorized as null, low (< 100 pg/ml), intermediate (≥ 100 < 1000 pg/ml) and high (≥ 1000 pg/ml) (Figure 8A).

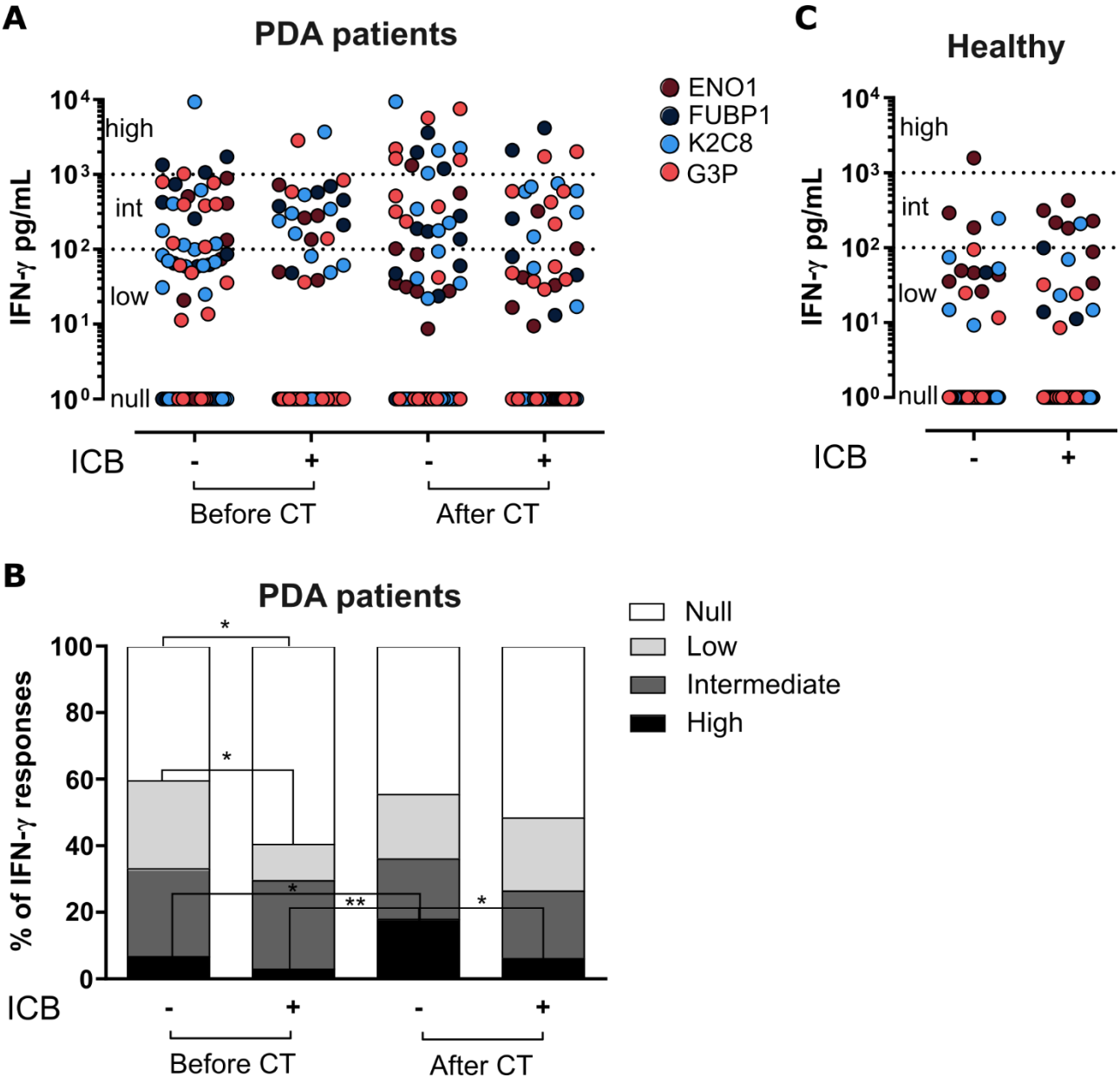

Figure 8. ICB effect on IFN-γ production from TAA-activated PBMC. A. IFN-γ levels (pg/ml) in supernatant of TAA-activated PDA patients' PBMC before and after CT (n. 18), and in presence of ICB (n. 16); null responses: no detection, low responses: < 100 pg/ml, intermediate responses: ≥ 100 < 1000 pg/ml, high responses: ≥ 1000 pg/ml. **B.** Percentage of null, low, intermediate and high responses before and after CT, in presence or not of ICB; statistics was calculated by Chi-square test. **C**. IFN-γ levels (pg/ml) of TAA-activated healthy subjects' PBMC in presence or not of ICB (n. 13).

Before CT the percentage of null responses was 39% and significantly raised 59% in the presence of ICB (Figure 8B). The percentage of low IFN-γ responses significantly decreased from 28% to 11% when ICB was added, whereas it did not affect the percentage of intermediate responses, since before CT they were about 26% with or without ICB. Instead, the high production of IFN-γ was halved from 7% to 3% in the presence of ICB before CT.

The percentage of high IFN-γ response increased significantly after CT compared to before CT, from 7% to 18%. No differences were found after CT for the null, low and intermediate IFN-γ response, since 44%, 19% and 18% response were detected respectively, and 51%, 22% and 20% of responses in presence of ICB. High IFN-γ responses after CT were significantly reduced from 18% to 6% in the presence of ICB.

PBMC from healthy subjects in response to TAA showed a prevalence of null responses (68%), while the low, intermediate and high IFN-γ responses were 25%, 6% and 2% respectively (Figure 8C). The addition of ICB did not result in any significant differences with 21%, 12% and 0 responses respectively, and the null responses remained at 67%.

These data demonstrate that in PDA patients the high production of IFN-γ in response to TAA is better induced after CT and particularly in the absence of ICB.

Effect of ICB and CT on immunological tone of TAA-stimulated PBMC: classification in subgroups of responses

To understand the immunological tone of the TAA-stimulated PBMC, the production of IL-10 was also measured and the ratio between IFN-γ and IL-10 production was evaluated, allowing to evaluate the effects of CT and ICB on the balance between functional and regulatory tone.
The predominance of IFN-γ was considerate as an effector like response (IFN-γ/IL10 ratio > 1 in red); while the regulatory like response was characterized by the predominance of IL-10 (IFN-γ/IL10 ratio < 1 values in blue) (Figure 9).

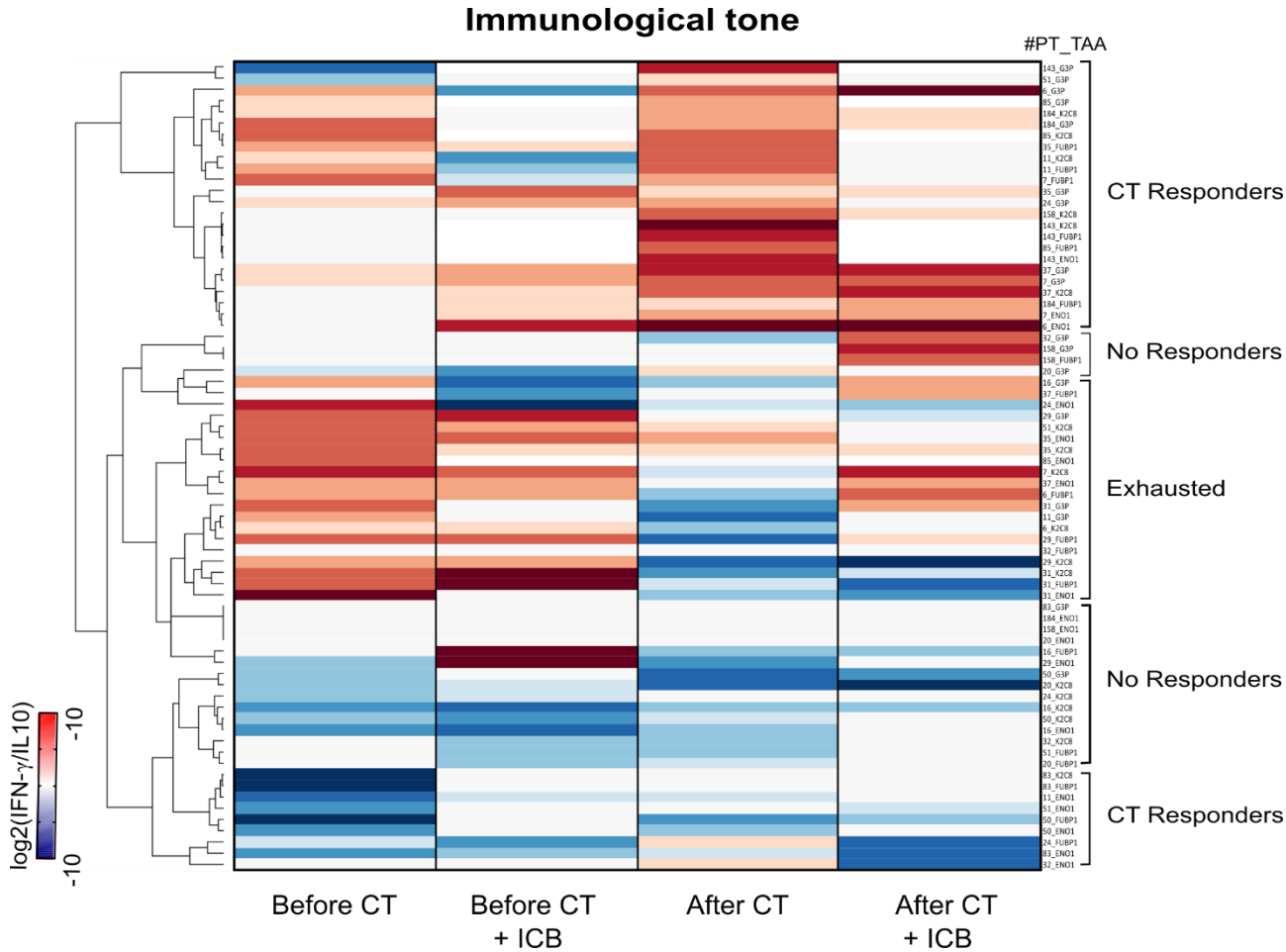

Figure 9. **Hierarchical clustering analysis of IFN-γ and IL10 ratio of TAA-activated PBMC from PDA patients before and after CT, in presence or not of ICB.** Cytokine production was detected by ELISA and the ratio between IFN-γ and IL-10 was measured. Heat map representing the ratio of cytokine response of patients' PBMC stimulated with ENO1, G3P, K2C8 and FUBP1 (#PT_TAA) in absence of ICB (18 patients: 72 responses) and in presence of ICB (16 patients: 64 responses), before and after the CT treatment. IFN-γ predominant production is shown in red, whereas blue indicates more abundant IL-10 production.

Clustering analysis of the immunological tone identified three groups of responses: i) “No responders” that displayed a greater regulatory tone, that in some cases could be decreased by ICB; ii) “Exhausted” that displayed a greater functional tone before CT, maintained with ICB addition in some cases but decreased after CT; iii) “CT responders”, that displayed a greater functional tone mostly after CT (Figure 9).

Before CT the 17% of patients (pt 6, 31 and 35) displayed an effector response against all the four TAA; 22% of patients against three (pt 7, 11, 29 and 85) and two (pt 24, 37, 143 and 184) TAA; 11% of patients (pt 16 and 51) against only one TAA and PBMC from 28% of patients (pt 20, 32, 50, 83 and 158) did not showed an effector response to any TAA (Table 3).

Table 3. Number of TAA with effector and shifted to effector responses by PDA patients’ PBMC before and after CT, in presence or not of ICB.

	Effector response	**Shift to effector response**		
Patients	Before CT	ICB only	CT only	CT+ICB
6	4	1	2	**3**
7	3	2	2	2
11	3	1	**3**	0
16	1	1	1	**3**
20	0	1	1	0
24	2	2	**3**	1
29	3	**2**	0	0
31	4	**2**	0	0
32	0	0	**1**	**1**
35	4	1	1	1
37	2	1	2	**3**
50	0	0	**2**	1
51	1	0	**2**	0
83	0	1	**3**	0
85	3	NA	3	NA
143	2	NA	4	NA
158	0	0	1	**3**
184	2	1	**2**	**2**
	69% (11/16)	**13% (2/16)**	**69% (11/16)**	
	% of patients with one or more responsive TAA	% of patients with the greater number of responsive TAA		

The effect of ICB and/or CT was evaluated considering the shift of immunological tone to a more intense effector response, namely when the IFN-γ/IL-10 ratio increased compared to before CT, and the higher number of responsive TAA for each patient is reported in bold in Table 3. The 13% of patients (pt 29 and 31) displayed a higher number of responsive TAA adding the ICB before CT. By contrast the percentage of patients who achieved the greater number of responsive TAA after CT was 31% (pt 11, 24, 50, 51 and 83) and 25% if ICB was added (pt 6, 16, 37 and 158). Patients 32 and 184 showed the same number of responsive TAA after CT and in combination with ICB, but still

higher compared to the only ICB. Whereas patients 7, 20 and 35 did not display any differences in the number of responsive TAA between ICB only and after CT. PBMC from patients 85 and 143 were not tested in ICB condition, however CT could increase the effector tone to three and four TAA respectively.

To summarize, CT alone or in combination with ICB could shift the PBMC effector response to a greater number of TAA in 69% of the patients, significantly higher compared to the 13% of patients with ICB only (p value=0,0012 CHI square test).

Profiling of ENO1-specific clonotypes by TCRB sequencing of PBMC in PDA patients before and after CT

Together with the proliferation also the potential role of CT in modifying the expansion of TAA-specific clones was investigated. PBMC from 6 PDA patients before and after CT were *in vitro* stimulated with ENO1. The profiling of the TCRB was performed by the NGS approach on mRNA extracted from PBMC. Patients' clinical data are reported in Table 2.

Each clone, characterized by a different CDR3 region, is indicated as "clonotype" and it corresponds to a specific V(D)J rearrangement; of note, more than one clonotype can correspond to the same V(D)J rearrangement.

The frequency of each clonotype present with ENO1 stimulation (ENO1) was compared to the frequency measured in the basal condition (medium) by subtraction of the clonotype proportion. Only the clonotypes with a significant variation were considered.

One representative patient is shown in Figure 10. Patient 10 displayed only two clonotypes with a significant ENO1-dependent variation both before and after CT (underlined in green), one clonotype shifted from an ENO1-contracted to ENO-1-expanded trend, whereas the other one maintained the same ENO1-expanded trend but with a greater extent after CT. In addition to those in common, before CT were observed three clonotypes with significant differences (underlined in black), two were ENO1-contracted and one was ENO1-expanded. After CT instead six significant different clonotypes (underlined in red) were found, only one was ENO1-contracted and five were ENO1-expanded. Globally patient 10 showed 7 clonotypes with a grater expansion after CT (red arrows), and only one clonotype before CT (black arrow).

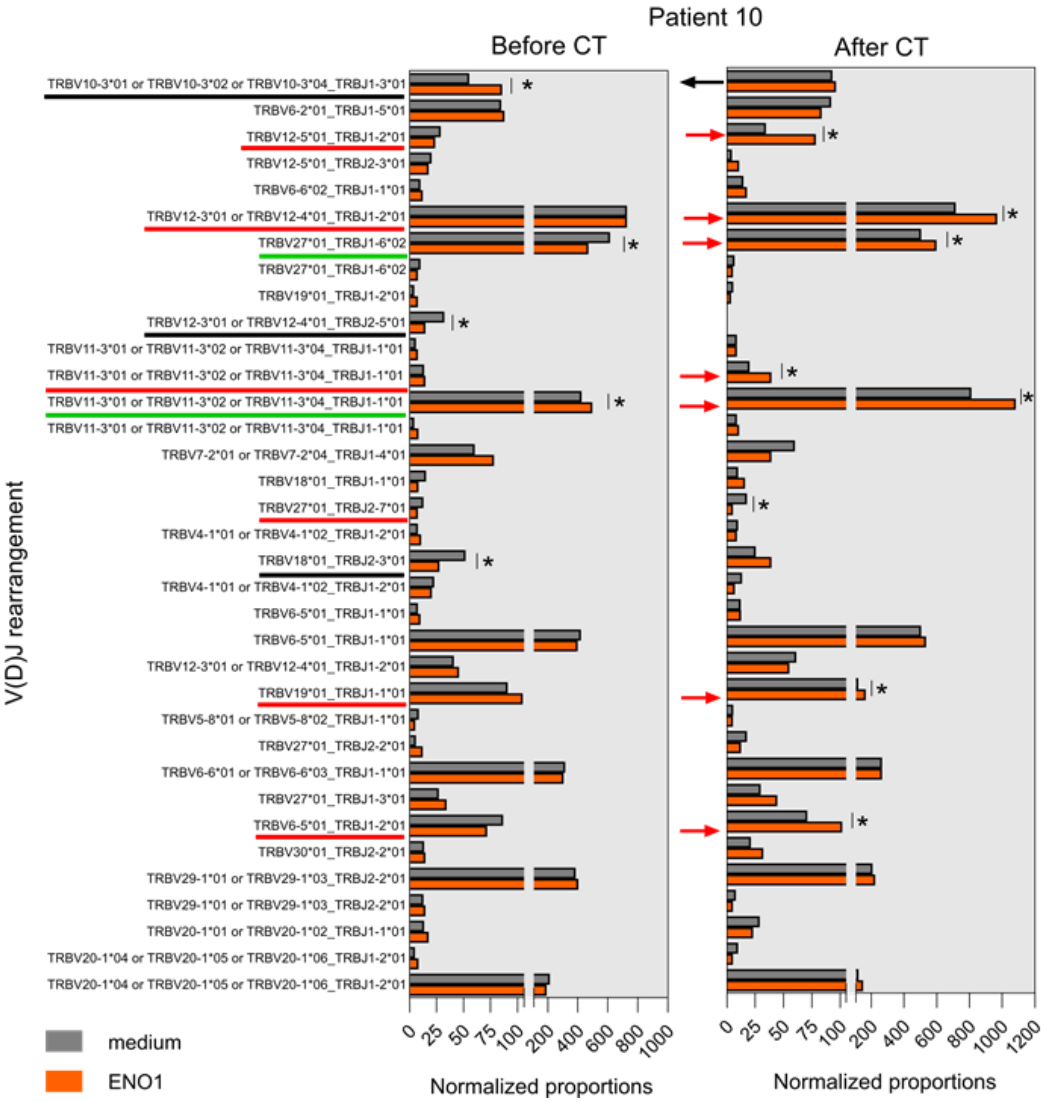

Figure 10. Difference in the frequency of significant TCRB clonotypes with ENO1 stimulation before and after CT. Bar plots show for each clonotype the normalized proportion every 10000 clones from the representative patient 10. Statistically significant ENO1-dependent expansion or contraction are indicated. Statistics were calculated with Chi-square test.

The other patients 32, 186, 163, 99 and 117 showed respectively thirteen, four, eight, six and six clonotypes with significant ENO1-dependent expansion before CT; whereas after CT were observed respectively seven, zero, eight, zero and five significant ENO1-expanded clonotypes (Figure 11, Table 4). Before CT in the same patients were observed respectively zero, two, eight, zero and ten clonotypes with significant ENO1-dependent contraction, while after CT they showed respectively zero, one, seven, eight and four significant ENO1-contracted clonotypes (Figure 11, Table 4).

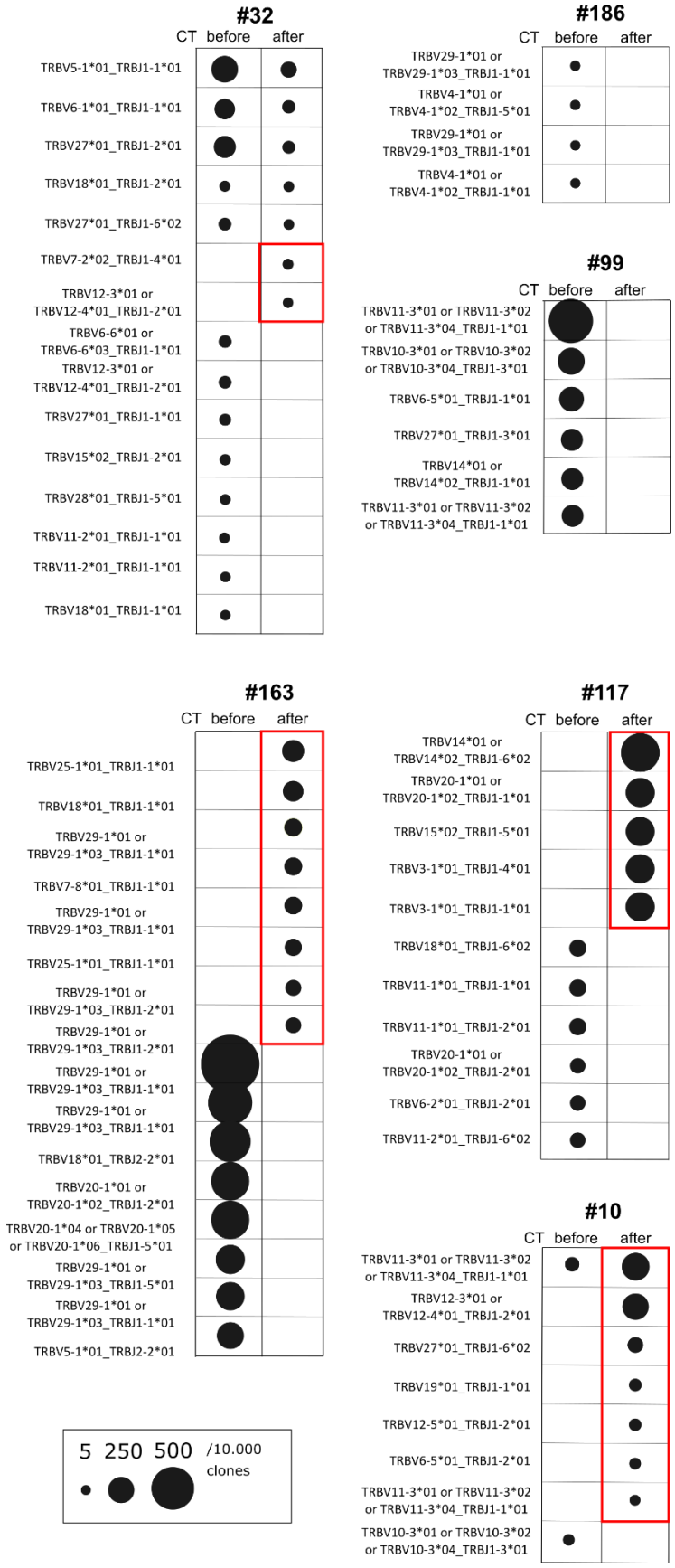

Figure 11. Statistically significant ENO1-dependent expansion before and after CT. List of clonotypes significantly expanded following ENO1 stimulation before and after CT. Each circle represents a unique V(D)J rearrangement, and its dimension indicates the delta of clones' number between ENO1 stimulation and medium.

Table 4. List of unique clonotypes from PBMC following ENO1-stimulation in 6 PDA patient before and after CT.

V(D)Jrearrangement	CDR3	CT	32		163		186		10		99		117	
			before	after	before	after	before	after	before	after	before	after	before	after
TRBV10-3*01 or TRBV10-3*02 or TRBV10-3*04_TRBJ1-2*01	AISESPGVYGYT													
TRBV10-3*01 or TRBV10-3*02 or TRBV10-3*04_TRBJ1-3*01	**AIRQDLSGNTIY**													
	AIRQDLSGNTIY													
TRBV11-1*01_TRBJ1-1*01	ASSLEHNEAF													
TRBV11-1*01_TRBJ1-2*01	ASSLAGNGYT													
TRBV11-2*01_TRBJ1-1*01	ASSLGENTEAF													
TRBV11-2*01_TRBJ1-4*01	ASSLWSTNEKLF													
TRBV11-2*01_TRBJ1-6*02	ASSSQLSGTPEGVYNSPLH													
	ASSPRGSSYNSPLH													
TRBV11-3*01 or TRBV11-3*02 or TRBV11-3*04_TRBJ1-1*01	**ASSLDLTGNTEAF**													
	ASSLDLTGNTEAF													
	ASSLDLTGNTEAF													
	ASSLDLTGHTEAF													
	ASSLDPTGNTEAF													
TRBV12-3*01 or TRBV12-4*01_TRBJ1-2*01	ASSPDSYGYT													
	ASSPYTYGYT													
	ASSFGGASGYT													
TRBV12-3*01 or TRBV12-4*01_TRBJ2-5*01	ASSLAGGEETQY													
TRBV12-5*01_TRBJ1-2*01	ASGLVPGQTHGYT													
TRBV14*01 or TRBV14*02_TRBJ1-1*01	ASSPPLGFNTEAF													
	ASSQDYGRDTEAF													
	ASSRERLTGNTEAF													
TRBV14*01 or TRBV14*02_TRBJ1-2*01	ASSPSGQGYGYT													
TRBV14*01 or TRBV14*02_TRBJ1-4*01	ASSPVNDDEKLF													
TRBV14*01 or TRBV14*02_TRBJ1-6*02	ASSQDSDWRGYGNSPLH													
TRBV14*01 or TRBV14*02_TRBJ1-6*02	ASSATGTIVPNSPLH													
TRBV15*02_TRBJ1-2*01	ATSRDIQGGGYT													
TRBV15*02_TRBJ1-5*01	ATSRDPAGDQPQH													
TRBV18*01_TRBJ1-1*01	ASSPERGRTEAF													
	ASSPRQGAGAATEAF													
	ASSPAGTEAF													
	ASSPDMNTEAF													
	ASSPLGSKNTEAF													
	ASSPLAGTAEAF													
	ASSAGTANTEAF													
TRBV18*01_TRBJ1-2*01	ASSPGLSLYGYT													
TRBV18*01_TRBJ1-6*02	ASSPGMDNSPLH													
TRBV18*01_TRBJ2-2*01	ASSPAGTGELF													
TRBV18*01_TRBJ2-3*01	ASSQRFTDTQY													
TRBV19*01_TRBJ1-1*01	ASSVGHTNTEAF													
TRBV19*01_TRBJ1-2*01	ASSRNYGYT													
TRBV2*01 or TRBV2*02_TRBJ1-6*01	ASSSYGGSPLH													
TRBV20-1*01 or TRBV20-1*02_TRBJ1-1*01	SATGGTEAF													
	SAQPENTEAF													
TRBV20-1*01 or TRBV20-1*02_TRBJ1-2*01	SAVREDGGYGYT													
	SARDWDRRSGYT													
TRBV20-1*04 or TRBV20-1*05 or TRBV20-1*06_TRBJ1-5*01	SARDPGTGNNQPQH													
TRBV23-1*01_TRBJ1-5*01	ASSRPIQGVGQPQH													
TRBV25-1*01_TRBJ1-1*01	ASTKLTEAF													
TRBV25-1*01_TRBJ1-1*01	ASSSDRVNTEAF													
TRBV27*01_TRBJ1-1*01	ASSSTAAAEAF													
TRBV27*01_TRBJ1-2*01	ASSLLPDPANYGYT													
TRBV27*01_TRBJ1-3*01	ASSYRGGNTIY													
TRBV27*01_TRBJ1-6*02	ASSLSFGRRYSNSPLH													
	ASSFTYARDRNGSPLH													
TRBV27*01_TRBJ2-7*01	ASSPTVAWEQY													
TRBV28*01_TRBJ1-5*01	ASSFQGSGHNQPQH													
TRBV28*01_TRBJ1-6*02	ASSPQDTRSYNSPLH													
TRBV29-1*01 or TRBV29-1*03_TRBJ1-1*01	SAKRQVNTEAF													
	SVDREQGEESTEAF													
	SVVGARRVAEAF													
	SVSLNTEAF													
	SVQINTEAF													
	SVPGPGQREAF													
	SVERGGRVNTEAF													
	SVEEEENTEAF													
	SLQGLSNTEAF													
	SGGEEEAF													
TRBV29-1*01 or TRBV29-1*03_TRBJ1-2*01	SVLTGTAGYT													
TRBV29-1*01 or TRBV29-1*03_TRBJ1-2*01	SAPYGGLFNYGYT													
TRBV29-1*01 or TRBV29-1*03_TRBJ1-3*01	SAPSGNTIY													
TRBV29-1*01 or TRBV29-1*03_TRBJ1-4*01	SVEYSATNEKLF													
TRBV29-1*01 or TRBV29-1*03_TRBJ1-5*01	SVAGQLDQPQH													
	SVGLRGGNQPQH													
TRBV29-1*01 or TRBV29-1*03_TRBJ2-2*01	SVELGLSTGELF													
TRBV29-1*01 or TRBV29-1*03_TRBJ2-2*01	SGRGPSGELF													
TRBV3-1*01_TRBJ1-1*01	ASSQMGRENTEAF													
	ASSQGGNTEAF													
	ASSQGRGYEAF													
TRBV3-1*01_TRBJ1-4*01	ASSHRTGEKLF													
	ASSQSEKLF													
TRBV3-1*01_TRBJ1-6*02	ASSQGLDNSPLH													
TRBV4-1*01 or TRBV4-1*02_TRBJ1-1*01	ASSQVNTEAF													
TRBV4-1*01 or TRBV4-1*02_TRBJ1-5*01	ASSLYQSVDSMYSNQPQH													
TRBV4-2*01_TRBJ1-2*01	ASSQSQGEFDGYT													
TRBV5-1*01_TRBJ1-1*01	ASSLVRPHTEAF													
	ASSRQGGEAF													
	ATKLQGSTEAF													
TRBV5-1*01_TRBJ2-2*01	ASSYKQGTGELF													
	ASSEGASNTGELF													
TRBV5-4*01 or TRBV5-4*03_TRBJ1-1*01	ASSFRDTEAF													
TRBV6-1*01_TRBJ1-1*01	ASSEGGVVEAF													
TRBV6-2*01_TRBJ1-2*01	ASSYGGRSSGYT													
TRBV6-5*01_TRBJ1-1*01	ASSRQGTTEAF													
TRBV6-5*01_TRBJ1-2*01	ASRLQGFGGYT													
	ASSYRRDYGYT													
TRBV6-6*01 or TRBV6-6*03_TRBJ1-1*01	ASGGVDDEAF													
TRBV7-2*01 or TRBV7-2*04_TRBJ1-5*01	ASSLGGASNQPQH													
TRBV7-2*02_TRBJ1-4*01	ASSLLGRDEKLF													
TRBV7-8*01_TRBJ1-1*01	ASSLGGRLNTEAF													
TRBV7-9*01 or TRBV7-9*02 or TRBV7-9*03_TRBJ1-1*01	ASSSGSGNEAF													
TRBV7-9*01 or TRBV7-9*02 or TRBV7-9*03_TRBJ1-6*01	ASSQDGTGGSPLH													
Significant ENO1-induced T cell expansions			13	7	8	8	4	0	2	7	6	0	6	5
Significant ENO1-induced T cell contractions			0	0	8	7	2	1	3	1	0	8	10	4

ENO1-dependent expansions are indicated in red and significant values in dark red; ENO1-dependent contractions are indicated in green and significant values in dark green. Common V(D)J rearrangements and CRD3 regions are highlighted in bold.

Interestingly, also if a lower number of clonotypes was expanded after CT, these clonotypes are mostly different compared to before CT. This observation suggests the presence of T cell clones unresponsive to ENO1 stimulation which could be restored after CT. Conversely, the evidence of the significant contraction following ENO1 stimulation could indicate the apoptotic or exhaustive state of those ENO1-specific T cell clones.

Considering all the patients, 67 clonotypes showed a significant expansion before or after CT, and among these, two clonotypes with the same CDR3 region were found in more than one patient (Table 4). Moreover, patients showed nine common V(D)J rearrangements with an analogue trend of ENO1- expansion, suggesting that certain rearrangements could have higher affinity to ENO1 stimulation (Table 4).

Overall, CT seemed to reprogram the ability to significantly expand ENO1-specific T cell clones since different a pattern of clonotypes was observed before and after CT.

Conclusions

The evaluation of the ICB effect before and after CT, allowed to verify the hypothesis that CT-dependent increased anti-tumor immune response could be influenced by the action of the ICB. The results obtained both from the proliferation and from the IFN-γ production support the thesis that generally the immune response of PDA patients does not benefit from the addition of ICB. However, a moderate effect can be observed in the reduction of regulatory tone. Immunological tone analysis identifies subgroups of PDA patient and different T cell clones expand in response to ENO1 before or after CT, supporting the need to further direct the future research towards personalized medicine in PDA patients.

Materials and Methods

Patients: From 2005 to 2011, 18 patients with PDA (Table 1) were enrolled in this study and provided sera and PBMC. The protocol was approved by the local research ethical committee (Azienda Ospedaliero-Universitaria Città della Salute e della Scienza di Torino, IT) and investigations were performed according to the Helsinki Declaration principles. All participants in the protocol signed a declaration of informed consent. PBMC samples were collected from venous blood before and after one cycle of CT. PBMC were separated by Ficoll-Hipaque (Sigma-Merck, Darmstadt DE) and frozen and stored in liquid nitrogen until use.

PBMC culture: PBMC were thawed and cultured at 5x105 cells/ml in 96-well round bottom plate with RPMI (Gibco-ThermoFischer, Waltham MA) plus 5% Certified FBS (Gibco-ThermoFischer, Waltham MA) in the presence or not of 5 µg/ml each recombinant protein, ENO1 (Sigma-Merck, Darmstadt DE) FUBP1, K2C8, G3P (Origene, Rockville, MD) and in the presence or not of a mixture of mAb anti-PD1 (10 µg/ml, Biolegend, San Diego, CA) plus mAb anti-CTLA4 (5 µg/ml, Yervoy-ipilimumab).

Cytokine evaluation: At three days of culture supernatant from TAA-stimulated PBMC was collected and stored at -20°C until the use. Supernatant were diluted 1:4 in assay diluent and tested in ELISA for the presence of IFN-γ and IL-10 following the manufacturer's instruction (Biolegend, San Diego, CA). Optical Density (OD) at 450 nm (reference wavelength: 570 nm) was detected with VICTOR® Nivo™ Multimode Microplate Reader (PerkinElmer, Waltham, MA).

Proliferation: At four days of culture BrdU was added at final concentration of 10 µM. After 18h the specific proliferation of TAA-stimulated PBMC was evaluated by Cell Proliferation ELISA BrdU incorporation, following the manufacturer's instruction (Roche-Merck Darmstadt DE). OD at 450 nm (reference wavelength: 690 nm) was detected with VICTOR® Nivo™ Multimode Microplate Reader (PerkinElmer, Waltham, MA). Stimulation Index (S.I.) referred as the OD ratio between the BrdU incorporation in the presence of TAA and BrdU incorporation control medium condition.

TRCB sequencing: PBMC were thawed and cultured in presence or not of ENO1 as previously describe. At five days PBMC were harvested, pelleted, and processed to mRNA extraction following the manufacturer's instructions with Maxwell® RSC simplyRNA Cells Kit compatible with Maxwell® RSC Instrument (Promega, Madison, WI). The concentration of mRNA was evaluated with QuantiFluor® RNA System (Promega, Madison, WI). RT-PCR was performed with SuperScript™ III Reverse Transcriptase (Invitrogen-ThermoFischer, Waltham MA) to obtained cDNA; concentration of cDNA was assumed the same as the mRNA used. Manufacturer's instructions of LymphoTrack® TRB Assay – MiSeq® (Invivoscribe, San Diego, CA) were followed to generate the library pool which was sequencing with MiSeq™ System (Illumina, San Diego, CA) using the MiSeq Reagent Nano Kit v2 (500-cycles) (Illumina, San Diego, CA).

Statistics and bioinformatics analysis: Hierarchical clustering analysis of IFN-γ/IL10 ratio was performed with Cluster 3.0 using Euclidean distance as similarity metric; data were $\log_2$ transformed then normalized. Heatmap figure of immunological tone was presented with Prism 8.0. Analysis of TCRB sequencing was performed with the online tool IMGT® System starting from the fastq files and the list of unique clonotypes was generated. Only clonotypes with >2 counts were considered in the following analysis. Normalized proportion = n. of clonotype counts / n. of total counts x 10000. The difference in proportions between ENO1 and medium was statistically analyzed with Chi-square test.

Discussion

PDA is a very dismal disease with a low overall survival since most PDA patients receive the diagnosis when the tumor has an advanced stage; moreover, PDA is mainly resistant to CT. To try increasing the outcome of PDA patients, in this thesis are proposed several combinatorial approaches based on immunotherapy, in particular DNA vaccination against TAA. For this reason, the identification of multiple TAA as effective targets is required.

ENO1 overexpression has been correlated with prognosis in PDA patients and the presence of ENO1-specific autoantibodies support its role as target for immunotherapy. ENO1 involvement in PDA invasiveness is demonstrated in the study of Principe et al., since ENO1 silencing inhibited adhesion, invasion, and metastasis in PDA cells, due to changes in actin cytoskeleton organization, integrin profile and uPAR expression. The interplay between ENO1 with integrins and uPAR critically controlled PDA progression, indeed the absence of ENO1 in PDA cells promoted cellular stress and senescence in a uPAR-dependent manner, confirming the role of ENO1 as a promising target in PDA treatment.

From an immunological point of view, ENO1 vaccine elicited an integrated humoral and cellular response to counteract tumor growth without affecting normal tissues, and several anti-tumor immunological mechanisms induced by the ENO1 vaccine were demonstrated in preclinical models. ENO1 vaccination may also benefit from the combined treatments: the next generation immunotherapy of PDA will take advantage of evidence on the CT effects to extend TAA-specific antibody and T cell response, as well as on data demonstrating the effectiveness of the PI3K-γ inhibition to unleash anti-tumor responses. Moreover, Trabectedin effectively depleted TAM and epigenetic reprogrammed TIL into anti-tumor Teff. Finally, also the pharmacological inhibition of ENO1 may contribute to reducing the proliferative and invasive ability of PDA cells.

ENO1 belongs to the GE group and proteomic analysis of PDA patients' sera revealed the presence of a specific antibody response for many GE, which constitute an interesting platform of target for immunotherapy. The overexpressed state of GE in PDA and their involvement in tumor progression support them as a target-group also to reprogram aberrant cancer metabolism and to shrink tumor aggressiveness.

Of note, CT increases TAA-specific immune response in PDA patients. CT induced a progressive increase of antibodies to many TAA indicating a robust antigenic spreading; to support this observation evidence from GEM+ENO1 treatment in the mouse model showed antibody and cellular response to another TAA aside from ENO1. The positive correlation between survival and the increased antibody response to G3P and K2C8 suggest the utility to boost or induce an immune response to PDA-related TAA in patients. TAA-specific antibody production could be stimulated or potentiated through CT, and the interaction with PDA cells can induce a stronger CDC, as the study of Mandili et al. demonstrated. Future immunotherapy based on the TAA vaccination may also synergize with CT to render the antibodies an effective tool against tumor cells.

The combination of CT with ENO1 vaccination elicited a strong anti-tumor activity in KC mice, although seemed to be much more effective in reducing PanIN lesions rather than invasive PDA. However, vaccines against multiple TAA plus CT have yet to be studied in mouse models, maybe exploiting also combinatorial treatments to potentiate the effectiveness against advanced PDA.

The pivotal role of CD4+ T cells in the PDA model is shown by the depletion of CD4+ T cells in untreated mice which led to overly aggressive growth of tumors. While some reports showed that effective tumor immunity can occur in the absence of CD4+ T cells, most indicated that CD4+ T cells are important for generating tumor specific CD8+ T cells. Indeed, most of the identified TAA were intracellular and loaded onto HLA-II by APC after phagocytosis of dying PDA cells exposed to CT. Generation of CD4+ T cells specific for TAA favors the production of specific IgG by B cells (and favors CDC) and the generation of CTL by CD8+ T cells.

In PDA patients CT increased TAA-induced Teff responses, supporting the idea that despite the tumor stage selected patients could benefit from a combined therapy of CT and TAA vaccination, since the study of Mandili et al. showed the presence of T cells responsive to TAA in the patients' peripheral blood mainly after CT. The evaluation of TAA-specific TIL remains an interesting feature to investigate. However, the immunosuppressed PDA microenvironment and the typical consequent T cell exhaustion play a role in immune resistance. Indeed, not in all the patients was observed an effector response to a specific antigen, for this reason a multiple targeting approach could be considered developing a vaccine toward more than one TAA.

Data from a second cohort of PDA patients indicated that CT did not significantly alter the proliferative response of TAA-stimulated PBMC, but high production of IFN-γ in response to TAA was

better induced after CT. A proliferative response to at least one TAA was observed for all patients, considering the four conditions in which PBMC were tested (before CT, after CT, +/-ICB), suggesting that the studied TAA could be considered as potential vaccine targets for many PDA patients at some point of their therapeutic path. Of note, only patients that recognized more TAA after CT had a better survival. This evidence could underline an effective implication of CT-dependent immune response against TAA in slowing tumor progression.

Evaluation of the IFN-γ production following TAA stimulation gives a better understanding of the TAA-specific effector response compared to proliferation alone. Of note, the prevalence of IFN-γ high responses showed a low proliferative response, suggesting the possible memory phenotype of those T cells. Evidence from literature showed that CD8+ T memory cells rapidly produced cytokines, such as IFN-γ, following TCR stimulation [45], and they could have a lower proliferation rate than Teff that will be derived from their progeny [46]. The presence of circulating T memory cells were found also in PDA patients [47].

As opposed to CT, ICB reduced the high proliferative and high IFN-γ responses in PDA patients both before and after CT, suggesting that it suppresses T cell activation. The same trend was observed in healthy subjects, also if the high responses were underrepresented compared to PDA patients. However, ICB increased the number of recognized TAA in some PDA patients but not in healthy subjects, whose PBMC are generally not in an exhausted state. The evaluation of IFN-γ production indicated a negative ICB effect before CT, as the null responses increased, while the group of low responses was reduced, suggesting that exhausted lymphocytes characterized by weak IFN-γ production were not rescued by the addition of ICB. It must be considered that the effect of the ICB was studied only *in vitro*, and we cannot rule out that treating patients with ICB in combination with CT prior to a multiple TAA vaccination, may affect the tumor progression. Anyway, the addition of ICB did not favor a proliferative expansion, but on the contrary decreased the number of highly proliferative and effector responses both before and after CT; this suggests that in PDA patients' peripheral blood the expected effect of the ICB, in rescue the T cell response from immunosuppressive mechanisms, is not possible to achieve.

The inefficacy of ICB could be due to molecular expression signature of T cells since the addition of ICB occurred *in vitro*, thus outside the typical immunosuppressive state of PDA tumor microenvironment. The function of ICB in tumor immunotherapy is based on the higher expression of immune checkpoint molecules, such as PD1 and CTLA4, in T cells. The previous observations could

suggest that peripheral T cells from PDA patients did not express PD1 or CTLA4 molecules, as expected from healthy subjects, since generally in both groups ICB failed to raise a relevant proliferative and effector response. So far data on the expression of PD1 or CTLA1 have been reported only in immune cells infiltrating the tumor but not in the peripheral blood of PDA patients. However, data from non-small-cell lung cancer and breast cancer showed higher expression of PD1 also in peripheral T cells in cancer patients compared to healthy donors [48,49].

Of note, recent evidence showed that other molecules play a central role, more relevant that PD1, in establishing T cell exhaustion, such as TCF-1, which supports the exhausted T cell precursor development by antagonizing Teff-like cell differentiation through multiple transcription factors [50]. The comprehension of active immune checkpoint signaling, together with novel involved transcription factor, in PDA patients' peripheral T cells is an interesting field to investigate; thus, PBMC gene expression analysis through mRNA next generation sequencing (NGS) is currently in progress in a subset of PDA patients before and after CT.

The analysis of IL-10 production was added to IFN-γ, to allow a view of the immunological tone of the immune response, which can be mainly effector (prevalence of IFN-γ) or regulatory (prevalence of IL-10). Despite ICB did not induce a relevant effector response, the adding of ICB (mainly after CT) could moderate the intensity of regulatory response via the impairment of IL-10 production. These observations suggest a potential role of ICB in affecting Treg functions, which should be deepened. Three groups of responses have been clustered on the base of the greater effector response: before CT, after CT and under no circumstances. This clustering highlights the possibility to stratify patients in subgroups with similar characteristics for the major number of TAA. In some PDA patients TAA-specific T cells showed up a strong effector phenotype already at the diagnosis, which was subsequently lost suggesting their exhaustive state. However, the exhaustion may be due to a molecular pathway different from PD1 and CTLA4, since the adding of ICB did not generally potentiate the effector response. Other PDA patients instead benefited from CT (in some cases also with the *in vitro* addition of ICB) which recovered or boosted the effector response of TAA-specific not exhausted T cells. This observation corroborates the previous results on the effect of CT in shaping the immune system of PDA patients in response to TAA. However, several patients cannot even receive a proper CT treatment due their clinical poor condition and multiple combined treatments need to be fine-tuned for these patients.

Finally, CT reprogrammed the pattern of ENO1-specific T cell clones, in some patients only before CT the PBMC maintained the ability to significantly expand ENO1-specific clonotypes. These data support the previous observations in which before CT patients showed TAA-specific T cells, that lost the ability to be activated after CT due to their state of exhaustion. By contrast, after CT other different ENO1-specific clonotypes appeared expanded, pointing out the CT effect in unleashed the activation of certain TAA-specific T lymphocytes. However, molecular expression profiles of before or after CT-related clones need to be further studied.

In conclusion, the profiling of immune response in patients with pancreatic cancer, together with the preclinical mouse model validations, provide a proof-of-concept that multiple TAA vaccination is a cornerstone for novel precision PDA treatments and its anti-tumor efficacy can be increased by the combination of DNA vaccine and specific pharmacological approaches such as CT.

Abbreviation list

PDA: Pancreatic Ductal Adenocarcinoma
CT: Chemotherapy
GEM: Gemcitabine
TME: Tumor Microenviroment
ECM: Extracellular Matrix
TAM: Tumor-Associated Macrophages
MDSC: Myeloid-Derived Suppressor Cells
Treg: Regulatory T Cells
Teff: Effector T Cells
SERPA: SERological Proteome Analysis
TAA: Tumor-Associated Antigens
PBMC: Peripheral Blood Mononuclear Cells
TIL: Infiltrating-Tumor T Cells
Th1: T helper1 cells
Th17: T helper 17 cells
TCRB: T cell receptor Vβ chains
CDC: Complement-Dependent Cytotoxicity
VN: Vitronectin
ROS: Reactive Oxygen Species
DAMP: damage-associated molecular patterns
APC: antigen presenting cells
ICB: Immune Checkpoint Blockade

Author's contributions

The candidate contributed to the writing the following reviews: Cappello, et al. Front Biosci, 2017; Cappello, et al. Cancers, 2018 and Curcio, et al. Molecules, 2021.
In the paper of Principe, et al. the candidate performed the senescent and apoptosis experiments.
In the paper of Mandili, et al. JITC, 2020 the candidate: contributed to the in vitro experiments with murine splenocytes; helped in the collection of tumor and other organs from mice at the sacrifice; performed the in vitro experiments with human PBMC.
The latest experiments of unpublished data were all performed by the candidate.

Bibliography

1. Siegel, R.L.; Miller, K.D.; Jemal, A. Cancer Statistics, 2020. *CA: A Cancer Journal for Clinicians* **2020**, *70*, 7–30, doi:10.3322/caac.21590.
2. Werner, J.; Combs, S.E.; Springfeld, C.; Hartwig, W.; Hackert, T.; Büchler, M.W. Advanced-Stage Pancreatic Cancer: Therapy Options. *Nature Reviews Clinical Oncology* **2013**, *10*, 323–333, doi:10.1038/nrclinonc.2013.66.
3. Reni, M.; Cereda, S.; Rognone, A.; Belli, C.; Ghidini, M.; Longoni, S.; Fugazza, C.; Rezzonico, S.; Passoni, P.; Slim, N.; et al. A Randomized Phase II Trial of Two Different 4-Drug Combinations in Advanced Pancreatic Adenocarcinoma: Cisplatin, Capecitabine, Gemcitabine plus Either Epirubicin or Docetaxel (PEXG or PDXG Regimen). *Cancer Chemother. Pharmacol.* **2012**, *69*, 115–123, doi:10.1007/s00280-011-1680-2.
4. Conroy, T.; Desseigne, F.; Ychou, M.; Bouché, O.; Guimbaud, R.; Bécouarn, Y.; Adenis, A.; Raoul, J.-L.; Gourgou-Bourgade, S.; de la Fouchardière, C.; et al. FOLFIRINOX versus Gemcitabine for Metastatic Pancreatic Cancer. *N. Engl. J. Med.* **2011**, *364*, 1817–1825, doi:10.1056/NEJMoa1011923.
5. Von Hoff, D.D.; Ervin, T.; Arena, F.P.; Chiorean, E.G.; Infante, J.; Moore, M.; Seay, T.; Tjulandin, S.A.; Ma, W.W.; Saleh, M.N.; et al. Increased Survival in Pancreatic Cancer with Nab-Paclitaxel plus Gemcitabine. *N. Engl. J. Med.* **2013**, *369*, 1691–1703, doi:10.1056/NEJMoa1304369.
6. von Ahrens, D.; Bhagat, T.D.; Nagrath, D.; Maitra, A.; Verma, A. The Role of Stromal Cancer-Associated Fibroblasts in Pancreatic Cancer. *Journal of Hematology & Oncology* **2017**, *10*, 76, doi:10.1186/s13045-017-0448-5.
7. Apte, M.V.; Wilson, J.S.; Lugea, A.; Pandol, S.J. A Starring Role for Stellate Cells in the Pancreatic Cancer Microenvironment. *Gastroenterology* **2013**, *144*, 1210–1219, doi:10.1053/j.gastro.2012.11.037.
8. Clark, C.E.; Hingorani, S.R.; Mick, R.; Combs, C.; Tuveson, D.A.; Vonderheide, R.H. Dynamics of the Immune Reaction to Pancreatic Cancer from Inception to Invasion. *Cancer Res* **2007**, *67*, 9518–9527, doi:10.1158/0008-5472.CAN-07-0175.
9. Upadhrasta, S.; Zheng, L. Strategies in Developing Immunotherapy for Pancreatic Cancer: Recognizing and Correcting Multiple Immune “Defects” in the Tumor Microenvironment. *J Clin Med* **2019**, *8*, doi:10.3390/jcm8091472.
10. Pardoll, D. Cancer and the Immune System: Basic Concepts and Targets for Intervention. *Semin Oncol* **2015**, *42*, 523–538, doi:10.1053/j.seminoncol.2015.05.003.
11. Sahin, U.; Türeci, Ö.; Pfreundschuh, M. Serological Identification of Human Tumor Antigens. *Current Opinion in Immunology* **1997**, *9*, 709–716, doi:10.1016/S0952-7915(97)80053-2.
12. Old, L.J.; Chen, Y.-T. New Paths in Human Cancer Serology. *Journal of Experimental Medicine* **1998**, *187*, 1163–1167, doi:10.1084/jem.187.8.1163.
13. Naour, F.L. Contribution of Proteomics to Tumor Immunology. *PROTEOMICS* **2001**, *1*, 1295–1302, doi:10.1002/1615-9861(200110)1:10<1295::AID-PROT1295>3.0.CO;2-F.
14. Tomaino, B.; Cappello, P.; Capello, M.; Fredolini, C.; Ponzetto, A.; Novarino, A.; Ciuffreda, L.; Bertetto, O.; De Angelis, C.; Gaia, E.; et al. Autoantibody Signature in Human Ductal Pancreatic Adenocarcinoma. *J. Proteome Res.* **2007**, *6*, 4025–4031, doi:10.1021/pr070281a.
15. Cappello, P.; Principe, M.; Bulfamante, S.; Novelli, F. Alpha-Enolase (ENO1), a Potential Target in Novel Immunotherapies. *Front Biosci (Landmark Ed)* **2017**, *22*, 944–959.
16. Tomaino, B.; Cappello, P.; Capello, M.; Fredolini, C.; Sperduti, I.; Migliorini, P.; Salacone, P.; Novarino, A.; Giacobino, A.; Ciuffreda, L.; et al. Circulating Autoantibodies to Phosphorylated

α-Enolase Are a Hallmark of Pancreatic Cancer. *J. Proteome Res.* **2011**, *10*, 105–112, doi:10.1021/pr100213b.
17. Mandili, G.; Curcio, C.; Bulfamante, S.; Follia, L.; Ferrero, G.; Mazza, E.; Principe, M.; Cordero, F.; Satolli, M.A.; Spadi, R.; et al. In Pancreatic Cancer, Chemotherapy Increases Antitumor Responses to Tumor-Associated Antigens and Potentiates DNA Vaccination. *J Immunother Cancer* **2020**, *8*, e001071, doi:10.1136/jitc-2020-001071.
18. Capello, M.; Caorsi, C.; Bogantes Hernandez, P.J.; Dametto, E.; Bertinetto, F.E.; Magistroni, P.; Rendine, S.; Amoroso, A.; Novelli, F. Phosphorylated Alpha-Enolase Induces Autoantibodies in HLA-DR8 Pancreatic Cancer Patients and Triggers HLA-DR8 Restricted T-Cell Activation. *Immunology Letters* **2015**, *167*, 11–16, doi:10.1016/j.imlet.2015.06.008.
19. Cappello, P.; Tomaino, B.; Chiarle, R.; Ceruti, P.; Novarino, A.; Castagnoli, C.; Migliorini, P.; Perconti, G.; Giallongo, A.; Milella, M.; et al. An Integrated Humoral and Cellular Response Is Elicited in Pancreatic Cancer by Alpha-Enolase, a Novel Pancreatic Ductal Adenocarcinoma-Associated Antigen. *Int. J. Cancer* **2009**, *125*, 639–648, doi:10.1002/ijc.24355.
20. Amedei, A.; Niccolai, E.; Benagiano, M.; Della Bella, C.; Cianchi, F.; Bechi, P.; Taddei, A.; Bencini, L.; Farsi, M.; Cappello, P.; et al. Ex Vivo Analysis of Pancreatic Cancer-Infiltrating T Lymphocytes Reveals That ENO-Specific Tregs Accumulate in Tumor Tissue and Inhibit Th1/Th17 Effector Cell Functions. *Cancer Immunol. Immunother.* **2013**, *62*, 1249–1260, doi:10.1007/s00262-013-1429-3.
21. Niccolai, E.; Cappello, P.; Taddei, A.; Ricci, F.; D'Elios, M.M.; Benagiano, M.; Bechi, P.; Bencini, L.; Ringressi, M.N.; Coratti, A.; et al. Peripheral ENO1-Specific T Cells Mirror the Intratumoral Immune Response and Their Presence Is a Potential Prognostic Factor for Pancreatic Adenocarcinoma. *Int. J. Oncol.* **2016**, *49*, 393–401, doi:10.3892/ijo.2016.3524.
22. Ramanathan, R.K.; Lee, K.M.; McKolanis, J.; Hitbold, E.; Schraut, W.; Moser, A.J.; Warnick, E.; Whiteside, T.; Osborne, J.; Kim, H.; et al. Phase I Study of a MUC1 Vaccine Composed of Different Doses of MUC1 Peptide with SB-AS2 Adjuvant in Resected and Locally Advanced Pancreatic Cancer. *Cancer Immunol. Immunother.* **2005**, *54*, 254–264, doi:10.1007/s00262-004-0581-1.
23. Staff, C.; Mozaffari, F.; Frödin, J.-E.; Mellstedt, H.; Liljefors, M. Telomerase (GV1001) Vaccination Together with Gemcitabine in Advanced Pancreatic Cancer Patients. *Int. J. Oncol.* **2014**, *45*, 1293–1303, doi:10.3892/ijo.2014.2496.
24. Shima, H.; Tsurita, G.; Wada, S.; Hirohashi, Y.; Yasui, H.; Hayashi, H.; Miyakoshi, T.; Watanabe, K.; Murai, A.; Asanuma, H.; et al. Randomized Phase II Trial of Survivin 2B Peptide Vaccination for Patients with HLA-A24-Positive Pancreatic Adenocarcinoma. *Cancer Science* **2019**, *110*, 2378–2385, doi:10.1111/cas.14106.
25. Zhang, Y.; Ma, J.-A.; Zhang, H.-X.; Jiang, Y.-N.; Luo, W.-H. Cancer Vaccines: Targeting KRAS-Driven Cancers. *Expert Review of Vaccines* **2020**, *19*, 163–173, doi:10.1080/14760584.2020.1733420.
26. Dranoff, G.; Jaffee, E.; Lazenby, A.; Golumbek, P.; Levitsky, H.; Brose, K.; Jackson, V.; Hamada, H.; Pardoll, D.; Mulligan, R.C. Vaccination with Irradiated Tumor Cells Engineered to Secrete Murine Granulocyte-Macrophage Colony-Stimulating Factor Stimulates Potent, Specific, and Long-Lasting Anti-Tumor Immunity. *Proc. Natl. Acad. Sci. U.S.A.* **1993**, *90*, 3539–3543.
27. Jaffee, E.M.; Hruban, R.H.; Biedrzycki, B.; Laheru, D.; Schepers, K.; Sauter, P.R.; Goemann, M.; Coleman, J.; Grochow, L.; Donehower, R.C.; et al. Novel Allogeneic Granulocyte-Macrophage Colony-Stimulating Factor–Secreting Tumor Vaccine for Pancreatic Cancer: A Phase I Trial of Safety and Immune Activation. *JCO* **2001**, *19*, 145–156, doi:10.1200/JCO.2001.19.1.145.

28. Haas, A.R.; Tanyi, J.L.; O'Hara, M.H.; Gladney, W.L.; Lacey, S.F.; Torigian, D.A.; Soulen, M.C.; Tian, L.; McGarvey, M.; Nelson, A.M.; et al. Phase I Study of Lentiviral-Transduced Chimeric Antigen Receptor-Modified T Cells Recognizing Mesothelin in Advanced Solid Cancers. *Molecular Therapy* **2019**, *27*, 1919–1929, doi:10.1016/j.ymthe.2019.07.015.
29. Wang, Z.; Troilo, P.J.; Wang, X.; Griffiths, T.G.; Pacchione, S.J.; Barnum, A.B.; Harper, L.B.; Pauley, C.J.; Niu, Z.; Denisova, L.; et al. Detection of Integration of Plasmid DNA into Host Genomic DNA Following Intramuscular Injection and Electroporation. *Gene Ther* **2004**, *11*, 711–721, doi:10.1038/sj.gt.3302213.
30. Hingorani, S.R.; Wang, L.; Multani, A.S.; Combs, C.; Deramaudt, T.B.; Hruban, R.H.; Rustgi, A.K.; Chang, S.; Tuveson, D.A. Trp53R172H and KrasG12D Cooperate to Promote Chromosomal Instability and Widely Metastatic Pancreatic Ductal Adenocarcinoma in Mice. *Cancer Cell* **2005**, *7*, 469–483, doi:10.1016/j.ccr.2005.04.023.
31. Cappello, P.; Rolla, S.; Chiarle, R.; Principe, M.; Cavallo, F.; Perconti, G.; Feo, S.; Giovarelli, M.; Novelli, F. Vaccination With ENO1 DNA Prolongs Survival of Genetically Engineered Mice With Pancreatic Cancer. *Gastroenterology* **2013**, *144*, 1098–1106, doi:10.1053/j.gastro.2013.01.020.
32. Cappello, P.; Curcio, C.; Mandili, G.; Roux, C.; Bulfamante, S.; Novelli, F. Next Generation Immunotherapy for Pancreatic Cancer: DNA Vaccination Is Seeking New Combo Partners. *Cancers* **2018**, *10*, 51, doi:10.3390/cancers10020051.
33. Castino, G.F.; Cortese, N.; Capretti, G.; Serio, S.; Di Caro, G.; Mineri, R.; Magrini, E.; Grizzi, F.; Cappello, P.; Novelli, F.; et al. Spatial Distribution of B Cells Predicts Prognosis in Human Pancreatic Adenocarcinoma. *Oncoimmunology* **2016**, *5*, e1085147, doi:10.1080/2162402X.2015.1085147.
34. Cappello, P.; Tonoli, E.; Curto, R.; Giordano, D.; Giovarelli, M.; Novelli, F. Anti-α-Enolase Antibody Limits the Invasion of Myeloid-Derived Suppressor Cells and Attenuates Their Restraining Effector T Cell Response. *Oncoimmunology* **2016**, *5*, e1112940, doi:10.1080/2162402X.2015.1112940.
35. Curcio, C.; Brugiapaglia, S.; Bulfamante, S.; Follia, L.; Cappello, P.; Novelli, F. The Glycolytic Pathway as a Target for Novel Onco-Immunology Therapies in Pancreatic Cancer. *Molecules* **2021**, *26*, 1642, doi:10.3390/molecules26061642.
36. Ceruti, P.; Principe, M.; Capello, M.; Cappello, P.; Novelli, F. Three Are Better than One: Plasminogen Receptors as Cancer Theranostic Targets. *Experimental Hematology & Oncology* **2013**, *2*, 12, doi:10.1186/2162-3619-2-12.
37. Walsh, J.L.; Keith, T.J.; Knull, H.R. Glycolytic Enzyme Interactions with Tubulin and Microtubules. *Biochimica et Biophysica Acta (BBA) - Protein Structure and Molecular Enzymology* **1989**, *999*, 64–70, doi:10.1016/0167-4838(89)90031-9.
38. Principe, M.; Borgoni, S.; Cascione, M.; Chattaragada, M.S.; Ferri-Borgogno, S.; Capello, M.; Bulfamante, S.; Chapelle, J.; Di Modugno, F.; Defilippi, P.; et al. Alpha-Enolase (ENO1) Controls Alpha v/Beta 3 Integrin Expression and Regulates Pancreatic Cancer Adhesion, Invasion, and Metastasis. *J Hematol Oncol* **2017**, *10*, 16, doi:10.1186/s13045-016-0385-8.
39. Warburg, O.; Wind, F.; Negelein, E. THE METABOLISM OF TUMORS IN THE BODY. *J Gen Physiol* **1927**, *8*, 519–530, doi:10.1085/jgp.8.6.519.
40. Mahoney, K.M.; Freeman, G.J.; McDermott, D.F. The Next Immune-Checkpoint Inhibitors: PD-1/PD-L1 Blockade in Melanoma. *Clinical Therapeutics* **2015**, *37*, 764–782, doi:10.1016/j.clinthera.2015.02.018.

41. Le, D.T.; Durham, J.N.; Smith, K.N.; Wang, H.; Bartlett, B.R.; Aulakh, L.K.; Lu, S.; Kemberling, H.; Wilt, C.; Luber, B.S.; et al. Mismatch Repair Deficiency Predicts Response of Solid Tumors to PD-1 Blockade. *Science* **2017**, *357*, 409–413, doi:10.1126/science.aan6733.
42. Brahmer, J.R.; Tykodi, S.S.; Chow, L.Q.M.; Hwu, W.-J.; Topalian, S.L.; Hwu, P.; Drake, C.G.; Camacho, L.H.; Kauh, J.; Odunsi, K.; et al. Safety and Activity of Anti-PD-L1 Antibody in Patients with Advanced Cancer. *N. Engl. J. Med.* **2012**, *366*, 2455–2465, doi:10.1056/NEJMoa1200694.
43. Royal, R.E.; Levy, C.; Turner, K.; Mathur, A.; Hughes, M.; Kammula, U.S.; Sherry, R.M.; Topalian, S.L.; Yang, J.C.; Lowy, I.; et al. Phase 2 Trial of Single Agent Ipilimumab (Anti-CTLA-4) for Locally Advanced or Metastatic Pancreatic Adenocarcinoma. *Journal of Immunotherapy* **2010**, *33*, 828–833, doi:10.1097/CJI.0b013e3181eec14c.
44. Schoenborn, J.R.; Wilson, C.B. Regulation of Interferon-γ During Innate and Adaptive Immune Responses. In *Advances in Immunology*; Academic Press, 2007; Vol. 96, pp. 41–101.
45. Lee, Y.J.; Jameson, S.C.; Hogquist, K.A. Alternative Memory in the CD8 Lineage. *Trends Immunol* **2011**, *32*, 50–56, doi:10.1016/j.it.2010.12.004.
46. Restifo, N.P.; Gattinoni, L. Lineage Relationship of Effector and Memory T Cells. *Curr Opin Immunol* **2013**, *25*, doi:10.1016/j.coi.2013.09.003.
47. Hang, J.; Huang, J.; Zhou, S.; Wu, L.; Zhu, Y.; Zhu, L.; Zhou, H.; Xu, K.; Jiang, H.; Yang, X. The Clinical Implication of CD45RA+ Naïve T Cells and CD45RO+ Memory T Cells in Advanced Pancreatic Cancer: A Proxy for Tumor Biology and Outcome Prediction. *Cancer Medicine* **2019**, *8*, 1326–1335, doi:10.1002/cam4.1988.
48. Bao, Y.; Mo, J.-F.; Wu, J.-Y.; Cao, C.-X. Expression of PD1 and BTLA on the CD8+ T Cell and ΓδT Cell Subsets in Peripheral Blood of Non-Small Cell Lung Cancer Patients. *Chin Med Sci J* **2019**, *34*, 248–255, doi:10.24920/003498.
49. Noda, M.; Masuda, T.; Ito, S.; Tobo, T.; Kitagawa, A.; Hu, Q.; Shimizu, D.; Eguchi, H.; Etoh, T.; Ohno, S.; et al. Circulating PD-1 MRNA in Peripheral Blood Is a Potential Biomarker for Predicting Survival of Breast Cancer Patients. *Ann Surg Oncol* **2020**, *27*, 4035–4043, doi:10.1245/s10434-020-08375-z.
50. Chen, Z.; Ji, Z.; Ngiow, S.F.; Manne, S.; Cai, Z.; Huang, A.C.; Johnson, J.; Staupe, R.P.; Bengsch, B.; Xu, C.; et al. TCF-1-Centered Transcriptional Network Drives an Effector versus Exhausted CD8 T Cell-Fate Decision. *Immunity* **2019**, *51*, 840-855.e5, doi:10.1016/j.immuni.2019.09.013.